

Aspects of Geometry and Topology in Liquid Crystalline Phases

Thomas John Machon

Submitted for the degree
of
Doctor of Philosophy

University of Warwick

September 2015

CONTENTS

List of Figures	iii
List of Tables	vii
Acknowledgements	xi
Declaration	xiii
Abstract	xv
1 Liquid Crystals, Defects and Topology	1
1.1 Free Energies for Liquid Crystals	2
1.2 Topological Defects	5
1.3 The Homotopy Theory of Defects	9
1.4 The General Theory	13
1.5 Biaxial Nematics	15
2 Global Theory of Topological Defects in Nematic Liquid Crystals	17
2.1 Orientable Textures	20
2.2 Non-orientable Textures	22
2.2.1 The Covering Space for a Nematic Domain	23
2.2.2 Branch Sets for a Nematic Domain	25
2.2.3 The Pontryagin-Thom Construction for Maps into S^2 .	28
2.2.4 Equivariant Maps	29
2.3 Nematic Textures on Tori	32

2.3.1	Textures on T^2	32
2.3.2	Textures on T^3	35
2.4	Knotted Line Defects	38
2.4.1	Interpretation of the Topology of Knotted Defects	45
3	Umbilic Lines and the Geometry of Orientational Order	49
3.1	Local Geometry of Orientational Order	51
3.2	Global Definition of Umbilics and their Topology	55
3.3	Local Profiles of Umbilic lines	62
3.4	The Local Profile of Tensor Field Zeros in 2D	65
3.5	Umbilic Loops	68
3.6	Examples of Line Fields: Blue Phases	75
4	Synthesis: the Case of the Cholesteric	81
4.1	Observed Defects in Cholesterics	82
4.2	The Theory of the Pitch Axis	84
4.2.1	Remedies for the Pitch Axis	86
4.3	Umbilic Lines and Cholesteric Defects	87
4.4	Two-dimensional Smectics	91
4.5	The Weakly Twisted Case	92
4.6	The Free Energy and Geometry of a Cholesteric	94
4.7	Cholesterics and Contact Structures	95
4.7.1	Solitons in a Cholesteric Background	98
4.8	Overtwistedness and Umbilic Lines	100
4.9	Floer Theories and Beyond	101
5	Defects Induced by Non-Orientable Colloids	105
5.1	Colloids and the Topology of Surfaces	106
5.2	Simulations of Non-Orientable Colloids	109
6	Constructing Knotted Textures with Milnor Fibrations	115
6.1	Constructing Knotted Textures	117

6.1.1	The Topology of the Texture	118
6.2	The Hopf Link and Conjugate Polynomials	119
6.3	Adding Skyrmions and Hedgehogs	121
6.3.1	Examples and practicalities	124
Bibliography		127

FIGURES

1.1	Molecular structure of MBBA.	2
1.2	Schlieren texture.	6
1.3	Defect Profiles in Two-Dimensional Nematics.	8
1.4	Escape in the third dimension.	8
1.5	Changing the basepoint.	11
1.6	The real projective plane.	12
1.7	Combining line defects.	13
1.8	Visualisation of various types of order.	15
1.9	Crossing of Defect Lines.	16
2.1	Defects in a domain corresponding to all of \mathbb{R}^3 minus a point at the origin.	21
2.2	Defects in a domain corresponding to all of \mathbb{R}^3 except two points.	22
2.3	Nematic covering spaces when the domain is the torus.	24
2.4	Examples of branching sets for nematic domains.	26
2.5	Intersection of cycles on \mathbb{RP}^2 .	26
2.6	Showing that $n _B$ must be null-homotopic.	28
2.7	The effect on the Pontryagin-Thom representation of a map $\Omega \rightarrow S^2$ under the antipodal map.	30
2.8	Schematic illustration of equivariant homotopy.	32
2.9	Equivariant homotopies and nematic textures on T^2 .	34
2.10	Orientable textures on T^3 .	36

2.11	Equivariant homotopy on the double cover of the torus.	37
2.12	Pulling a twist off a link to form a twisted circle.	38
2.13	The unknot and the Hopf link.	40
2.14	Examples of Seifert surfaces for the trefoil knot and the Hopf link.	41
2.15	Various cycles relating to \mathcal{B} and L	42
2.16	The relationship $a_i^+ - a_i^- = c_{2g+i}$	43
2.17	Skyrmion tube entangling a trefoil knot defect.	46
2.18	Disconnected spanning surface for the $(4, 4)$ torus link.	47
3.1	Umbilic lines.	53
3.2	The splitting $T\mathbb{R}^3 \cong L_n \oplus \xi$ induced by orientational order.	56
3.3	Anatomy of an umbilic line.	60
3.4	Umbilic lines in a Skyrmion lattice.	61
3.5	Transient monopoles and umbilic lines.	63
3.6	Umbilic lines in a toron.	70
3.7	The self-linking number for transverse umbilic loops.	71
3.8	Umbilic lines in the Hopf fibration.	73
3.9	Umbilic lines in the blue phases.	78
4.1	Two helical cholesterics in a slab of height L	83
4.2	Defects in Cholesterics.	84
4.3	Twisting of a director.	85
4.4	Solomon's Seal in a cholesteric.	90
4.5	Umbilic Crossing a Disclination.	91
4.6	Surfaces in two dimensional smectics.	92
4.7	Umbilic lines in a Saturn's ring configuration.	93
4.8	Soliton against a cholesteric background.	99
4.9	Hopf linked defects in a cholesteric.	103
5.1	Saturn's ring defect line around a spherical colloid with homeotropic anchoring.	106

5.2	Topological characterisation of surfaces with homeotropic boundary conditions in a three-dimensional, nematic liquid crystal.	108
5.3	Simulation results of a Möbius strip with homeotropic boundary conditions.	111
5.4	Knotted and linked disclinations in chiral nematics stabilised by the presence of twisted strip colloids.	112
5.5	Comparison of configurations for a quintuply twisted strip.	113
5.6	Field Structure of knotted disclination lines.	114
6.1	Milnor Fibrations	116
6.2	PT Surfaces in Milnor Fibrations.	121
6.3	Extending the Milnor Construction.	122
6.4	Gallery of knotted defect textures.	125

TABLES

1.1	Homotopy groups for the quotient of $SO(3)$ by various symmetry subgroups.	14
2.1	$H_1(\Sigma(L))$ for (p, q) torus links with $2 \leq (p, q) \leq 20$	48
3.1	Local structure of zeros for a spin 2 field.	69

There is only one name on this thesis, but it is the work of many people. My supervisor, Gareth Alexander, has gone far beyond any reasonable expectation one might have of their supervisor. His patience, wisdom and insight never ran dry; my debt to him can be done no justice here. I would like to acknowledge my second supervisor, Miha Ravnik, and also Randall Kamien for their generosity and for many helpful conversations and both Bryan Chen and Simon Čopar, whose work has influenced mine greatly.

The soft matter group at Warwick have been excellent and stimulating place to spend the last three years. In particular I would like to mention Davide Michieletto, Dario Papavassiliou, Alex Rautu and Diana Khoromskaia for their good advice and good company.

I shared many great times with my fellow students in the 2011 complexity cohort: Peter Dawson, Dominic Kerr, Yuri Lifanov, Michael Maitland, Aran Tamsett, Ellen Webborn and Rachel Wilkerson, my officemates in D2.14: Matt Graham and Joel Nicholls and also Ben Collyer, Matthew Dale and Felicity Kendrick.

I would like to thank my family, my mother Barbara, my father Paul and my brother George for their love and support.

Finally, for the rest and for everything, I thank Elena.

DECLARATION

This thesis is submitted to the University of Warwick in support of my application for the degree of Doctor of Philosophy. It has been composed by myself and has not been submitted in any previous application for any degree. Part of the material in this thesis has been published in the following papers:

Material from Chapter 5 has been published in:

T. Machon and G.P. Alexander, *Knots and non-orientable surfaces in chiral nematics*, Proc. Natl. Acad. Sci. USA **110**, 14174 (2013).

A summary of some material in Chapter 2 has been published in:

T. Machon and G.P. Alexander, *Knotted Defects in Nematic Liquid Crystals*, Phys. Rev. Lett. **113**, 027801 (2014).

The arguments in §4.2-3 formed a small part of the publication:

D.A. Beller, T. Machon, S. Čopar, D.M. Sussman, G.P. Alexander, R.D. Kamien and R.A. Mosna, *Geometry of the Cholesteric Phase*, Phys. Rev. X **4**, 031050 (2014).

The material in Chapter 3 has been submitted for publication and material from Chapters 2,4 and 6 is currently being prepared for publication.

ABSTRACT

Liquid crystals exhibit a rich set of phenomena with a geometric and topological flavour. In this thesis the study nematic and cholesteric phases of liquid crystals from the perspective of geometry and topology. We show that a global extension of the homotopy theory of defects in three dimensional nematics allows one to associate a topological ‘internal state’ to knotted and linked defects lines, such as those made experimentally. This internal state reflects the way in which the liquid crystal ‘wraps around’ the defects in the system and can be associated to baby Skyrmion tubes and relative orientations. Moving on from this we give a geometric analysis of orientational order, showing that there are a natural set of lines, realised as geometric singularities, the generalisation of the umbilical points of a surface. These lines can be identified with a number of structures seen experimentally in chiral systems such as double twist cylinders, the centres of Skyrmions and λ lines. We describe the theoretical properties of these lines, in particular how they reflect the topology of the underlying orientation by furnishing a representation of (four times) the Euler class of the orthogonal 2-plane bundle. We then combine these two theoretical structures to give a description of the cholesteric phase. In particular, our description allows all structures to be derived from the orientational order, and we show how previous theories and interesting structures such as τ lines fit into this scheme. We extend this theory by making the connection between cholesteric liquid crystals and contact structures, where we show that one can obtain additional topological distinctions between field configurations. We discuss topological aspects of colloidal inclusions and show that non-orientable colloids can precipitate the creation of knotted defect lines *in silico*. Finally, we show how one can use Milnor fibrations to give explicit formulae for director fields that contain knotted defect lines.

"We shall not cease from exploration, and the end of all our exploring will be to arrive where we started and know the place for the first time."

T.S. Eliot, *Little Gidding*

CHAPTER 1

LIQUID CRYSTALS, DEFECTS AND TOPOLOGY

Liquid crystals are phases of matter lying between liquid and crystalline order. Typically composed of long, thin molecules such as N-(4-Methoxybenzylidene)-4-butylaniline (MBBA), shown in Figure 1.1, they flow as a liquid but experience the long-range orientational correlations and elastic distortions of a solid [1]. There are several different liquid crystalline mesophases, the most basic being the nematic phase, but others such as cholesteric (chiral) and smectic (layered) liquid crystals also exist, along with their own set of complex phenomena. The nematic phase is typically obtained by cooling from the isotropic (liquid) phase through a first order phase transition [2]. Upon this transition, and common to all liquid crystalline phases, is the creation of orientational order due to a non-zero average local molecular alignment. In theoretical descriptions of liquid crystals this is typically coarse-grained to produce a unit magnitude orientation field, known as the director [3]. One of the key aspects of liquid crystalline order that this orientation is apolar, it picks out only an unoriented direction in space, rather than the oriented direction given by a vector. While the order is apolar, it is traditional in the literature to represent it as a unit vector, \mathbf{n} . Locally there is no issue with this as one can always locally orient a director field. Globally, however, this orienting is not always possible. As a consequence of this apolarity, liquid crystalline systems exhibit a huge variety of interesting phenomena that very often have a geometric or topological flavour. Of particular note are the line-

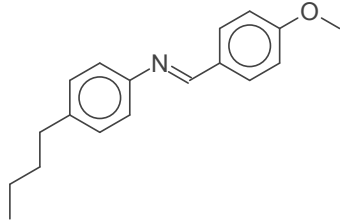


Figure 1.1: Molecular structure of MBBA, a material that forms a nematic phase at room temperature.

like structures one observes: disclinations, dislocations and others. Recent experimental work has given extremely fine control of these line structures, with the resulting creation of knotted defects lines [4, 5, 6], and a variety of other solitons [7, 8, 9]. These elaborate objects strengthen the connection between the physics of liquid crystals and the fields of geometry and topology, and provide a beautiful set of motivating examples for much of this thesis.

1.1 FREE ENERGIES FOR LIQUID CRYSTALS

The most elementary liquid crystal phase is the nematic, in which the system prefers a uniform molecular alignment with no positional order. As such, in the nematic phase distortions from uniform alignment are energetically costly. Static configurations of nematics can therefore be understood by constructing an appropriate elastic free energy in terms of distortions in \mathbf{n} [1, 2]. The first point to note, and this will be stressed throughout this thesis, is that \mathbf{n} represents a genuine direction in space, rather than an internal state. To construct an elastic free energy we should therefore look for symmetry protected quantities in $\nabla \mathbf{n}$, that is scalars that are left invariant under global rotations. This is a classical calculation, reformulated in Chapter 3 in terms of vector bundles, where it is shown that one can decompose the gradient tensor as

$$\nabla \mathbf{n} = \frac{\nabla \cdot \mathbf{n}}{2} (\mathbb{I} - \mathbf{n} \otimes \mathbf{n}) - \frac{\mathbf{n} \cdot \nabla \times \mathbf{n}}{2} J + \mathbf{n} \otimes (\mathbf{n} \cdot \nabla) \mathbf{n} + \Delta \quad (1.1)$$

where $J_{ij} = \epsilon_{ijk}n_k$ and Δ corresponds to the anisotropic orthogonal gradients, which are dealt with extensively in Chapter 3. Each of these pieces is orthogonal with respect to the inner product $\langle A, B \rangle = A_{ij}B_{ij}/2$ and the pieces transform among themselves under rotations. As such the symmetry protected quantities we can extract from $\nabla \mathbf{n}$ are precisely the magnitudes of each of these components. These scalars are

$$\frac{\nabla \cdot \mathbf{n}}{2}, \quad (1.2)$$

$$\frac{\mathbf{n} \cdot \nabla \times \mathbf{n}}{2}, \quad (1.3)$$

$$((\mathbf{n} \cdot \nabla) \mathbf{n})^2, \quad (1.4)$$

$$|\Delta|^2 = \left(\frac{\nabla \cdot \mathbf{n}}{2} \right)^2 + \left(\frac{\mathbf{n} \cdot \nabla \times \mathbf{n}}{2} \right)^2 - \frac{1}{2} \nabla \cdot ((\nabla \cdot \mathbf{n}) \mathbf{n} - (\mathbf{n} \cdot \nabla) \mathbf{n}). \quad (1.5)$$

The first three of these are known as splay, twist and bend. The final one is related to a quantity known as saddle-splay. The first two, splay and twist can take both positive and negative values, whereas bend and $|\Delta|^2$ are non-negative. Technically this is because splay and twist correspond to sections of line bundles, which are one dimensional. Note that $\nabla \cdot \mathbf{n}$ is not invariant under $\mathbf{n} \rightarrow -\mathbf{n}$, so we can only look at $(\nabla \cdot \mathbf{n})^2$. This slight complication comes from the deficiency of the description in terms of \mathbf{n} , really one should use a tensor, such as $\mathbf{n} \otimes \mathbf{n}$, and examine irreducible representations of $\nabla(\mathbf{n} \otimes \mathbf{n})$, at which point one would only find $(\nabla \cdot \mathbf{n})^2$ as an allowed scalar. With these quantities we can construct an elastic free energy as a weighted sum of these allowed scalars

$$\begin{aligned} F = & \int A(\nabla \cdot \mathbf{n})^2 + B\mathbf{n} \cdot \nabla \times \mathbf{n} + C(\mathbf{n} \cdot \nabla \times \mathbf{n})^2 + D((\mathbf{n} \cdot \nabla) \mathbf{n})^2 \\ & + E \left(\left(\frac{\nabla \cdot \mathbf{n}}{2} \right)^2 + \left(\frac{\mathbf{n} \cdot \nabla \times \mathbf{n}}{2} \right)^2 - \frac{1}{2} \nabla \cdot ((\nabla \cdot \mathbf{n}) \mathbf{n} - (\mathbf{n} \cdot \nabla) \mathbf{n}) \right). \end{aligned} \quad (1.6)$$

These terms are typically combined to form the Frank free energy [1]

$$F = \int \frac{K_1}{2} (\nabla \cdot \mathbf{n})^2 + \frac{K_2}{2} (q_0 + \mathbf{n} \cdot \nabla \times \mathbf{n})^2 + \frac{K_3}{2} ((\mathbf{n} \cdot \nabla) \mathbf{n})^2 - \frac{K_{24}}{2} \nabla \cdot ((\nabla \cdot \mathbf{n}) \mathbf{n} - (\mathbf{n} \cdot \nabla) \mathbf{n}) \quad (1.7)$$

where the fourth term is now saddle-splay proper. There are a few points we will make about this equation. The first is that if $q_0 \neq 0$ then the free energy is chiral, and corresponds to a type of liquid crystal known as cholesteric that exhibits a particularly rich set of phenomena [10, 11], which will be explored in Chapter 4. The second point is that the saddle-splay term is a total divergence. This is because it corresponds to the ‘Gaussian curvature’ of the vector field, by which we mean that if \mathbf{n} defines a foliation, *i.e.* a system of layers, then the saddle-splay is the Gaussian curvature of the layers. As such it is subject to a variant of the Gauss-Bonnet formula and can be reduced to boundary information, something that will again be explored in Chapter 3. The final point we will make is that, as a consequence of (1.1), if one sets $A = C = D = E$ and $B = 0$ in (1.6), then the free energy density is proportional to $|\nabla \mathbf{n}|^2 = (\partial_i n_j)(\partial_i n_j)$; this is known as the one elastic constant approximation [12].

As a unit magnitude director, the Frank free energy is not capable of acting as an order parameter [13]. This is not only an issue in understanding phase transitions, but also in the study of defects, where the elastic energy diverges in many situations. To solve these issues one turns to the Q -tensor theory, commonly known as Landau-de Gennes theory [1]. Briefly, in this theory the order parameter is a traceless symmetric rank 2 tensor Q . This tensor has two independent invariants, $\text{Tr}(Q^2)$ and $\text{Tr}(Q^3)$, and a Landau theory can then be constructed as

$$F_{bulk} = A \text{Tr}(Q^2) + B \text{Tr}(Q^2) + C(\text{Tr}(Q^2))^2 \quad (1.8)$$

which indicates a first order transition to an ordered phase. An elastic energy

density can also be given as

$$F_{el} = \frac{L_1}{2}(\partial_a Q_{ab})^2 + \frac{L_2}{2}(\epsilon_{abc}\partial_b Q_c)^2. \quad (1.9)$$

This free energy has been shown to be remarkably effective when used as a basis for computer simulations, with a number of exotic structures correctly predicted *in silico* before later being realised experimentally [14, 15, 16]. Many of the simulation results shown in this thesis were achieved using a finite difference code using this free-energy.

Finally, of some relevance to this thesis is the correspondence between the Q tensor and director field descriptions. A generic Q tensor has three distinct eigenvectors, and so picks out a triad of directions (a so-called biaxial liquid crystal). However, typically, the free energy favours a uniaxial form with only one non-degenerate eigenvector. Indeed, experimentally uniaxial liquid crystals are observed and, in particular, the topology is that of uniaxial liquid crystals; the predicted distinctive topology of biaxial nematics has not been observed experimentally. This uniaxial Q tensor can be related to a director field as

$$Q_{ij} = s_1(n_i n_j - \frac{1}{3}\delta_{ij}). \quad (1.10)$$

As such, we will focus our efforts on understanding uniaxial liquid crystals, though those for which the Q tensor is not uniaxial will play an important role.

1.2 TOPOLOGICAL DEFECTS

Take a sample of nematic and place it between two cross-polarisers. Under an optical microscope you will observe a Schlieren texture, a beautiful pattern of light and dark brushes meeting at points [17]. An example is given in Figure 1.2. Remarkably for a macroscopic image, Figure 1.2 can be used to infer microscopic information about the local orientation of the nematic at each point in the sample [8, 19, 20]. Because the nematic is between cross-

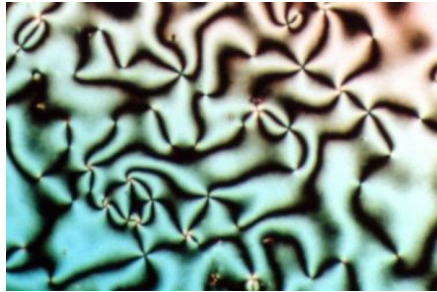


Figure 1.2: Schlieren texture obtained from a thin sample of nematic liquid crystal between cross-polarisers. The dark regions are where the local orientation of the nematic is aligned with either of the polarisers. The lightest regions are where the molecular orientation is at an angle of (approximately) $\pi/4$ to both polarisers. Reproduced from [18].

polarisers, no light will pass if it is aligned with either of the polarisers – these are the dark brushes. If, however, the nematic is oriented at an angle of approximately $\pi/4$ to either (and hence both) of the cross-polarisers, light will pass – these are the light brushes. What of the points where the brushes meet? At these points the transition from light to dark and back again is extremely fast, this indicates that the gradients of \mathbf{n} diverge and we find a singularity in the order, a topological defect. Of course, in reality $\nabla \mathbf{n}$ does not diverge, at the defect core the liquid crystal locally melts into the isotropic phase [1].

We can understand the nature of the defects purely by counting the brushes. There are two types of defects, those with two dark brushes and those with four. Since the nematic is thin, we can treat it as a two dimensional system with \mathbf{n} lying tangent to the plane. In the vicinity of a defect with two dark brushes, we must have that the director is vertical and horizontal (supposing that these are the two orientations of the polarisers) only once each and so the director must wind by π around the defect, whereas for the defects with four brushes the director must be vertical and horizontal twice, and so the director must wind by 2π around the defect. We can make this more formal as follows. Firstly, in the vicinity of the of a half strength defect a description in terms of a vector, $\mathbf{n} = (n_1, n_2)$, is no longer sufficient, and we must use an orientationless description. The simplest is the tensor $\mathbf{n} \otimes \mathbf{n}$ given (locally)

by

$$\mathbf{n} \otimes \mathbf{n} = \begin{pmatrix} n_1^2 & n_1 n_2 \\ n_1 n_2 & n_2^2 \end{pmatrix}, \quad (1.11)$$

which has \mathbf{n} as its only eigenvector with non-zero eigenvalue. Removing the isotropic part (corresponding to $(\text{Tr}(\mathbf{n} \otimes \mathbf{n})/2)\mathbb{I} = (1/2)\mathbb{I}$, since $n_1^2 + n_2^2 = 1$) we obtain the Q tensor

$$Q = \frac{1}{2} \begin{pmatrix} n_1^2 - n_2^2 & 2n_1 n_2 \\ 2n_1 n_2 & n_2^2 - n_1^2 \end{pmatrix}. \quad (1.12)$$

Since $(n_1^2 + n_2^2)^2 = (n_1^2 - n_2^2)^2 + (2n_1 n_2)^2 = 1$, we can rewrite this as

$$Q = \frac{1}{2} \begin{pmatrix} \cos \theta & \sin \theta \\ \sin \theta & -\cos \theta \end{pmatrix}, \quad (1.13)$$

where now $\mathbf{n} = (\cos \theta/2, \sin \theta/2)$. In this way we can describe the local orientation with the angle θ which is well-defined everywhere. Suppose one has a defect in a Schlieren texture then, in order to be well-defined, around that defect that angle θ must wind by $q2\pi$, $q \in \mathbb{Z}$, corresponding to the director field winding by an angle of $q\pi$. This integer q labels the charge of the defect, and example profiles are illustrated in Figure 1.3. Note that if q is odd then the director is non-orientable around the defect line. The existence of these non-orientable defects is a direct consequence of the non-orientability of the nematic order.

What happens if we bring together two defects of charge p and q ? Consider the function $f_\epsilon(z) = (z - \epsilon)^p(z + \epsilon)^q$, where $z = x + iy$ is the standard complex coordinate in the plane. We can then construct an associated Q by writing $\theta_\epsilon = \text{Arg}(f_\epsilon)$. For any non-zero value of ϵ , θ_ϵ has two singularities, one at $(\epsilon, 0)$ and one at $(-\epsilon, 0)$. From the form of f_ϵ one can see that the singularity at $(\epsilon, 0)$ will have winding p and the other winding q . In the limit $\epsilon \rightarrow 0$ the two singularities are brought together and we are left with $f_0 = z^{p+q}$, which

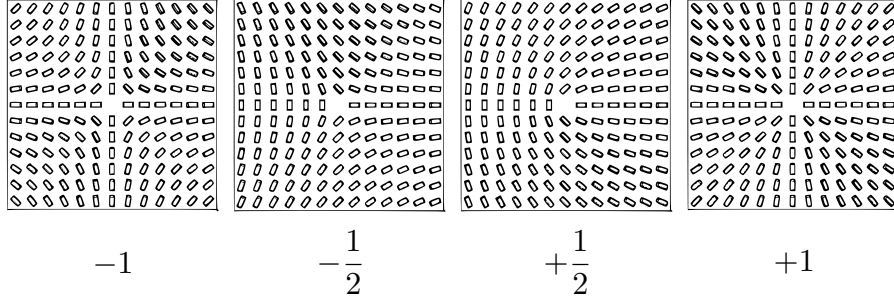


Figure 1.3: Defect profiles in two-dimensional nematics with $|q/2| \leq 1$. Note that if q is odd, then the defect is non-orientable.

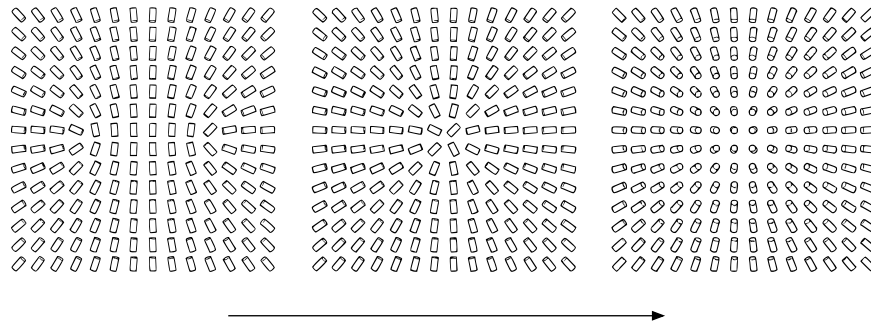


Figure 1.4: Escape in the third dimension. Two half strength defects are brought together, if the system is in two dimensions this is still a topological defect with winding +1. In three dimensions, however, the singularity can be removed by rotating the director to the vertical, as shown in the far right image. This process is an illustration of the fact that $\pi_1(\mathbb{RP}^2) \cong \mathbb{Z}_2$ and that $1 + 1 \equiv 0 \pmod{2}$.

contains a single singularity of winding $p + q$; bringing defects together adds their charges.

While the two dimensional case is instructive the most interesting phenomena are found in one dimension higher. In three dimensions the defects that were points in two dimensions become line defects, or disclinations (one can think of them as being extruded along the third axis). It is arguable that from a theoretical perspective these characteristic disclinations are the most interesting aspect of liquid crystalline order; indeed the term nematic comes from the Greek $\nu\epsilon\mu\alpha$, meaning thread, referring to the thread-like disclination lines observed in a three dimensional sample.

This move to three dimensions has profound consequences for the topo-

logical properties of the defects in the system. Singularities corresponding to an integer winding of n in two dimensions become removable in three dimensions. Perhaps the most famous example of this is the so-called ‘escape in the third dimension’ [21, 22, 23], illustrated in Figure 1.4, where a $+1$ winding profile is removed by rotating the director field towards the vertical as one approaches the singularity. Because a singularity with winding p can be split into two singularities with winding $q + r = p$ and since every half-integer is equal to $q + 1/2$, $q \in \mathbb{Z}$, this immediately means that not only are integer windings removable in three dimensions, but that all half-integer windings can be made equivalent. Not only this, but if we have two disclination lines, then they will each have half-integer profiles, which combine to create a removable integer profile, so disclination lines can self-annihilate. As well as disclination lines, three-dimensional nematic order also contains point defects. The most common of these is the so-called ‘hedgehog’, given by the radial texture $\mathbf{n} = \mathbf{e}_r$, found, for example, in nematic droplets [24].

1.3 THE HOMOTOPY THEORY OF DEFECTS

While the two-dimensional case is simple enough to understand on an intuitive basis, the more complex phenomena arising in three dimensions necessitate the development of a theoretical framework to give a precise description. Traditionally this has been supplied by the homotopy theory of defects [20, 25]. This theory studies configurations of an ordered material up to an equivalence relation of homotopy, that is \mathbf{n}_0 and \mathbf{n}_1 are held to be topologically equivalent if there is a one-parameter family of directors \mathbf{n}_t interpolating between them. The study of an individual defect in this scheme is done locally – defects are classified according to the topology of the director on an appropriate subset of the sample that either surrounds or encircles the defect. It is important to note that the homotopy theory of defects incorporates no information about the energetics. It is often the case that two topologically equivalent configurations are separated by a large energy

barrier and so may be considered as inequivalent configurations from an experimental perspective. Nevertheless, if the topological theory indicates a distinction between configurations, then the distinction is robust.

To give a flavour of the theory, we can study the two-dimensional case. Suppose one has a defect in a nematic at a point $p \in \mathbb{R}^2$. Consider an open neighbourhood $N(p)$, given by the set of points $\{x \in \mathbb{R}^2 : |x - p| < \epsilon\}$ for $\epsilon > 0$. Then locally we can treat \mathbf{n} as a director field defined on the set $D = N(p) - p$. If we give a local basis for tangent vectors, $\{\mathbf{e}_1, \mathbf{e}_2\}$, then at a point $a \in D$, \mathbf{n} describes an unoriented direction. The space of unoriented directions in two dimensions is the real projective line \mathbb{RP}^1 , given by identifying antipodal points on the circle. We can then extend $\{\mathbf{e}_1, \mathbf{e}_2\}$ to a basis over the entirety of D and regard \mathbf{n} as a map, $\mathbf{n} : D \rightarrow \mathbb{RP}^1$. The homotopy theory of defects then states that we should consider classes of maps up to the relation of homotopy, which we denote $[D, \mathbb{RP}^1]$. Now our domain is an open annulus, $D \cong S^1 \times (0, 1)$ and is homotopy equivalent to the circle S^1 , an operation which can be visualised by making the annulus progressively thinner. As such $[D, \mathbb{RP}^1] \cong [S^1, \mathbb{RP}^1]$.

From the previous discussion we already know the answer to this problem, $[S^1, \mathbb{RP}^1] \cong \mathbb{Z}$, the winding number. To calculate this from a homotopy theoretic perspective we first consider a restricted set of maps, where we fix the value of \mathbf{n} at a given point, known as the basepoint. The set of all maps from S^1 to any space X with a fixed basepoint has the structure of a group (the group operation is composition of maps), and is known as the fundamental or first homotopy group $\pi_1(X)$ [26]. The first step in the homotopy classification is therefore computing the fundamental group of X . In our case it is a standard result that $\pi_1(\mathbb{RP}^1) \cong \mathbb{Z}$. The final step is allowing the basepoint, previously held fixed, to vary. Doing this gives an equivalence between $a \in \pi_1(X)$ and bab^{-1} for any $b \in \pi_1(X)$, as indicated in Figure 1.5. In our case \mathbb{Z} is abelian so $bab^{-1} = a$, and we find that homotopy classes of point defects in two-dimensional nematics are given by the integers.

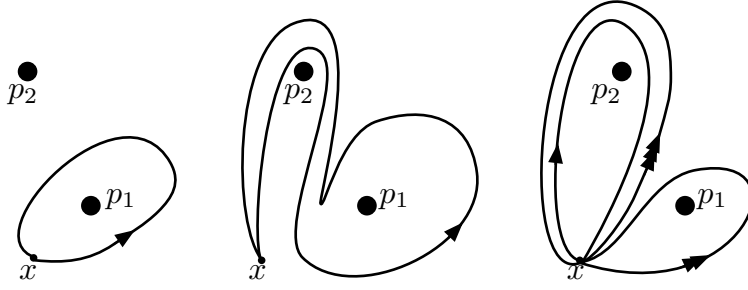


Figure 1.5: Changing the basepoint. Suppose the defects at p_1 and p_2 correspond to elements a and b respectively in $\pi_1(X)$, for an order parameter space X . By dragging the basepoint, x around p_2 a map corresponding to a is freely homotopic to bab^{-1} , for any $b \in \pi_1(X)$.

Now we need to generalise the procedure to other dimensions and systems. First we identify the order parameter space, X , for our system. We then examine homotopy classes of maps from the neighbourhood of a singularity into our order parameter space. In two dimensions the circle, S^1 , surrounded a point defect but in three dimensions it surrounds a line defect. By identical reasoning, point defects in three dimensions are given by studying maps from S^2 into the order parameter space. To do this we need to generalise the fundamental group to $\pi_n(X)$, denoting the group of homotopy classes of basepoint preserving maps from S^n to X . The topological type of point defects are then given by elements in $\pi_2(X)$, modulo an equivalence relation. This equivalence relation is similar to that in Figure 1.5, but instead of a simple conjugation of elements, $\pi_1(X)$ has a group action on all other homotopy groups, and it is this action that forms the equivalence relation. Finally, note that there is a relationship between the dimension of the surrounding sphere s , the defect r and the ambient space d , namely

$$s + r = d - 1$$

Before we use this theory to understand three-dimensional nematics, we note that for a space of dimension d , $\pi_d(X)$ (and its associated equivalence relation) can be used to understand topologically non-trivial non-singular states [27]. If one has a system described by a field $\phi(x) : \mathbb{R}^d \rightarrow X$ which

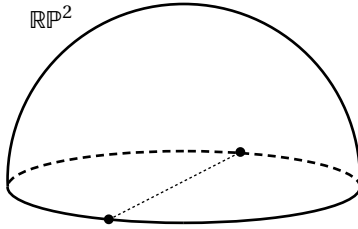


Figure 1.6: The real projective plane, \mathbb{RP}^2 , the order parameter space for nematics. It can be thought of as a hemisphere with antipodal points on the equator identified. The non-orientability of this space leads to the presence of line defects in nematics.

tends to a constant as $|x| \rightarrow \infty$, then the domain can be compactified to obtain a map $S^d \rightarrow X$, which can be classified with the homotopy theoretic techniques. A variety of topological solitons, such as baby Skyrmions and Hopf solitons can arise in this way.

Applying the theory to three dimensional nematics, the first challenge is to identify the order parameter space. Again we have a nematic described by a line field \mathbf{n} . At any point in space the possible lines are given by points in S^2 with antipodal points identified. This space is the real projective plane \mathbb{RP}^2 , and can be visualised as a hemisphere with antipodal points on the equator identified, as shown in Figure 1.6¹. The homotopy groups of this space are well known, and are given in Table 1.1, one finds that, as mentioned above, three dimensional nematics contain both point and line defects.

For line defects in three dimensional nematics, the appropriate homotopy group is $\pi_1(\mathbb{RP}^2)$, which is the two element group, \mathbb{Z}_2 . This is abelian and so describes the line defects in three dimensional nematics. The trivial element (0) represents a loop encircling no (or an even number of) defect(s) and the non-trivial element (1) represents a loop encircling an odd number of disclination lines. This simple classification (in fact it is the simplest possible classification of defects) reflects the fact that we uncovered earlier: there is only one local structure for disclination lines in nematics, and that they may mutually annihilate, as shown schematically in Figure 1.7.

¹Because it is a closed non-orientable surface, it does not embed in three dimensional space, and so any visual representation necessarily contains cuts or self-intersections.

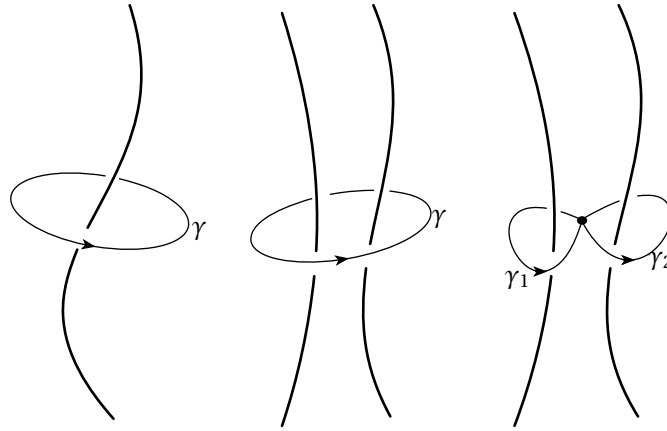


Figure 1.7: Combining line defects. Two line defects, of type a and b in $\pi_1(X)$ can combine to form a defect of type ab . In the case of disclinations in nematics, two line defects merging will always mutually annihilate, as $1 + 1 \equiv 0 \pmod{2}$.

Point defects are a little more complicated. As indicated by Table 1.1 the second homotopy group is given by $\pi_2(\mathbb{RP}^2) \cong \mathbb{Z}$. However, we need to take into account the action of π_1 on π_2 . In this case the action sends $x \rightarrow -x \in \mathbb{Z}$ and hence the classification of point defects is given by $\mathbb{Z}/(x \sim -x) \cong \mathbb{N}$, the natural numbers [20]. Essentially, because the nematic is unoriented one cannot distinguish between a point defect of type $\mathbf{n} = \mathbf{e}_r$ and $\mathbf{n} = -\mathbf{e}_r$. This raises potential issues. Suppose one has a system containing two point defects of type $p, q \in \mathbb{N}$. What happens when they are brought together? In the two dimensional case it is easy, the answer was $p + q$, but the three dimensional case is more complex. The answer may be $|p + q|$ or $|p - q|$. This ambiguity can only be solved by extending the homotopy theory to allow for global information, connecting the two defects, which is explored in Chapter 2.

1.4 THE GENERAL THEORY

In the 70's the theory of topological defects in ordered materials was put on a general footing within the paradigm of broken symmetry. The classic text in this field is the review article by Mermin [25], but we will give a recapitulation

	H	π_1	π_2	π_3
Ferromagnet	$SO(2)$	1	\mathbb{Z}	\mathbb{Z}
Nematic	$O(2)$	\mathbb{Z}_2	\mathbb{Z}	\mathbb{Z}
Frame Field	1	\mathbb{Z}_2	1	\mathbb{Z}
Biaxial	D_2	Q	1	\mathbb{Z}

Table 1.1: Homotopy groups for the quotient of $SO(3)$ by various symmetry subgroups, H . Q denotes the group generated by $\langle i, j \rangle$ under quaternionic multiplication.

since the ideas will play a role throughout this thesis.

One supposes that the system has some symmetry group G which is spontaneously broken in the ground state to a subgroup H . The canonical example and one which is relevant for us is ferromagnetism in three dimensions. The Hamiltonian of a ferromagnet is invariant under the action of $SO(3)$, corresponding to rotations of the system, the ground state of the system is a unit vector which breaks the $SO(3)$ symmetry and is only invariant under an $SO(2)$ subgroup of $SO(3)$ corresponding to rotations about the axis of the ferromagnetic order.

In this picture distinct ground states are labelled by elements in the quotient space G/H , which can be thought of as the order parameter space. The local description of topological defects is then given by homotopy classes of maps from measuring spheres into G/H . We will suffer through two trivial examples before discussing an interesting one, all are detailed in Table 1.1 and Figure 1.8. The first trivial example is the aforementioned case of the ferromagnet. Here we have an initial $SO(3)$ broken to an $SO(2)$ which preserves an oriented axis. The quotient space $SO(3)/SO(2)$ is S^2 , so the local topology of defects in ferromagnets is given by homotopy groups of S^2 . Nematics are similar, however the symmetry is broken to $O(2)$, since we need only preserve an unoriented axis. The quotient space $SO(3)/O(2)$ is the real projective plane, as discussed above, which leads to the presence of disclination lines.

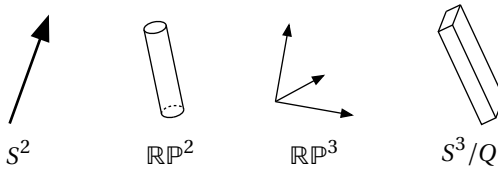


Figure 1.8: Visualisation of various types of order. From left to right: ferromagnetic order, described by a point in S^2 , can be viewed as a unit vector; nematic order, given by \mathbb{RP}^2 , can be visualised as a field of cylinders or lines; $SO(3)$ order can be viewed as a field of oriented triads and has $\mathbb{RP}^3 \cong SO(3)$ as an order parameter space; biaxial nematics, viewed as a brick invariant under π rotations about the principal axes, have the manifold S^3/Q as their order parameter space, where S^3 is viewed as the unit quaternions.

1.5 BIAXIAL NEMATICS

One of the most interesting applications of the homotopy theory of defects is to biaxial nematics. This example is well known as being one of the simplest to exhibit more elaborate topological phenomena [20, 28]. We discuss it because it is interesting and because one of the main focuses of this thesis, the topology of cholesterics, has previously been approximated as that of biaxial nematics [11]. In these materials the local order is given by three principal unoriented directions, e_1 , e_2 and e_3 . One can think of this as a brick, invariant under π rotations about each of the principal axes, as illustrated in Figure 1.8. More formally we identify the subgroup H of $SO(3)$ as consisting of rotations of π about each of the principal axes. So now we need to consider the order parameter space $SO(3)/H$. It is easier in this situation to use the $SU(2) \rightarrow SO(3)$ homomorphism and regard $SU(2)$ as the unit quaternions whence H becomes the subgroup $Q = (\pm 1, \pm i, \pm j, \pm k)$. As a manifold $SU(2) \cong S^3$ and so to understand line defects in biaxial nematics we are required to calculate $\pi_1(SU(2)/Q)$. Fortunately, there is a theorem [25, 26] that says if G is a simply connected Lie group (such as $SU(2)$) and H a discrete subgroup, then $\pi_1(G/H) \cong H$. Therefore $\pi_1(SU(2)/Q) \cong Q$. Of course, as discussed above, to get the full classification one must consider conjugacy classes of Q . There are 5 such classes, corresponding to $\{1\}$, $\{-1\}$, $\{i, -i\}$,

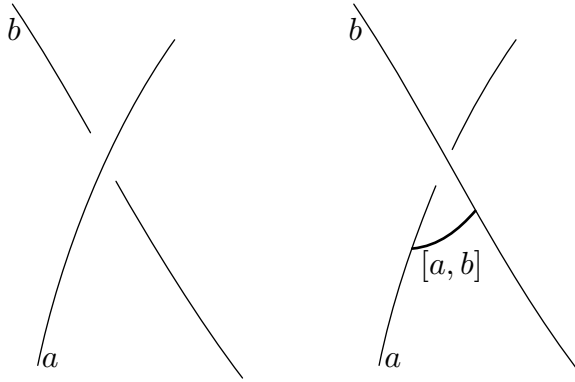


Figure 1.9: Crossing of defect lines. The attempted crossing of defect lines of types a and b will result in a tether of type $[a, b] = aba^{-1}b^{-1}$.

$\{j, -j\}, \{k, -k\}$. The first of these is the trivial element, corresponding to no defect. The last three correspond to singularities in each of the three principle directions. The second type, the $\{-1\}$, is associated to the fact that $SO(3)$ is not simply connected.

There are many subtleties coming from this formalism, we will highlight one which will be relevant to our discussion of cholesterics in Chapter 4. As observed by Poénaru and Toulouse [28], because Q is non-Abelian, defect lines may not necessarily be able to cross. If one has two line defects of type a and $b \in \pi_1(G/H)$, then their attempted crossing will result in a tether defect whose type is equivalent to the commutator $[a, b] = aba^{-1}b^{-1}$, as indicated in Figure 1.9. In biaxials, then, defects of type $\{i, -i\}$, $\{j, -j\}$ and $\{k, -k\}$ may not cross without leaving a tether of type -1 , e.g. $(i)(j)(-i)(-j) = k^2 = -1$. We will show in Chapter 4 that an entirely different theory can reproduce these rules.

CHAPTER 2

GLOBAL THEORY OF TOPOLOGICAL DEFECTS IN NEMATIC LIQUID CRYSTALS

In this chapter we will study the global properties of defects in nematic liquid crystals. The traditional method of classification involves studying a local neighbourhood of a defect, and looking for the possible topological classes of texture that may be obtained. We take a slightly different approach. We consider a nematic liquid crystal in a domain Ω . For example, Ω may be all of \mathbb{R}^3 . We exclude the defect set from Ω , so for example in the case of a single point defect at the origin, the domain is $\mathbb{R}^3 - \{0\}$, though our primary focus will be when the defect set is a knot or link. We then examine the topology of the nematic texture by considering homotopy classes of maps from the entire domain into \mathbb{RP}^2 . Unlike the standard local approach [20, 25] this global approach throws away no information and avoids the usual ambiguities involved in the interaction of defects in nematics. Previous work on the topology of linked defects in nematics [28, 29, 30, 31] has also not taken this global approach. We are not aware that the result is explicitly present in the maths literature. The analogous case of maps of a 3-complex into S^2 was solved completely by Pontryagin in the 1940s [32, 33] and extended by Thom in the 1950s [34]. This is described later in the chapter.

The main result of this chapter is the following. Let \mathbf{n} be a director field for a nematic liquid crystal in \mathbb{R}^3 with a defect set \mathcal{D} , we can split \mathcal{D} up as

$\mathcal{D} = \mathcal{P} \cup \mathcal{L}$ where \mathcal{P} is the set of point defects and \mathcal{L} is the set of line defects. Furthermore, $\mathcal{L} = \cup_i L_i$ where each of the L_i is a non-split knot or link. Then the topology of the texture \mathbf{n} is given by an element of the set

$$\left(\bigoplus_{p_i \in \mathcal{P}} \mathbb{Z} \right) \oplus \left(\bigoplus_{L_j \in \mathcal{L}} (\mathbb{Z} \oplus H_1(\Sigma(L_j))) \right) / \sim . \quad (2.1)$$

Where $H_1(\Sigma(L_j))$ is the first singular homology group of the branched double cover of S^3 over L_j and \sim is the equivalence relation $x \sim -x$. This formula can be given the following interpretation. Each point defect $p_i \in \mathcal{P}$ has a charge, given by an integer, \mathbb{Z} , this is the first factor. The second factor has two terms. Each split component $L_j \in \mathcal{L}$ has a charge, as if it were a point defect, which is the first factor of \mathbb{Z} . The second part relates to the internal topology of \mathbf{n} for each component. If one considers each link component as a knotted particle, then this data can be thought of as an ‘internal state’ associated to the knot or link. Aspects of this internal state can be interpreted as Skyrmion tubes, or in cholesterics λ lines, discussed in Chapters 3 and 4, entangling the knot or link. Finally, the equivalence relation comes about because of the global sign ambiguity for nematics – the calculations are done by temporarily orienting \mathbf{n} . An important point to note, which will be explored with the case of the Hopf link, is that any particular identification of homotopy classes of textures with elements in this set is not canonical, though one can always fix the class of a set of reference textures to avoid any ambiguity. In particular, any automorphism of the group (before taking the equivalence relation) in (2.17) by an element of order 2, gives a valid relabelling of the textures.

There have been a series of fascinating experiments in which such knotted defect lines have been created experimentally through the use of colloidal particles [4], knotted colloids [5] and toroidal droplets [6]. We hope that our work will help understand these experimental results. To give an example of such an applicable result, in §2.4 we show that there are two dis-

tinct textures associated to simply linked defect loops and in Chapter 6 we will show that certain representatives of these can be interpreted as having linking number ± 1 . Such linked defects can now be readily created in the laboratory, but it is not known, for a given system, which of the two types (if any) is easier to create.

Before we get to this result we must first build up the technical machinery in order to perform the calculation. Suppose now we have a nematic in three dimensions. We use the term three dimensions liberally, we suppose an arbitrary differentiable, oriented 3-manifold, we can choose a trivialisation of $T\Omega$ and then view \mathbf{n} as a map $\mathbf{n} : \Omega \rightarrow \mathbb{RP}^2$. We will not worry about classes of trivialisations, since our intended application is to nematics in real space, we are always supplied with a natural trivialisation coming from the Cartesian one. Our goal is to compute homotopy classes of maps from a Ω (or a subset thereof) into \mathbb{RP}^2 . These homotopy classes will represent the different topological classes of nematic texture on the domain. We should note also that we may take Ω to be a two dimensional subset of the domain, for example a torus enclosing a defect line so really the problem is ‘homotopy classes of maps from a two or three dimensional oriented manifold into \mathbb{RP}^2 .

As one may have surmised by this point, the main novelty in considering line fields rather than vector fields is that line fields may be non-orientable, you may not be able to put arrowheads on the sticks in a consistent manner. While this is the correct intuitive notion, we must make it precise in order to calculate with it. In fact, it turns out that a thorough understanding of the implications of non-orientability forms the bulk of the calculation presented in this chapter. So, let \mathbf{n} be a director field, considered as a map $\Omega \rightarrow \mathbb{RP}^2$. There is then an induced map on homology, $\mathbf{n}^* : H_1(\Omega) \rightarrow H_1(\mathbb{RP}^2)$, or

$$\mathbf{n}^* : H_1(\Omega) \rightarrow \mathbb{Z}_2. \quad (2.2)$$

This map measures whether \mathbf{n} reverses orientation along each homology cy-

cle in the domain. The texture is orientable if this map sends every cycle $\gamma \in H_1(\Omega)$ to $0 \in \mathbb{Z}_2$ and non-orientable if the map is surjective. Note that as a linear function from H_1 to \mathbb{Z}_2 , this can be thought of as an element of $H^1(\Omega, \mathbb{Z}_2)$. This element is the first Stiefel-Whitney class of the line bundle of vectors parallel to \mathbf{n} .

2.1 ORIENTABLE TEXTURES

Before we explore non-orientable textures we will examine those that are orientable. In this case the only difference between a nematic and a unit vector field is a global sign ambiguity of $\mathbf{n} \sim -\mathbf{n}$, the implications of which have been discussed at length in the literature [20]. Suppose now we are given an orientable texture, one can then lift it to a map $\hat{\mathbf{n}} : \Omega \rightarrow S^2$. The homotopy classes of orientable nematic textures on a domain are therefore simply given by classes of maps from Ω to S^2 , with the map corresponding to $\hat{\mathbf{n}}$ identified with the map corresponding to $-\hat{\mathbf{n}}$.

As a simple example consider Ω to be \mathbb{R}^3 minus the origin, as illustrated in Figure 2.1. This can be thought of as modelling the region surrounding a single point defect at the origin. Now $\mathbb{R}^3 - \{0\}$ is homotopy equivalent to S^2 , and so one simply has to compute classes of maps $[S^2, \mathbb{RP}^2]$. By the discussion above, these are given by classes of maps $[S^2, S^2]/ \sim \cong \mathbb{Z}/x \sim -x \cong \mathbb{N}$, as previously established. This tells you that the topology of this system is purely determined by the local topology (or ‘charge’) of the defect, there is no more structure.

Things become more interesting when one looks at more complicated domains. Take now Ω to be $\mathbb{R}^3 - \{p_1, p_2\}$ where $\{p_1, p_2\}$ are two distinct points, illustrated in Figure 2.2. This is now modelling the topology of a system consisting of two distinct point defects. This example illustrates a well-known difficulty [20] with liquid crystal topology, corresponding to the ‘addition of charges’ for point defects. If one takes only local information, then each of the two defects, located at p_1 and p_2 are assigned an integer

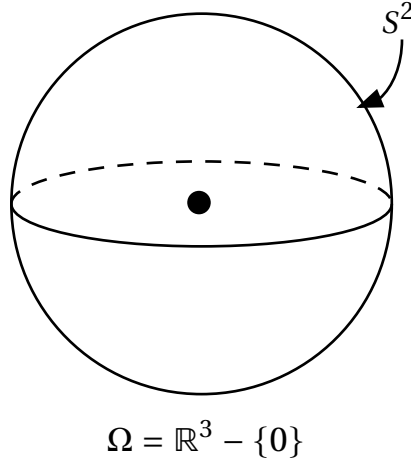


Figure 2.1: Domain corresponding to all of \mathbb{R}^3 minus a point at the origin. It is homotopy equivalent to a sphere; the topology of a nematic texture consisting of a single point defect is simply determined by the defect type.

$q_i \in \mathbb{N}$. The ambiguity arises when one considers the result of bringing the two defects together, which is either $|q_1 + q_2|$ or $|q_1 - q_2|$. The resolution involves incorporating global information about the texture that connects the two neighbourhoods of p_1 and p_2 . This can be, and has been, done in a number of ways. For example, one can consider a common basepoint for both local neighbourhoods or use the Pontryagin-Thom construction. With our method we take our domain to be $\mathbb{R}^3 - \{p_1, p_2\}$. This space deformation retracts to a wedge sum of spheres, $S^2 \vee S^2$. So now we must consider free homotopy classes of maps $[S^2 \vee S^2, \mathbb{RP}^2]$. It is true [26] that for pointed maps $[A \vee B, C]_* \cong [A, C]_* \times [B, C]_*$. Hence we know $[S^2 \vee S^2, S^2]_* \cong \mathbb{Z} \times \mathbb{Z}$. Now our goal, $[S^2 \vee S^2, \mathbb{RP}^2]$, is simply found by acting on $[S^2 \vee S^2, S^2]_*$ with the equivalence relation. So we have

$$[S^2 \vee S^2, \mathbb{RP}^2] \cong \mathbb{Z} \times \mathbb{Z}/(x_1, x_2) \sim -(x_1, x_2) \cong \mathbb{N} \times \mathbb{Z} \quad (2.3)$$

and therefore we find that including global information removes any ambiguity. The classes of maps are given by the set $\mathbb{N} \times \mathbb{Z}$, *i.e.* the ambiguity is a global sign ambiguity, we can fix the charge of the defect at, say, p_1 , but then all the charges relative to that defect are fixed, and so the absolute value of

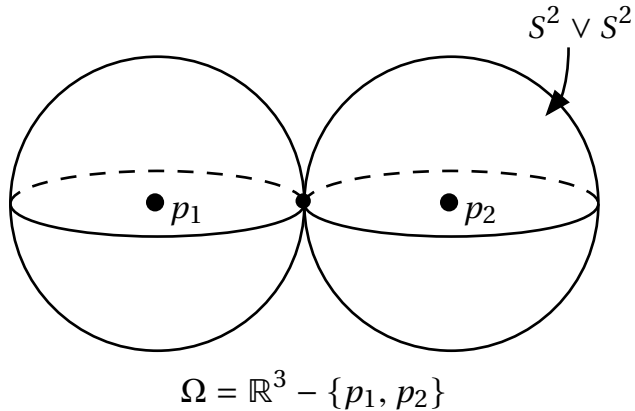


Figure 2.2: Domain corresponding to all of \mathbb{R}^3 except two points which one supposes to be point defects. The space is homotopy equivalent to the wedge sum of two spheres. The topology of the nematic in the surrounding area is given by free homotopy classes of maps from $S^2 \vee S^2$ to \mathbb{RP}^2 . The result is the set $\mathbb{N} \times \mathbb{Z}$. The factor of \mathbb{Z} says that if one assumes that the charge of the first defect is positive (given by \mathbb{N}), then the sign of the second can be either positive or negative, removing the ambiguity in adding the signs.

ponp

their sum is unambiguously defined.

2.2 NON-ORIENTABLE TEXTURES

We now turn to non-orientable textures. To do this we need to introduce two natural geometric objects associated to the map n^* . The first is a class of sets \mathcal{B} , which for a d dimensional domain is class of $d - 1$ dimensional sets relating the non-orientability of n to intersections of 1-cycles with \mathcal{B} . The second is a double cover of the domain $\widehat{\Omega}$. The idea is as follows: homotopy classes of maps to S^2 are computable through the work of Pontryagin [32, 33], so one would like to turn every problem into computing the classes of maps from some space into S^2 . In the case of a non-orientable nematic texture, to do this requires changing the domain, Ω , to a double cover. Once this has been done, we can define a map to S^2 on this double cover. Once we have this double cover we split it up into two pieces and consider maps on each piece. The topological relationship between these two pieces determines the way information about the texture can be moved between them. The re-

sult of this is a tool for the computation of the topological classes of nematic textures for any domain. The argument below is split into sections. The first defines the covering space we use. The second defines the sets \mathcal{B} associated to the map \mathbf{n}^* . The third is a short discussion of the Pontryagin-Thom construction and the fourth section makes use of these tools to show how to compute homotopy classes of nematic textures on a specific domain.

2.2.1 THE COVERING SPACE FOR A NEMATIC DOMAIN

We now construct the appropriate covering space for a given nematic texture in a particular domain, X . A covering space \tilde{X} for X is a space \tilde{X} equipped with a surjective projection operator $p : \tilde{X} \rightarrow X$ such that for every $x \in X$ there is an open neighbourhood U with $p^{-1}(U)$ a disjoint union of open sets homeomorphic to U . A double cover is a covering space for which $p^{-1}(x)$ corresponds to two distinct points in \tilde{X} , for any $x \in X$.

Connected covering spaces for a given space X are classified by conjugacy classes of subgroups of the fundamental group $\pi_1(X)$ [26]. Specifically, let \tilde{X} be a covering space. Then the projection map p , induces a map $p^* : \pi_1(\tilde{X}) \rightarrow \pi_1(X)$, and so $\pi_1(\tilde{X})$ is a subgroup of $\pi_1(X)$. Changing the base point corresponds to conjugating the subgroup by the projection of the path in \tilde{X} between the base points. The order of the covering is then the index of the subgroup inside $\pi_1(X)$.

So which covering space do we choose for our nematic domain Ω ? The purpose of our covering space is to allow us to orient \mathbf{n} . The obstruction to doing this is the induced map on homology $\mathbf{n}^* : H_1(\Omega) \rightarrow \mathbb{Z}_2$ being non-zero. The criterion for \mathbf{n} to be orientable on the covering space $\widehat{\Omega}$ is as follows. $H_1(\Omega)$ is the commutator subgroup of $\pi_1(\Omega)$. Thus, for a covering space, $\widehat{\Omega}$, there is an induced map $h \circ p : \pi_1(\widehat{\Omega}) \rightarrow H_1(\Omega)$, where h , the Hurewicz map, is equivalent to Abelianisation. This can then be composed with \mathbf{n}^* to form a map $\pi_1(\widehat{\Omega}) \rightarrow \mathbb{Z}_2$. \mathbf{n} is orientable on $\widehat{\Omega}$ if this map is trivial.

The idea is to construct the ‘smallest’ covering space on which \mathbf{n} is ori-

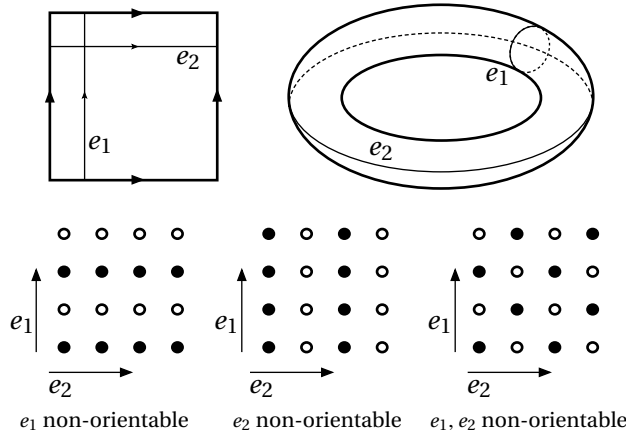


Figure 2.3: Nematic covering spaces when the domain is the torus. *Top left:* schematic of the torus as a square with opposite sides identified, with generators for $\pi_1(T^2)$ illustrated. *Top right:* as top left, but with the torus drawn as an embedding in \mathbb{R}^3 . *Bottom left:* subgroup of \mathbb{Z}^2 in the case that n is non-orientable along e_1 . \mathbb{Z}^2 is drawn as a lattice, filled in circles correspond to the elements that are part of the subgroup. Note that it is all group elements corresponding to cycles on the torus along which n is orientable. *Bottom middle & bottom left:* the same but for the other two cases. Note that in all cases the resulting covering space is another torus.

entable, corresponding to the subgroup consisting of all loops in $\pi_1(\Omega)$ which map to $0 \in \mathbb{Z}_2$. To do this, look at the kernel, K , of the homomorphism $n^* \circ h : \pi_1(\Omega) \rightarrow \mathbb{Z}_2$. Then it is an elementary result that K is a normal subgroup of $\pi_1(\Omega)$, and furthermore, since $n^* \circ h$ is non-trivial, the index of K must be 2. So $\widehat{\Omega}$ is constructed from the subgroup corresponding to the kernel of $n^* \circ h$.

As an example we will consider possible covering spaces when the domain is the torus, T^2 , show in Figure 2.3. We have $\pi_1(T^2) = \mathbb{Z}^2$, which is generated by two elements e_1, e_2 that correspond to a meridian and longitude of the torus respectively. Then there are three non-trivial possibilities:

1. e_1 is non-orientable under the map to \mathbb{Z}_2 and e_2 is orientable.
2. e_2 is non-orientable and e_1 is orientable.
3. Both e_1 and e_2 are non-orientable.

Our covering space corresponds to the subgroup of \mathbb{Z}^2 which is the kernel

of the map to \mathbb{Z}_2 . In case 1, this is the subgroup $\langle 2e_1, e_2 \rangle$. In case 2, it is the subgroup $\langle e_1, 2e_2 \rangle$ and in case 3 it is the subgroup $\langle e_1 + e_2, e_1 - e_2 \rangle$. In all these cases the resulting covering space $\widehat{\Omega}$ is once again a torus.

2.2.2 BRANCH SETS FOR A NEMATIC DOMAIN

Associated to each choice of map \mathbf{n}^* are a class of branch sets, which can be thought of as an analogue of the familiar branch cuts in complex analysis. These branch cuts will be central to furthering our discussion, so we develop them here. Suppose that our domain Ω has dimension d . Then there is an intersection pairing in homology

$$H_1(\Omega) \times H_{d-1}(\Omega, \partial\Omega) \rightarrow \mathbb{Z} \quad (2.4)$$

which, if one represents homology cycles as submanifolds, counts the intersection between the two submanifolds with sign. Choosing a particular class $[\mathcal{B}] \in H_{d-1}(\Omega, \partial\Omega)$ and reducing the final \mathbb{Z} modulo 2 creates a map $b_{[\mathcal{B}]} : H_1(\Omega) \rightarrow \mathbb{Z}_2$. Branch sets are then orientable sets \mathcal{B} for which $b_{[\mathcal{B}]} = \mathbf{n}^*$ as maps on homology.

This construction has a simple geometric interpretation. One constructs a set \mathcal{B} , which is a surface if Ω is three dimensional or a line if Ω is two dimensional, such that if γ is a loop along which \mathbf{n} is non-orientable, then γ must intersect \mathcal{B} an odd number of times. Examples of branch sets for a given domain are shown in Figure 2.4.

Note that if we lift the requirement that \mathcal{B} is orientable, then we could work in a theory with \mathbb{Z}_2 coefficients. While doing this is a more general approach, it gives the same answer, so we will not adopt it. As a point of interest, however, taking this approach leads to the definition of something similar to a Gordon-Litherland form rather than a Seifert matrix when considering knotted defect lines. In this non-orientable setting a canonical set of branch sets are given through the Pontryagin-Thom construction [8, 19]. Take a director field \mathbf{n} and pick a generic fixed direction, if one is in \mathbb{R}^3 then

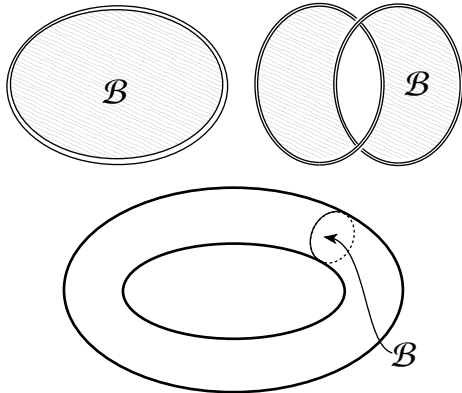


Figure 2.4: Examples of branching sets. *Top left:* The loop is a defect line around which \mathbf{n} is non-orientable. A branching set \mathcal{B} consists of the disk whose boundary is the defect. Note that because the domain has a boundary (the defect line), the set \mathcal{B} can be thought of as a cycle in relative homology. *Top right:* The same situation as the top left, only now the defect lines are linked. *Bottom:* the case where Ω is a torus. Here \mathbf{n} is non-orientable along the cycle e_2 from Figure 2.3, the branch set \mathcal{B} is homologous to e_1 .

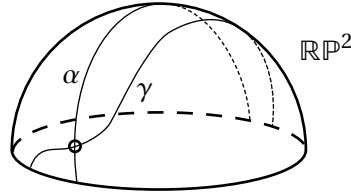


Figure 2.5: Two non trivial cycles α and γ on \mathbb{RP}^2 must intersect an odd number of times.

one may choose the vertical direction. Plot all points where \mathbf{n} points orthogonal to this direction, this defines a surface in the domain where \mathbf{n} is orthogonal to some direction. On S^2 the set of directions orthogonal to a given direction forms a great circle, which projects to a non-trivial cycle, α , in \mathbb{RP}^2 . Suppose now that γ is a loop along which \mathbf{n} is non-orientable. Then along γ \mathbf{n} must map to a non-contractible loop in \mathbb{RP}^2 . The image of γ on \mathbb{RP}^2 and the cycle α must intersect an odd number of times, illustrated in Figure 2.5, and so γ must pass through the surface an odd number of times, satisfying the requirement in the definition of \mathcal{B} .

Branch sets have a connection to the covering space $\widehat{\Omega}$ which will be es-

sential in what follows. Intuitively the idea is that the set \mathcal{B} can be thought of as a ‘portal’. Going through this portal takes you between the two sheets of $\widehat{\Omega}$. Formally, let \mathcal{B} be a branch set for a nematic domain Ω , with covering space $\widehat{\Omega}$ and projection p . Then the lift $\widehat{\mathcal{B}} = p^{-1}(\mathcal{B}) \subset \widehat{\Omega}$ has two components. Cutting $\widehat{\Omega}$ along $\widehat{\mathcal{B}}$ defines two submanifolds $\widehat{\Omega}_1$ and $\widehat{\Omega}_2$ such that $\widehat{\Omega}_1 \cup \widehat{\Omega}_2 = \widehat{\Omega}$ and $\widehat{\Omega}_1 \cap \widehat{\Omega}_2 = p^{-1}(\mathcal{B})$. Furthermore, for a given $x \in \Omega$, $p^{-1}(x)$ will be two points, one in $\widehat{\Omega}_1$ and one in $\widehat{\Omega}_2$ unless $x \in \mathcal{B}$ in which case $p^{-1}(x)$ will be two points in the intersection of $\widehat{\Omega}_1$ and $\widehat{\Omega}_2$.

The final part of this section will be to show that if \mathcal{B} is a branch set, then $\mathbf{n}|_{\mathcal{B}}$ is null-homotopic. $\mathbf{n}|_{\mathcal{B}}$ must be orientable. Suppose it wasn’t, then there would be a closed loop $\gamma \subset \mathcal{B}$ where $\mathbf{n}|_{\gamma}$ was a non-trivial map $S^1 \rightarrow \mathbb{RP}^2$. Now push γ off \mathcal{B} into Ω (we demanded \mathcal{B} was orientable). \mathbf{n} is non-orientable along this new loop γ' , but the loop does not intersect \mathcal{B} . But \mathcal{B} must intersect all loops along which \mathbf{n} is non-orientable, which is a contradiction and so $\mathbf{n}|_{\mathcal{B}}$ must be orientable.

If \mathcal{B} is one-dimensional, then we are done. Suppose \mathcal{B} is two-dimensional. Homotope \mathbf{n} such that $\mathbf{n}|_{\mathcal{B}}$ is constant except in a small neighbourhood, N , of some point $x \in \mathcal{B}$ such that $\mathbf{n}|_{\partial N(x)}$ is constant. By compactifying $N(x)$ to S^2 , the topology of $\mathbf{n}|_{\mathcal{B}}$ is fully determined by the topology of the resulting map $S^2 \rightarrow \mathbb{RP}^2$. Consider a loop γ along which \mathbf{n} is non-orientable and which intersects \mathcal{B} at x . Take a solid torus, $S^1 \times D^2$ whose restriction to \mathcal{B} is $N(x)$ and which contains γ running along the S^1 factor. The boundary of the solid torus is then $S^1 \times S^1$. Restricting the first factor to zero gives $0 \times S^1 = \partial N(x)$. Since $S^1 \times S^1$ can be seen as a one-parameter family of circles, \mathbf{n} on each $\theta \times S^1$ must be null-homotopic as \mathbf{n} on $\partial N(x)$ is constant. Homotope \mathbf{n} such that it is constant on each $\theta \times S^1 \subset \partial S^1 \times D^2$ and compactify to form a map $\tilde{\mathbf{n}} : S^1 \times S^2 \rightarrow \mathbb{RP}^2$. This operation is illustrated in Figure 2.6.

Now we need to study the map $\tilde{\mathbf{n}} : S^1 \times S^2 \rightarrow \mathbb{RP}^2$. Restricting it to a fixed $\theta \in S^1$ will give us a map $S^2 \rightarrow \mathbb{RP}^2$. The classification of this map, in

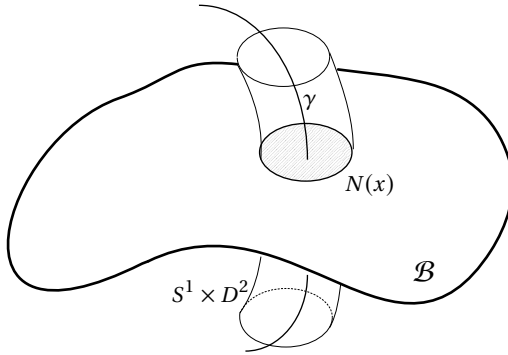


Figure 2.6: Showing that $n|_{\mathcal{B}}$ must be null-homotopic. All the data about $n|_{\mathcal{B}}$ is contained in the shaded neighbourhood of x , $N(x)$, with n constant on the boundary. γ is a cycle along which n is non-orientable, we extend $N(x)$ along a solid torus and examine n there.

terms of \mathbb{N} , will give us the topology of $n|_{\mathcal{B}}$ by the above discussion. Give a temporary orientation to \tilde{n} on $\theta \times S^2$. Then we have a map $m : S^2 \rightarrow S^2$ and it will be classified by an integer q . Now consider the continuous one-parameter family of maps $m_t : S^2 \rightarrow S^2$ given by restricting \tilde{n} to $\theta + t \times S^2$. But because we know by construction that \tilde{n} is non-orientable along the S^1 factor, $m_{2\pi} = -m$ and so the degree of $m_{2\pi}$ is $-q$, so we have constructed a continuous family of maps taking a degree q map to a degree $-q$ map. This is only possible if $q = 0$. Hence the map on $\theta \times S^2$ is null homotopic and so the restriction of n to \mathcal{B} is also null-homotopic.

2.2.3 THE PONTRYAGIN-THOM CONSTRUCTION FOR MAPS INTO S^2

The Pontryagin-Thom construction [34] for maps into S^2 provides a way to represent maps from a manifold M into S^2 as framed submanifolds of M , most of our discussion here follows Milnor [35] and tom Dieck [36]. We will first define a framed submanifold. Suppose U is a submanifold of Ω , then a framing of U is a map from each point $x \in U$ to a basis (v_1, v_2, \dots, v_s) of the normal bundle NU , the orthogonal complement of TU , given as $NU \oplus TU \cong T\Omega|_U$.

Now we define a cobordism between submanifolds. Two submanifolds

U and U' are cobordant in Ω if there is a submanifold $C \subset \Omega \times [0, 1]$ such that $\partial_C = U \sqcup \bar{U}'$, where \bar{U}' denotes orientation reversal. Furthermore we require that $C \cap \Omega \times 0 = U$ and $C \cap \Omega \times 1 = \bar{U}'$.

Finally, a framed cobordism between two framed submanifolds (U, fr) , (U', fr') is a cobordism C with a $(s + 1)$ dimensional framing for which the first s components agree with the framings of U and U' when restricted to $\Omega \times 0$ and $\Omega \times 1$ respectively.

The Pontryagin-Thom construction for maps to S^2 states that homotopy classes of maps $[\Omega, S^2]$ are in one to one correspondence with framed cobordism classes of $d - 2$ dimensional embedded submanifolds, where d is the dimension of Ω . We will also need the statement for manifolds with boundary. Suppose Ω is a manifold with boundary. Form its double, $D(\Omega)$ consisting of two copies of Ω glued via the identity map along the boundary. Then $D(\Omega)$ is a closed manifold and the Pontryagin-Thom construction applies. Finally, restricting one's viewpoint to just Ω , we see that homotopy classes of maps are given by cobordism classes of properly embedded framed submanifolds, where properly embedded implies that the boundary of the submanifold is in the boundary of Ω .

The final thing we need from the Pontryagin-Thom construction is the effect of the antipodal map. Suppose one has a map $v : M \rightarrow S^2$, represented as a framed submanifold (U, fr) . Construct a new map $v' : M \rightarrow S^2$ by composing v with the antipodal map A . Then what are the corresponding (U, fr) ? Since A is an orientation reversing bijection of S^2 , up to cobordism, the corresponding pair for v' must be $(U, -fr)$. Where by $-fr$ we mean the framing with the orientation reversed, which one can take as equal to fr but with v_1 sent to $-v_1$. This is illustrated in Figure 2.7.

2.2.4 EQUIVARIANT MAPS

Now that we have our machinery in place we can begin to study the topology of \mathbf{n} . Using $\hat{\Omega}$ we can lift \mathbf{n} to a map $\hat{\mathbf{n}}$ such that the following diagram

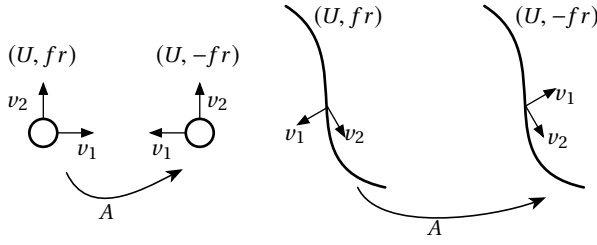


Figure 2.7: The effect on the Pontryagin-Thom representation of a map $\Omega \rightarrow S^2$ under the antipodal map A . The resulting submanifold is cobordant to the original, but the orientation of the framing is reversed (that is $v_1 \rightarrow -v_1$). Shown are examples for Ω being two and three dimensional.

commutes

$$\begin{array}{ccc} \widehat{\Omega} & \xrightarrow{\hat{\mathbf{n}}} & S^2 \\ \downarrow p_1 & & \downarrow p_2 \\ \Omega & \xrightarrow{\mathbf{n}} & \mathbb{RP}^2 \end{array} \quad (2.5)$$

where $p_1 : \widehat{\Omega} \rightarrow \Omega$ is the covering space projection for Ω and $p_2 : S^2 \rightarrow \mathbb{RP}^2$ is the projection for S^2 as a double cover of \mathbb{RP}^2 where $p_2^{-1}(x)$ gives two antipodal points on S^2 for any $x \in \mathbb{RP}^2$.

Now we have a map $\widehat{\Omega} \rightarrow S^2$ we can classify homotopy classes of maps.

There are some restrictions. Because (2.5) must be satisfied we require

$$\hat{\mathbf{n}}(x) = -\hat{\mathbf{n}}(t(x)) \quad (2.6)$$

where $t, t^2 = 1$, is the deck transformation for the covering space $\widehat{\Omega}$ that simply permutes the sheets of the cover. We will denote such maps as equivariant. So we must classify equivariant maps up to equivariant homotopy. Note that the orientable case also fits into this picture, except that one takes $\widehat{\Omega}$ to be the trivial double cover consisting of two disjoint copies of Ω .

The idea is to use our branch sets, these separate our covering space $\widehat{\Omega}$ into two pieces, each of which looks like Ω cut along the branch set. We look at maps restricted to one of the pieces, then study the result of ‘pushing’ the map through the branch set. This then induces an equivalence relation on maps defined on each piece which we exploit to characterise the maps.

Let \mathcal{B} be a branch set for Ω . Then $p_1^{-1}(\mathcal{B})$ separates $\widehat{\Omega}$ into $\widehat{\Omega}_1$ and $\widehat{\Omega}_2$.

Each of these two spaces look like Ω cut along \mathcal{B} . By the Pontryagin-Thom construction, homotopy classes of maps $\widehat{\Omega} \rightarrow S^2$ will be given by cobordism classes of properly embedded $d-2$ dimensional framed submanifolds. Suppose we have such a submanifold (U, fr) . Because $\mathbf{n}|_{\mathcal{B}}$ is null-homotopic, we can assume that $U \cap p_1^{-1}(\mathcal{B})$ is empty. This means we can split (U, fr) into two pieces, (U_1, fr_1) and (U_2, fr_2) , which are contained in $\widehat{\Omega}_1$ and $\widehat{\Omega}_2$ respectively. Now, because $\hat{\mathbf{n}}$ is equivariant, we know that up to cobordism $t((U_2, fr_2)) = (U_1, -fr_1)$, where t is the deck transformation, since the antipodal map reverses the orientation of the framing, that is (U_1, fr_1) completely determines (U_2, fr_2) .

Now we consider equivariant homotopies, illustrated in Figure 2.8. Suppose we have our pair of framed submanifolds, (U_1, fr_1) and (U_2, fr_2) , we can push (U_1, fr_1) through $p_1^{-1}(\mathcal{B})$ into $\widehat{\Omega}_2$ with equivariance demanding we also push (U_2, fr_2) from $\widehat{\Omega}_2$ into $\widehat{\Omega}_1$. There is thus an equivalence between (U_1, fr_1) and $T(U_2, fr_2)$, where T denotes the map induced by the homotopy. Now because $\widehat{\Omega}_1$ and $\widehat{\Omega}_2$ are homeomorphic to Ω cut along \mathcal{B} , the map T can be viewed as the composite operation of pushing (U_1, fr_1) through \mathcal{B} and then reversing the orientation of the framing. It is clear that all equivariant homotopies can be viewed this way.

Therefore, we can calculate homotopy classes of nematic textures in a domain Ω as follows. Let \mathcal{B} be a branch set for \mathbf{n} and Ω . Let C_{fr} be the space of framed cobordism classes of properly embedded submanifolds of dimension $d-2$ in $\Omega - \mathcal{B}$. Then the homotopy classes of textures for a given branch set \mathcal{B} is given as C_{fr}/\sim where \sim is the equivalence relation given by $(U, fr) \sim T(U, fr)$, with T the action of pushing (U, fr) through \mathcal{B} and then reversing the orientation of the framing. The final thing to do is, given this set of maps, quotient out by the equivalence relation that $\hat{\mathbf{n}}$ and $-\hat{\mathbf{n}}$ represent the same map.

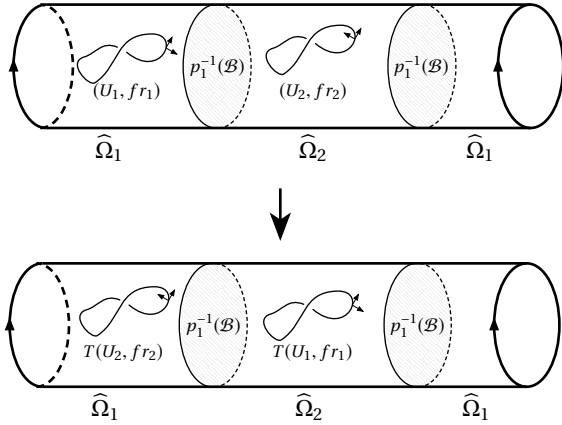


Figure 2.8: Schematic illustration of equivariant homotopy. The framed submanifold, (U_1, fr_1) in $\widehat{\Omega}_1$ is pushed through $p_1^{-1}(\mathcal{B})$, with the corresponding action taken on (U_2, fr_2) . The result is an equivalence relation between framed submanifolds.

2.3 NEMATIC TEXTURES ON TORI

With our tools in place we will perform some example computations where the domain Ω is a torus. These examples have physical relevance. The case $\Omega = T^2$ is a classical calculation in the topology of liquid crystals [30, 37, 20, 19] and is used to model the boundary of a local neighbourhood of a defect loop in three dimensional space. The case of $\Omega = T^3$ can be used to understand triply periodic, non-singular nematic textures. We should point out that we cannot find the discussion of the case $\Omega = T^3$ in the literature.

2.3.1 TEXTURES ON T^2

Suppose we have a map $\mathbf{n} : T^2 \rightarrow \mathbb{RP}^2$. As mentioned above, physically one can think of this as the boundary of a tubular neighbourhood of a line in a three dimensional sample. If \mathbf{n} is orientable on Ω then we can lift to a map $\tilde{\mathbf{n}} : T^2 \rightarrow S^2$. This map is characterised by its degree, and thus by the integers. Taking into account the ambiguity in the lift, these maps are characterised by the natural numbers \mathbb{N} . Physically one can think of this as a point defect of type $q \in \mathbb{N}$ sitting inside the torus.

Now we consider tori on which \mathbf{n} is not orientable. As mentioned in §2.2.1 there are three possibilities. If e_1 and e_2 correspond to a meridian and longitude of T^2 , then \mathbf{n} can be non-orientable along either e_1 , e_2 or both, and the classification in all three cases is identical. We will focus on the case where \mathbf{n} is non-orientable along e_1 , illustrated in Figure 2.9. In this case a branch set \mathcal{B} can be given as a representative of e_2 . Now since T^2 is two-dimensional, we should look at framed zero dimensional submanifolds, or points. Since these are points, there are only two possible framings: positive or negative. It is elementary to show that a framed cobordism from two points to the empty set exists only if they have the opposite framing. Since the submanifolds are points, the action of pushing them through \mathcal{B} is trivial, and one just reverses the orientation. Thus one can reduce the number of framed points modulo two. The global ambiguity $\hat{\mathbf{n}} \rightarrow -\hat{\mathbf{n}}$ leaves this count invariant. Therefore the classification of nematic textures with \mathbf{n} non-orientable along e_1 is given by \mathbb{Z}_2 , counting the number of framed points mod two. Note that the \mathbb{Z}_2 answer would not depend on which of the three combinations of cycles we chose to be non-orientable. Finally we note that this immediately extends to any closed genus g surface. If \mathbf{n} is a map from a closed orientable genus g surface and \mathbf{n} is non-orientable along any cycle, then the homotopy class of maps with this non-orientability is given by \mathbb{Z}_2 . We note that the visual presentation of this calculation is similar to the use of the Pontryagin-Thom construction for maps into \mathbb{RP}^2 given by Chen [19].

THE RELATIONSHIP WITH JÄNICH'S INDEX

In his paper ‘Topological Properties of Ordinary Nematics in 3-Space’ Jänich [30] introduced an index $\nu \in \mathbb{Z}_4$ used to characterise the tubular neighbourhood of a defect line. This index has been used by several authors to understand the topology of defect lines [31, 20]. We will show how this index relates to the homotopy classification of maps we have constructed. Suppose one has a defect loop in \mathbb{R}^3 . Consider \mathbf{n} restricted to the boundary of a tubular neigh-

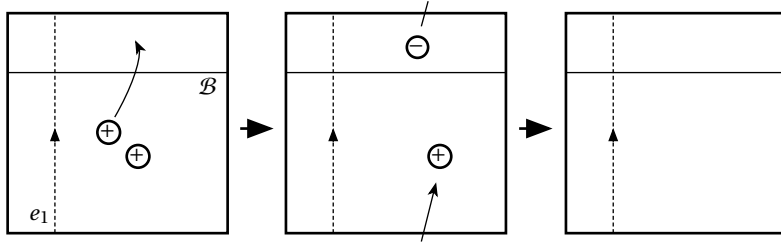


Figure 2.9: Equivariant homotopies and nematic textures on T^2 . n is non-orientable along e_1 . A branch set, \mathcal{B} , can be taken to be a representative of e_2 . Since the framed submanifolds are just framed points, pushing them through \mathcal{B} simply reverses the framing. Since there is a framed cobordism from a positively framed and negatively framed point to the empty set, the classification of nematic textures on T^2 with n non-orientable along e_1 is given by \mathbb{Z}_2 , counting the number of framed points without sign mod two.

bourhood of the defect line. This will give a map $T^2 \rightarrow \mathbb{RP}^2$ that is non-orientable along the meridian. So we need to classify homotopy classes of maps $n : T^2 \rightarrow \mathbb{RP}^2$ that are non-orientable along the meridian. The first step is determining the orientability of the map. The map is non-orientable along the meridian, and it may or may not be non-orientable along the longitude. Let $\mu_1 \in \mathbb{Z}_2$ denote whether or not n is non-orientable along the longitude. In each case there is a further index $\mu_2 \in \mathbb{Z}_2$, as illustrated above, that counts the mod 2 reduction of the number of framed 0-dimensional submanifolds representing n . Hence the topological classes of maps is given by an element in the set $\mu = \mu_1 \times \mu_2 = \mathbb{Z}_2 \times \mathbb{Z}_2 \cong \mathbb{Z}_4$, where the last isomorphism is one of sets (there is no group structure on the maps), this, up to an automorphism of \mathbb{Z}_4 is exactly Jänich's index. Finally we should give the physical interpretation of this index, where we follow Alexander *et al.* [20]. The first factor, saying whether n is non-orientable along the longitude of T^2 counts, modulo two, the number of defect lines linking the one inside the torus. The second index is more subtle. It can be thought of as counting, modulo two, the number of point defects inside the T^2 neighbourhood.

2.3.2 TEXTURES ON T^3

We now turn our attention to the three-dimensional torus, $T^3 \cong S^1 \times S^1 \times S^1$, and consider homotopy classes of maps $\mathbf{n} : T^3 \rightarrow \mathbb{RP}^2$. The case of \mathbf{n} orientable was solved by Pontryagin [32, 33] (see the papers by de Turck *et al.* [38, 39] for a comprehensive discussion of this classification). The classification states that the homotopy classes of maps are given by three integers (p, q, r) and a third invariant $\lambda \in \mathbb{Z}_d$ where $d = 2\text{gcd}(p, q, r)$. Understanding the details of this classification will prove useful in going forward. To this we, once again, turn to the Pontryagin-Thom construction. Because our domain is now three dimensional, the Pontryagin-Thom representation of the map will be in terms of cobordism classes of one-dimensional framed submanifolds, or framed links in T^3 . The framing is an ordered choice (v_1, v_2) of local normal vectors to the link. It thus induces an orientation on the link components¹. The integers (p, q, r) represent a homology class in $H_1(T^3)$ with a basis coming from the factorisation $T^3 = (S^1)^3$. The final invariant λ is given by the twisting of the framing along these lines – this twisting is related to the Hopf invariant of maps $S^3 \rightarrow S^2$. The contribution of a right handed twist to λ is +1. Note that under the antipodal map the framing reverses the orientation of the link component and the direction of the twist rotation, leaving the contribution to λ unchanged. Following de Turck *et al.* [38, 39], it is possible to put the framed submanifolds (U, fr) for maps $T^3 \rightarrow S^2$ into standard position, shown in Figure 2.10.

So, incorporating the ambiguity of sign in \mathbf{n} , we find that for orientable maps $\mathbf{n} : T^3 \rightarrow \mathbb{RP}^2$ the homotopy classification is given by $(p, q, r) \in \mathbb{Z}^3 / (x \sim -x)$ and $\lambda \in \mathbb{Z}_{2\text{gcd}(p, q, r)}$. Now we turn to the case where \mathbf{n} is non-orientable. As in the case of maps $T^2 \rightarrow \mathbb{RP}^2$, we have to specify along which homology cycles \mathbf{n} is non-orientable. Following the conventions of Figure 2.10 we will suppose that \mathbf{n} is non-orientable along e_3 . All other cases (there are $2^3 - 1$ in total) give an equivalent result. To understand these non-orientable maps

¹Just use the right-hand rule!

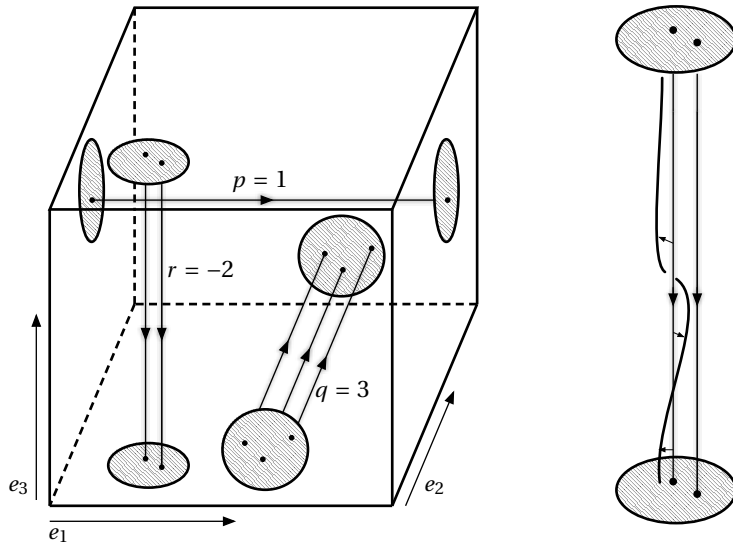


Figure 2.10: *Left:* a framed link in standard position on T^3 . There are three sets of lines, along e_1 , e_2 and e_3 . The framing of each link gives it an orientation and the integers (p, q, r) simply count the number of link components along each cycle. *Right:* The extra invariant $\lambda \in \mathbb{Z}_d$, $d = 2\text{gcd}(p, q, r)$ counts the twists in the framing. A right handed twist contributes $+1$ to λ . Note that under the antipodal map the framing reverses the orientation of the link component and the direction of the twist rotation, leaving the contribution to λ unchanged.

it is most convenient to look at the lifted map $\hat{\mathbf{n}} : \widehat{T^3} \rightarrow S^2$. In the case we are considering, with \mathbf{n} non-orientable along e_3 , this covering space can be viewed as a new torus formed by stacking two copies of the original domain on top of each other, separated by a branch set $p_1^{-1}(\mathcal{B})$. So now we have a map $\hat{\mathbf{n}} : T^3 \rightarrow S^2$. But we already know about the topology of these maps. First we shall examine the possible values of (p, q, r) . Since $\mathbf{n}|_{\mathcal{B}}$ is null-homotopic we know that $r = 0$. Furthermore, since $\hat{\mathbf{n}}$ is equivariant and the effect of the antipodal map is to reverse orientation of the links, we know that the contribution to (p, q) from $\widehat{\Omega}_1$ must be equal and opposite to that of $\widehat{\Omega}_2$ and hence $(p, q, r) = (0, 0, 0)$. Next we look at the invariant λ . Since $(p, q, r) = (0, 0, 0)$ it is defined on the full integers. As the antipodal map acts trivially on the twists in framings we know that the contribution to λ from $\widehat{\Omega}_1$ must be equal to that of $\widehat{\Omega}_2$, and so $\lambda \in 2\mathbb{Z}$.

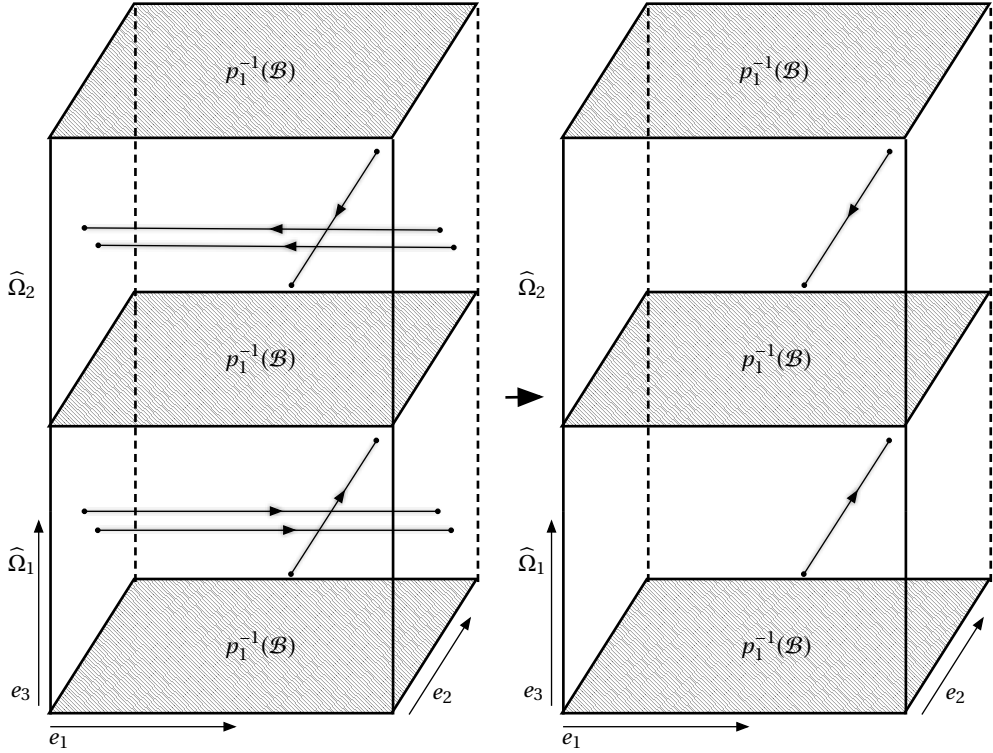


Figure 2.11: Equivariant homotopy on the double cover of the torus. One of the two cycles along e_1 in each of $\hat{\Omega}_1$ and $\hat{\Omega}_2$ can be pushed through $p_1^{-1}(\mathcal{B})$ and annihilated, giving a mod 2 reduction. The single pair along e_2 cannot be removed, since any attempt to push one through $p_1^{-1}(\mathcal{B})$, by equivariance, requires the same of the other, and so simply results in an orientation reversal.

Finally we have to look at the effect of equivariant homotopies. This is illustrated in Figure 2.11, the story is the same as that for T^2 . Cycles along either e_1 or e_2 can be reduced equivariantly modulo two. What of the the λ invariant? As shown in Figure 2.12, any twist in the framing can be pulled off a link to form a twisted loop. The effect on this loop of being pushed through $p_1^{-1}(\mathcal{B})$ is trivial and so we see that equivariant homotopies do not affect λ^2 . Finally we note that the action of $\hat{n} \rightarrow -\hat{n}$ is trivial on both the λ invariant and the \mathbb{Z}_2 invariants to obtain the result that, given a choice of non-orientable cycles for a nematic texture on T^3 , the possible topological classes of texture are given by an element of the set $\mathbb{Z}_2 \times \mathbb{Z}_2 \times \mathbb{Z}$.

²For an exceedingly thorough discussion of various cobordism moves, the reader is once again invited to consult the paper of De Turck *et al.* [38, 39].

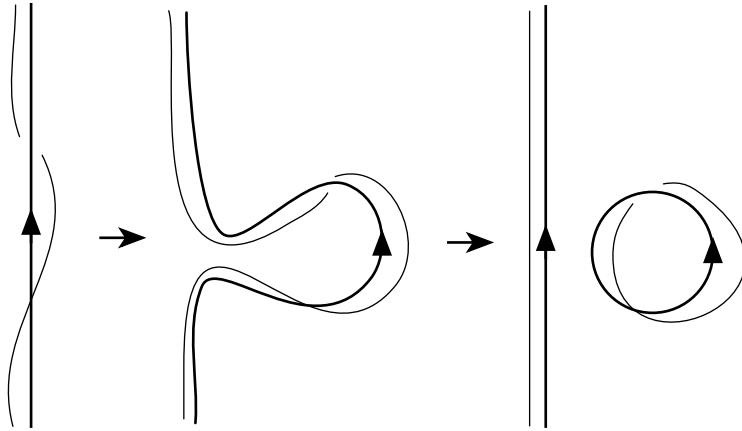


Figure 2.12: Pulling a twist off a link to form a twisted circle.

This gives a classification of non-singular triply periodic nematic textures. It is interesting to note that the factor of \mathbb{Z} corresponding to the Pontryagin invariant is free to be any integer, whereas in the case when the texture is orientable it is defined only modulo $2\text{gcd}(p, q, r)$. A natural mathematical question to ask at this point is whether this phenomenon is general, that is: is the Pontryagin invariant for a map from a closed 3-manifold to \mathbb{RP}^2 always a full integer. It is likely that this question has a fairly easy solution within reach of the methods above, but we leave it to the reader.

2.4 KNOTTED LINE DEFECTS

We now come to the central calculation of this chapter, that of the number – up to smooth deformation – of nematic textures surrounding a given set of line defects. We will be precise in our formulation of this problem. We will consider a nematic texture in \mathbb{R}^3 with a prescribed set of line defects and no other singularities. Furthermore, we will assume that $\lim_{|x| \rightarrow \infty} \mathbf{n}(x) = \mathbf{n}_0$, a constant – we will relax this assumption later. Given this setup, we ask for the number of distinct nematic textures with this defect set. Our assumption that \mathbf{n} is uniform at infinity allows us to compactify the domain and consider maps $\mathbf{n} : S^3 - N(L) \rightarrow \mathbb{RP}^2$, where $N(L)$ is a small neighbourhood of the

defect lines. This is done for technical reasons, to ensure the boundary is two dimensional, but it is also a physical assumption – defect lines typically have a thickness of order 10^{-8}m [1], which is certainly not 0.

While in the calculation of textures on the torus we chose which cycles were non-orientable under n^* , in this case our choice is made for us: the texture is non-orientable around the defect lines. To be precise the first homology group of a link complement, $S^3 - L$, is given as $H_1(S^3 - L) = \mathbb{Z}^{|L|}$, where $|L|$ is the number of components of the link. We demand that the map $n^* : H_1(S^3 - L) \rightarrow \mathbb{Z}_2$ sends each generator to the generator of \mathbb{Z}_2 , in other words each link component represents a defect line. Before we do the calculation proper we will consider two toy cases: that of a simple circle (the ‘unknot’) and the case of two linked rings (the Hopf link) and solve them with different methods, before we turn to the general case.

The case of the unknot is simple. Let U be an unknot, then the complement $S^3 - U$ deformation retracts to S^1 . Then the question is simply reduced to studying maps $S^1 \rightarrow \mathbb{RP}^2$, these are indexed by \mathbb{Z}_2 , simply whether the texture is orientable or not. But we already know, by assumption, that the texture is non-orientable, so there is no more freedom left and we find that there is a unique nematic texture associated to the complement of an unknotted defect in the 3-sphere³. One might be tempted to ask at this point about the relationship to Jänich’s \mathbb{Z}_4 index, and how this relates to the statement that there is only one type of unknotted defect. The answer is that any of Jänich’s indices other than 0 imply the existence of other defects in the system.

Consider now the Hopf link. The complement of the Hopf link in S^3 is fibered over S^1 with fibre a genus zero surface with two boundary components. This fibre deformation retracts onto a circle, so the complement of the Hopf link deformation retracts to the product of two circles, or the two-torus T^2 . Hence the number of nematic textures in the complement of a

³To save time we will be sloppy and often say ‘there is a unique unknot’ or similar when we are really talking about classes of maps.

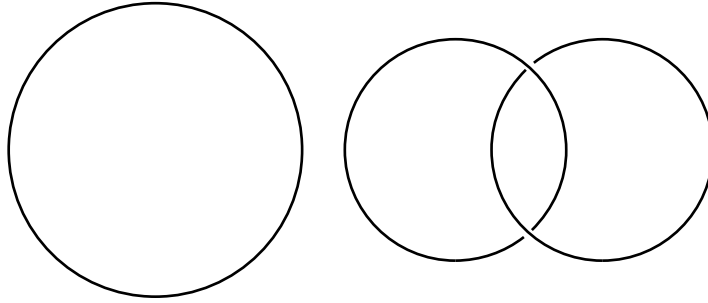


Figure 2.13: *Left*: An unknot, there is a unique nematic texture on the complement if the unknot is a defect. *Right*: A Hopf link, assuming that the lines are defects the complement of this link supports two distinct nematic textures.

Hopf link is equivalent to the number of nematic textures on a torus which are non-orientable along both e_1 and e_2 , which is just two. As we will see, these two different textures on the Hopf link can be interpreted as having linking number plus or minus one.

We now study the general case using the methods we have developed. First consider a branching set \mathcal{B} for a system containing line defects. From the original definition (2.4) of branch sets in terms of intersection forms we know that \mathcal{B} is a representative of a relative homology class in $H_2(S^3 - N(L), \partial N(L))$, where $N(L)$ is a neighbourhood of the link. Since relative homology cycles of low dimension can be represented as properly embedded submanifolds, \mathcal{B} is therefore an orientable surface whose boundary is L , which is nothing more than a Seifert surface for the link L . Seifert surfaces are a fundamental tool in the study of knot theory, and it is no accident that they show up here. Examples of Seifert surfaces are shown in the Figure 2.14. Now that we have our branch set, what of the covering space? It turns out that the covering spaces here are well-known and termed the double cyclic cover for the link complement [40].

Now we have the pieces in place, we should apply our method. The first point to note is that since our domains all have boundary, any twists in the framing of submanifolds can be pushed into the boundary⁴. The only thing

⁴An alternative statement is that the complement of a link deformation retracts onto a 2-complex.

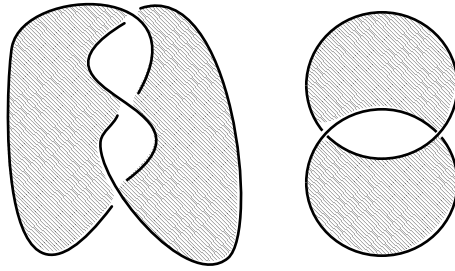


Figure 2.14: Examples of Seifert surfaces for the trefoil knot and the Hopf link. These serve as branch sets \mathcal{B} if the lines are thought of as defects.

that is preserved is the orientation induced by the framing. Hence in this case we need only consider regular cobordism classes of oriented links. But these are just given by the relative first homology group of the domain. So in the first instance we need to examine $H_1(S^3 - N(L) - \mathcal{B}, \partial N(L) - \mathcal{B})$. Since $\partial\mathcal{B} = L$ it is clear that this group can be replaced by $H_1(S^3 - \mathcal{B}, \partial\mathcal{B})$ by collapsing $N(L)$ onto L . We start with a piece of the long exact sequence for relative homology, namely

$$H_1(\partial\mathcal{B}) \longrightarrow H_1(S^3 - \mathcal{B}) \longrightarrow H_1(S^3 - \mathcal{B}, \partial\mathcal{B}) \longrightarrow H_0(\partial\mathcal{B}) \longrightarrow H_0(S^3 - \mathcal{B}) \quad (2.7)$$

which, by elementary computations, gives

$$\mathbb{Z}^{|L|} \longrightarrow \mathbb{Z}^{2g+|L|-1} \longrightarrow H_1(S^3 - \mathcal{B}, \partial\mathcal{B}) \longrightarrow \mathbb{Z}^{|L|} \longrightarrow \mathbb{Z} \quad (2.8)$$

From this sequence it is clear that a potentially over-complete set of generators for $H_1(S^3 - \mathcal{B}, \partial\mathcal{B})$ is given by $\{c_i\} \cup \{a_i\}$, where the $\{c_i\}$ are a set of generators for $H_1(S^3 - \mathcal{B})$ and the $\{a_i\}$, $i \in \mathbb{Z}_{|L|-1}$, are represented as tethers connecting the various link components, as illustrated in Figure 2.15. The $\{c_i\}$ are chosen so that, in relation to a basis $\{b_i\}$ for $H_1(\mathcal{B})$, $\text{Lk}(b_i, c_j) = \delta_{ij}$.

Now that we have a list of generators, we need to understand relationships between them. There are three such sets of relationships, which we

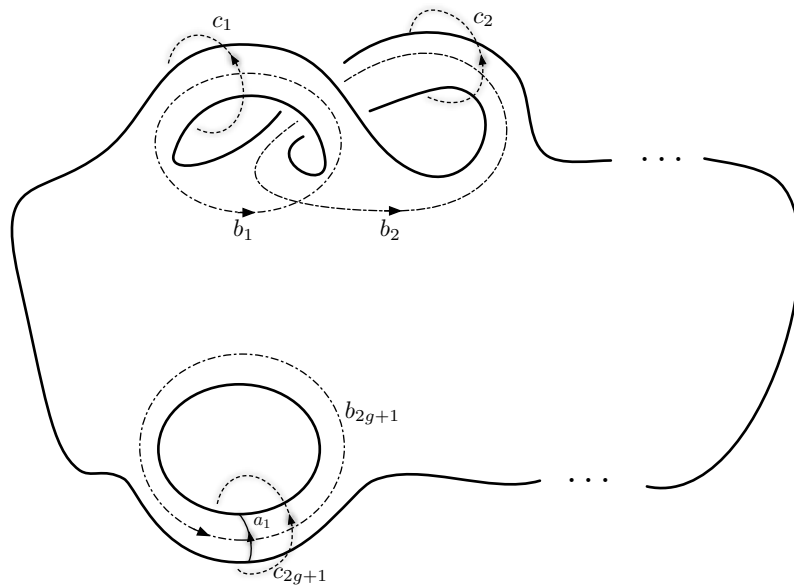


Figure 2.15: Various cycles relating to \mathcal{B} and L . \mathcal{B} is represented as a surface with g sets of double handles along the top and $|L| - 1$ sets of loops along the bottom. The basis a gives set of tethers that connect the link components. There is a complementary basis a^- , not shown, that involves pushing the a through \mathcal{B} . The basis b gives a basis for $H_1(\mathcal{B})$. The basis c gives basis for $H_1(S^3 - L)$. $\{a_i\} \cup \{c_i\}$ gives an overcomplete basis for $H_1(S^3 - \mathcal{B}, \partial\mathcal{B})$. The bases $\{b_i\}$ and $\{c_i\}$ are chosen such that $\text{Lk}(c_i, b_j) = \delta_{ij}$.

term A , B and C . Types A and C come from considering equivariant homotopies, whereas type B comes from the exact sequence (2.8) and simply consists of setting all longitudes (with respect to the framing given by \mathcal{B}) of link components to zero. There are $|L| - 1$ such independent longitudes and they can be thought of as setting either the positive or the equivalent negative pushoff from \mathcal{B} of the lower row of cycles in Figure 2.15 to zero.

As previously mentioned the second set of relations comes from equivariant homotopies. In particular, just above \mathcal{B} , any element of $\{c_i\}$ can be represented as some linear combination of cycles on \mathcal{B} pushed off in the positive direction. Such curves are given by a linear combination of $b_i^+, i \in \mathbb{Z}_{2g+|L|-1}$. We are only interested in the first $2g$ of these, since the others represent longitudes. Consider such a curve, b^+ lying just above \mathcal{B} . By pushing it through \mathcal{B} and reversing orientation we obtain a relationship $b_i^+ = -b_i^-$,

where b_i^- represents the linear combination of elements in $\{c_i\}$ coming from pushing b_i off \mathcal{B} in the negative direction.

Finally, by pushing a tether $a_i = a_i^+$ through \mathcal{B} , we find the relationship $a_i^+ = -a_i^-$. This can then be combined with the relationship $a_i^+ - a_i^- = c_{2g+i}$, shown in Figure 2.16, to obtain $2a_i^+ = c_{2g+i}$.

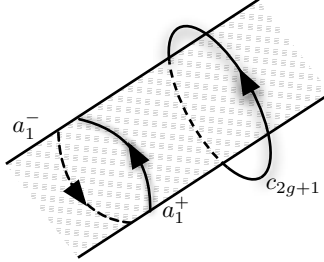


Figure 2.16: The relationship $a_i^+ - a_i^- = c_{2g+i}$.

Now, there are $2g$ relations of type A , and $|L| - 1$ relations of type B and C . Each of the three can be written out as

$$A_i := b_i^+ + b_i^- = \sum_{j=1}^{2g+|L|-1} \text{Lk}(b_j, b_i^+) + \text{Lk}(b_j, b_i^-) = 0 \quad (2.9)$$

$$B_i := b_{2g+i}^+ = \sum_{j=1}^{2g+|L|-1} \text{Lk}(b_j, b_{2g+i}^+) = 0 \quad (2.10)$$

$$C_i := 2a_i - c_{2g+i} = 0 \quad (2.11)$$

and combined into a block matrix, where the horizontal blocks correspond to the first $2g$ $\{c_i\}$, the last $|L| - 1$ $\{c_i\}$ and the $\{a_i\}$ and the vertical blocks correspond to relationships of type A , B and C , as

$$\begin{pmatrix} A^{(1)} & A^{(2)} & 0 \\ B^{(1)} & B^{(2)} & 0 \\ 0 & 1 & -2 \end{pmatrix}. \quad (2.12)$$

This is just a presentation matrix for an Abelian group. By taking into ac-

count relationships of type C , it is clear that an equivalent group is given by the matrix

$$\begin{pmatrix} A^{(1)} & 2A^{(2)} \\ B^{(1)} & 2B^{(2)} \end{pmatrix}. \quad (2.13)$$

Now let S be the Seifert matrix for the link L , then in our notation the matrix

$$S + S^T = \begin{pmatrix} A^{(1)} & A^{(2)} \\ 2B^{(1)} & 2B^{(2)} \end{pmatrix} \quad (2.14)$$

is a presentation matrix for the first homology of the branched double cover of $S^3 - L$ which we denote $H_1(\Sigma(L))$. The type of Abelian group given by a presentation matrix is simply given by the list of eigenvalues of the matrix.

For an arbitrary matrix we have

$$\det \begin{pmatrix} A & B \\ C & D \end{pmatrix} = \det(A)\det(D - CA^{-1}B) \quad (2.15)$$

from which it is clear that the matrices (2.13) and (2.14) have the same eigenvalues, and thus present the same group.

Finally we can say the following. Suppose one has a nematic texture in \mathbb{R}^3 with uniform boundary conditions at infinity and a set of line defects L . Then the number of topologically distinct nematic textures associated to that defect set is given by elements of $H_1(\Sigma(L))/\sim$, where the equivalence relation is $x \sim -x$. We are almost at our goal, (2.17), we just need to take account of a few more things. The first is the case of split links. A split link in S^3 is a link for which you can find an embedded sphere separating two or more components. The idea is to model a collection of defects. Indeed if one can surround a defect with a sphere, then it ought to have a charge as if it were a point defect, since on the sphere one cannot tell what type of defect, point, line knot *etc.* is inside the sphere. This is the case, and it is a

standard result [41] that for a link L with N split components, then

$$H_1(\Sigma(L)) = \mathbb{Z}^{N-1} \oplus \bigoplus_i H_1(\Sigma(L_i)). \quad (2.16)$$

The factors of \mathbb{Z} at the front can be thought of as corresponding to the point-defect charges of the split components. There are $N - 1$ of them rather than N because our uniform boundary conditions demand that the total charge is zero, which reduces the degrees of freedom by one. We can lift this condition by supposing that there is a point defect ‘at infinity’ in S^3 , the charge of this point defect compensates for the charges of all the other defects. Finally we can also add an arbitrary number of point defects into our system. Doing this we obtain the result quoted at the beginning of this chapter. Let \mathbf{n} be a director field for a nematic liquid crystal in \mathbb{R}^3 with a defect set \mathcal{D} , then $\mathcal{D} = \mathcal{P} \cup \mathcal{L}$ where \mathcal{P} is the set of point defects and \mathcal{L} is the set of line defects. Furthermore, $\mathcal{L} = \cup_i L_i$ where each of the L_i is a non-split knot or link. Then the topology of the texture \mathbf{n} is given by an element of the set

$$\left(\bigoplus_{p_i \in \mathcal{P}} \mathbb{Z} \right) \oplus \left(\bigoplus_{L_j \in \mathcal{L}} (\mathbb{Z} \oplus H_1(\Sigma(L_j))) \right) / \sim \quad (2.17)$$

2.4.1 INTERPRETATION OF THE TOPOLOGY OF KNOTTED DEFECTS

In this section we will try and understand some of the consequences of the above result. The first point to make is that for a knot, the quantity $|H_1(\Sigma(L))|$ is always a finite odd integer, and is a well known invariant termed the determinant of the knot. To motivate what might be considered interesting properties to examine, consider Table 2.1 which shows $H_1(\Sigma(L))$ for all torus links up to $(20, 20)$. We note two important things. Firstly, while for a knot $|H_1(\Sigma(L))|$ is always a finite odd integer, for a link it may be even. Secondly, not only may the order be even, but it may be infinite.

To explain the significance of the first observation we note that if an abelian group \mathbb{Z}_p has even p , then there is an order 2 element x such that $2x = 0$, or

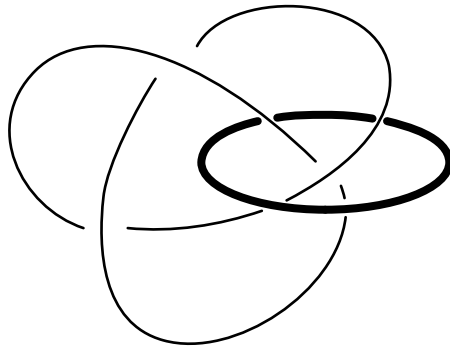


Figure 2.17: Skyrmion tube (thick line) entangling a trefoil knot defect. The creation of this line takes the state from 0 to 1 in \mathbb{Z}_3 .

$x = -x$. This connects to the nematic inversion symmetry. Suppose one had a knotted texture, then by the method detailed above, one must lift this to an orientable map on a covering space. A reasonable question is: when does the result not depend on the choice of lift from \mathbb{RP}^2 . The answer is when there are elements of order two. Under $\mathbf{n} \rightarrow -\mathbf{n}$ the appropriate element in $H_1(\Sigma(L))$ also changes sign. Order two elements are precisely those which are invariant with respect to this symmetry. For an example, take the Hopf link, it has $H_1(\Sigma(L)) = \mathbb{Z}_2$ which contains two elements 0 and 1. Under $x \rightarrow -x$ we have $0 \rightarrow 0$ and $1 \rightarrow 1$. As a counter example take the trefoil knot. It has $H_1(\Sigma(L)) = \mathbb{Z}_3$, with three elements 0, 1 and -1 . But under $x \rightarrow -x$ we have $0 \rightarrow 0$, $1 \rightarrow -1$ and $-1 \rightarrow 1$, so only one of the elements is invariant. This suggests we should partition states associated to a link based on their response – either symmetric or antisymmetric – to inversion symmetry. Consider the following question ‘given a director field, can I find another director field always orthogonal to the first?’ As we will discuss in later chapters, the answer to this question is given in terms of the Euler class of the orthogonal 2-plane bundle defined by \mathbf{n} , and it is precisely those textures that are order 2 that allow such an orthogonal direction to exist [42]. Physically, if one also demands that \mathbf{n} is a cholesteric, then symmetric states are those that can be realised without the presence of additional λ lines. More generally, for a nematic, one can think of states which are anti-symmetric

with respect to inversion as containing Skyrmion tubes entangling the knot or link (shown in Figure 2.17), whereas the symmetric states have no such tubes.

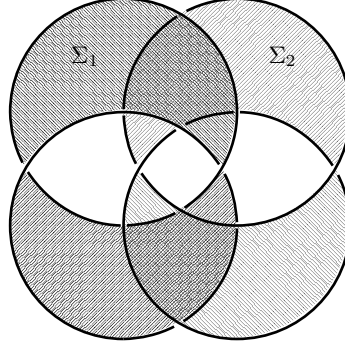


Figure 2.18: Disconnected spanning surface for the $(4, 4)$ torus link. One can think of it has two linked Hopf links. If this link represents a defect set in a nematic, then n is orientable on a closed torus surrounding either of the connected components of the surface. Since one can find a closed, non-contractible surface on which n is orientable, one can compute the degree of n on the surface. This gives a full integer and the effect is responsible for the integer summands given in Table 2.1.

Now we turn to links for which $|H_1(\Sigma(L))|$ is infinite. Algebraically the implication of this is clear. For a closed 3-manifold M we know that $H_2(M) = H_1(M)/\text{torsion}$ and hence the groups of infinite order imply that the branched double cover of S^3 over L has non-trivial second homology group. This has a nice geometric interpretation [40], in terms of the existence of disconnected spanning surfaces for the particular link, as shown in Figure 2.18. If such a link represents a defect set in a nematic, then n is orientable on a non-contractible closed surface surrounding a part of the link. Since one can find a closed, non-contractible surface on which n is orientable, one can compute the degree of n on the surface. This gives a full integer and the effect is responsible for the integer summands given in Table 2.1.

$p \setminus q$	2	3	4	5	6	7	8	9	10	11	12	13	14	15	16	17	18	19	20	
2	2	3	4	5	6	7	8	9	10	11	12	13	14	15	16	17	18	19	20	
3	3	3	2^2	3	\mathbb{Z}^2	1	\mathbb{Z}^2	1	3	1	\mathbb{Z}^2	1	3	2^2	3	1	\mathbb{Z}^2	1	3	
4	4	4	3	$2 \times \mathbb{Z}^2$	5	12	7	$4 \times \mathbb{Z}^2$	9	20	11	$6 \times \mathbb{Z}^2$	13	28	15	8 $\times \mathbb{Z}^2$	17	36	19	$10 \times \mathbb{Z}^2$
5	5	5	1	5^{24}	5	1	5	1	\mathbb{Z}^4	1	\mathbb{Z}^4	1	5	2^4	5	1	5	1	\mathbb{Z}^4	
6	6	6	\mathbb{Z}^2	12	5	$2 \times \mathbb{Z}^4$	7	24	30	11	$4 \times \mathbb{Z}^4$	13	42	$5 \times \mathbb{Z}^2$	48	17	$6 \times \mathbb{Z}^4$	19	60	
7	7	7	1	7	1	7^{26}	7	1	7	1	\mathbb{Z}^6	7	1	7	7	1	7	7	7	
8	8	8	3	$4 \times \mathbb{Z}^2$	5	24^{24}	7	$2 \times \mathbb{Z}^6$	9	40	11	$12 \times \mathbb{Z}^2$	13	56	15	$4 \times \mathbb{Z}^6$	17	72	19	$20 \times \mathbb{Z}^2$
9	9	9	2^2	9	1	$3 \times \mathbb{Z}^2$	1	9	2^8	9	1	$3 \times \mathbb{Z}^2$	1	9	2 ²	9	1	9	9	
10	10	10	3	20	\mathbb{Z}^4	30	7	40	9	$2 \times \mathbb{Z}^8$	11	60	13	70	$3 \times \mathbb{Z}^4$	80	17	90	19	$4 \times \mathbb{Z}^8$
11	11	11	1	11	1	11	1	11	1	2^{10}	11	1	11	1	11	11	1	11	11	
12	12	\mathbb{Z}^2	$6 \times \mathbb{Z}^2$	5	$4 \times \mathbb{Z}^4$	7	$12 \times \mathbb{Z}^2$	3	$\times \mathbb{Z}^2$	60	11	$2 \times \mathbb{Z}^{10}$	13	84	$5 \times \mathbb{Z}^2$	$24 \times \mathbb{Z}^2$	17	$12 \times \mathbb{Z}^4$	19	$30 \times \mathbb{Z}^2$
13	13	13	1	13	1	13	1	13	1	2^{12}	13	1	13	1	13	1	13	1	13	
14	14	14	3	28	5	42	\mathbb{Z}^6	56	9	70^{24}	11	84	13	$2 \times \mathbb{Z}^{12}$	15	112	17	126	19	140
15	15	15	2^2	15	2^{24}	5	$\times \mathbb{Z}^2$	1	15	2^2	1	$5 \times \mathbb{Z}^2$	1	15	2^{14}	15	1	$5 \times \mathbb{Z}^2$	1	$3 \times \mathbb{Z}^4$
16	16	16	3	$8 \times \mathbb{Z}^2$	5	48	7	$4 \times \mathbb{Z}^6$	9	80	11	$24 \times \mathbb{Z}^2$	13	112	15	$2 \times \mathbb{Z}^{14}$	17	144	19	$40 \times \mathbb{Z}^2$
17	17	17	1	17	1	17	1	17	1	17	1	17	1	17	2^{16}	17	17	17	17	
18	18	\mathbb{Z}^2	36	5	$6 \times \mathbb{Z}^4$	7	72	\mathbb{Z}^8	90	11	$12 \times \mathbb{Z}^4$	13	126	$5 \times \mathbb{Z}^4$	144	17	$2 \times \mathbb{Z}^{16}$	19	180	
19	19	19	1	19	1	19	1	19	1	19	1	19	1	19	2^{18}	19	19	19	$2 \times \mathbb{Z}^{18}$	
20	20	3	$10 \times \mathbb{Z}^2$	\mathbb{Z}^4	60	7	$20 \times \mathbb{Z}^2$	9	$4 \times \mathbb{Z}^8$	11	$30 \times \mathbb{Z}^2$	13	140	$3 \times \mathbb{Z}^4$	$40 \times \mathbb{Z}^2$	17	180	19	$2 \times \mathbb{Z}^{18}$	

Table 2.1: $H_1(\Sigma(L))$ for (p, q) torus links with $2 \leq (p, q) \leq 20$. x implies a group \mathbb{Z}_x , integer summands are given as usual.

CHAPTER 3

UMBILIC LINES AND THE GEOMETRY OF ORIENTATIONAL ORDER

The pure topological perspective explored in the previous chapter is illuminating, the abstraction allows one to see and say much. However, one also throws much away in doing this; a physical system is much more than its topology. This chapter is an exploration of the geometry of physical systems described by orientational order and ultimately how this geometry reflects the topology we have been discussing. In this way, in part, one can think of this chapter as a bridge between some of the abstract objects in the previous chapter and structures in physical systems. Seen in another light, this chapter is an attempt at a unification and elucidation of much of the lore concerning ‘double twist cylinders’ and their myriad companions in chiral systems. Still further, one might think of this chapter as a simple exercise in the geometry of vector fields.

In this chapter we are concerned with geometric features of orientational order. By this we mean systems which are described by either a unit vector or line field, such as magnetic or nematic systems. These systems typically contain line-like geometrical features. We will show that these lines can be identified as a set of natural geometric singularities in a unit vector field, which we call umbilic lines. These lines convey the global structure of the vector field through their role as Poincaré dual to the Euler class of a natural

vector bundle associated to the order. Later in this thesis we will show that these lines can be used to give a description of λ lines and related structures in cholesteric liquid crystals[9, 43, 44, 45, 46]. However, their appearance is not just confined to these systems, indeed they arise in superfluids as the cores of vortices [47, 48, 49, 50], and they can be identified in the Skyrmion¹ textures of chiral ferromagnets [51, 52, 53, 54, 55] and Bose-Einstein condensates [56, 57, 58, 59, 60, 61].

The umbilics we describe are generic traits, exhibited by any vector or line field, and closely analogous to several other structural degeneracies, for instance the lines of circular polarisation (C lines) in a generic electromagnetic field [62, 63, 64, 65] and the umbilic points of surfaces [66, 67] and random fields [68, 69, 70, 71, 72, 73, 74, 75], from which the terminology derives.

While we will give a detailed discussion of their relevance to cholesterics in Chapter 4, in general umbilic lines acquire extra significance in any material where the ground state has non-zero gradients where typically the vortex configurations surrounding umbilics correspond to local minima of the free energy. So for concreteness one can consider this chapter as concerning a system governed by the free-energy such as

$$F = \frac{K}{2} \int_{\mathbb{R}^3} \left[|\nabla \mathbf{n}|^2 + 2q_0 \mathbf{n} \cdot \nabla \times \mathbf{n} \right] d^3x, \quad (3.1)$$

where K is an elastic constant and q_0 is the strength of the chirality, or magnitude of spin-orbit coupling. This is the Frank free energy [1] for a bulk cholesteric under the one elastic constant approximation and also the Hamiltonian for elastic distortions in a chiral ferromagnet with a Dzyaloshinskii-Moriya interaction [76, 77]. We note that there is a connection of our local description with the work of Efrati and Irvine [78] on chiral shapes and structures. In their work they introduced a chirality pseudotensor to characterise the direction of twisting and sense of chirality of various materials.

¹We use the word ‘Skyrmion’ in the context of textures observed in chiral magnets, rather than in its original context of a non-linear field theory of pions.

We demonstrate a general connection with the shape operator for a surface or vector field, from which their chirality pseudotensor can be derived, and show that natural benefits are gained by considering both operators. Finally, analogous geometrical structures to the umbilics we describe have been discussed by Thorndike *et al.* [79], Čopar *et al.* [80], and Beller *et al.* [81], although not with the topological aspect that we give here.

3.1 LOCAL GEOMETRY OF ORIENTATIONAL ORDER

The local geometry of the orientational order at any point in the material can be given the following generic characterisation. Since \mathbf{n} is a unit vector its gradients are always perpendicular to itself. They separate naturally into gradients along the direction of the local orientation, which are bend distortions, and gradients along orthogonal directions, which correspond to the splay, twist, and saddle-splay deformations introduced in Chapter 1. These latter represent a linear transformation on the two-dimensional plane of directions perpendicular to the local orientation. If $\mathbf{d}_1, \mathbf{d}_2$ are unit vectors orthogonal to \mathbf{n} , such that $\{\mathbf{n}, \mathbf{d}_1, \mathbf{d}_2\}$ form a right-handed set, then the orthogonal gradients can be expressed in this local basis as a 2×2 real matrix with the decomposition

$$\nabla_{\perp} \mathbf{n} = \frac{\nabla \cdot \mathbf{n}}{2} \begin{bmatrix} 1 & 0 \\ 0 & 1 \end{bmatrix} + \frac{\mathbf{n} \cdot \nabla \times \mathbf{n}}{2} \begin{bmatrix} 0 & -1 \\ 1 & 0 \end{bmatrix} + \begin{bmatrix} \Delta_1 & \Delta_2 \\ \Delta_2 & -\Delta_1 \end{bmatrix}. \quad (3.2)$$

The first component is an identity transformation on the orthogonal directions, while the second is a skew transformation that provides the orthogonal directions with a complex structure. The coefficients of these two terms are known as the mean curvature and the mean torsion [82, 83], respectively, and correspond to scalar and pseudoscalar parts of the transforma-

tion. The last part is a deviatoric, or spin 2, component, Δ , that conveys the local ‘shear’. Its eigenvectors can be used to define principal directions of the curvature of the local orientation. In the case where \mathbf{n} is the normal to a surface, the transformation (3.2) is the derivative of the Gauss map, or shape operator of the surface, and the principal directions alluded to are the directions of principal curvature.

The geometric character of the orientational order is conveyed by this generic local description. The twist, $\mathbf{n} \cdot \nabla \times \mathbf{n}$, encodes the chirality of the order with surfaces of zero twist separating regions of different handedness, and also indicates whether \mathbf{n} is the normal to a system of layers. The splay, $\nabla \cdot \mathbf{n}$, measures how the flow of \mathbf{n} preserves volume, and $(\mathbf{n} \cdot \nabla)\mathbf{n}$ gives the geodesic curvature of the integral lines. Zeros of the deviatoric part of $\nabla_{\perp}\mathbf{n}$ occur along lines in three dimensions – they require both Δ_1 and Δ_2 to vanish and hence are codimension two – and correspond to degeneracies of the principal curvatures, or singularities of the principal curvature directions. They are the umbilics of the orientational order. At such points the transverse gradients are isotropic meaning that umbilics are naturally associated with the centres of vortex-like structures. A basis-independent expression can be given for these zeros purely in terms of the director; they correspond to the vanishing of the non-negative quantity

$$|\Delta|^2 = \left(\frac{\nabla \cdot \mathbf{n}}{2} \right)^2 + \left(\frac{\mathbf{n} \cdot \nabla \times \mathbf{n}}{2} \right)^2 - \frac{1}{2} \nabla \cdot [\mathbf{n}(\nabla \cdot \mathbf{n}) - (\mathbf{n} \cdot \nabla)\mathbf{n}], \quad (3.3)$$

this being the 2-norm of Δ . In the vicinity of an umbilic we may write

$$\Delta = |\Delta| \begin{bmatrix} \cos \theta & \sin \theta \\ \sin \theta & -\cos \theta \end{bmatrix}, \quad (3.4)$$

and around the umbilic the angle θ winds by an integer multiple of 2π . An umbilic is said to be generic if it has a winding number of ± 1 . Umbilics with

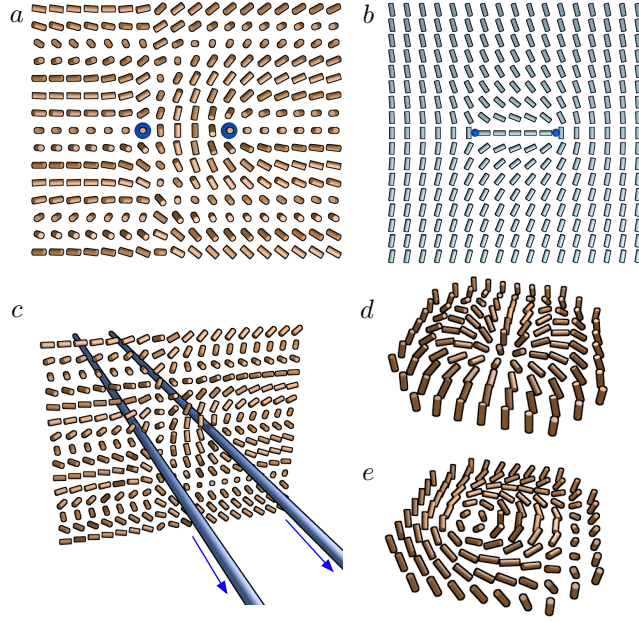


Figure 3.1: Umbilic lines. (a) $\lambda^+ \lambda^-$ dislocation in a cholesteric. It contains two generic umbilics. This combination of two generic umbilics can be identified as half a Skyrmion, or a meron. (b) Eigenvector field of Π for the dislocation. The two umbilics have opposite windings of the eigenvectors, but are counted with the same sign as n rotates by π when passing from one to the other. (c) Umbilic lines can be oriented in three dimensions. (d) & (e) Typical centres of vortices, based on curvature and torsion distortions respectively, that correspond to winding number 2 non-generic umbilics.

higher winding do occur, and indeed those with winding +2 are often observed in vortices, double twist cylinders and Skyrmions, with the degeneracy coming from an imposed axisymmetry. This can persist in certain experimental settings, either where there is axisymmetry or hexagonal symmetry, however, from a structural point of view they can be seen as a composite of winding ± 1 umbilics, into which they break apart under generic perturbation.

Illustrations can be given for a number of simple field conformations corresponding to textures observed in superfluid vortices, magnetic Skyrmions and the λ lines of cholesteric liquid crystals, shown in Figure 3.1. Two-dimensional sections of the full textures are shown on surfaces intersecting the umbilics transversally. The eigenvectors of Π – to be defined presently – shown in (b) identify the profiles of the umbilics in (a).

As we will show, the windings that we have just described are equivalent to the indices of the umbilics up to a sign, which arises because the orientation of \mathbf{n} ‘reverses’ from one umbilic to another. (The discrepancy is therefore absent if \mathbf{n} is the normal to a surface, since then there is no reversal of its orientation between umbilics, and the index is simply the local winding of the eigenvectors of Δ .) The sum of the indices of the umbilics yields a topological invariant, equal to four times the Skyrmion number of the texture on the two-dimensional surface. This calculation of the Skyrmion number is dual to the usual method of integrating a curvature form [84, 27]

$$q = \frac{1}{8\pi} \int_{\Sigma} \epsilon_{abc} n^a \partial_i n^b \partial_j n^c dx^i \wedge dx^j, \quad (3.5)$$

which computes the degree of the map $\mathbf{n} : \Sigma \rightarrow S^2$. The duality can be viewed as entirely analogous to that in the classical differential geometry of surfaces between the Gauss-Bonnet theorem – integral of the Gaussian curvature – and the calculation of the Euler characteristic using umbilic points of the surface.

Two additional aspects of the local description are worth bringing out before giving a global treatment. First, the complex structure $J = \begin{bmatrix} 0 & -1 \\ 1 & 0 \end{bmatrix}$ acts on the shape operator (3.2) by simple composition to produce an equivalent linear transformation

$$\begin{aligned} \chi = J \circ \nabla_{\perp} \mathbf{n} = & -\frac{\mathbf{n} \cdot \nabla \times \mathbf{n}}{2} \begin{bmatrix} 1 & 0 \\ 0 & 1 \end{bmatrix} + \frac{\nabla \cdot \mathbf{n}}{2} \begin{bmatrix} 0 & -1 \\ 1 & 0 \end{bmatrix} \\ & + \begin{bmatrix} -\Delta_2 & \Delta_1 \\ \Delta_1 & \Delta_2 \end{bmatrix}. \end{aligned} \quad (3.6)$$

This transformation, although equivalent to the shape operator, is independent from it in the sense that they are orthogonal with respect to the natural inner product between matrices, $\text{Tr}(\chi^T \nabla_{\perp} \mathbf{n}) = 0$, a property that turns out to be of some importance in the analysis of the topology of umbilics. χ is the

chirality pseudotensor given by Efrati and Irvine [78] in their study of chiral materials. The spin 2 component $\Pi = J \circ \Delta$ carries equivalent information to Δ . Its eigenvectors can be thought of as defining directions of principal torsion (or twist) and are simply rotated relative to those of Δ by $\pi/4$ about the director. Nonetheless, for materials with chiral interactions or structure, it is these directions, rather than the eigenvectors of Δ , that are often more visibly recognisable, as is elegantly illustrated in the experiments of Armon *et al.* [85] on the opening of chiral seed pods, and those of Efrati and Irvine [78] on stretched elastic sheets.

Second, if the umbilic forms a closed loop then the winding of the angle θ along the contour length of the umbilic (a longitude) conveys a second integer invariant. Of course, this latter depends on both the choice of longitude and the homotopy class of the local trivialisation $\{d_1, d_2\}$. We describe this in detail later.

3.2 GLOBAL DEFINITION OF UMBILICS AND THEIR TOPOLOGY

The umbilic lines we have identified convey topological information about the vector field n , specifically the Euler class of the orthogonal 2-plane bundle, ξ , through a combination of the Gauss-Bonnet-Chern theorem [86, 87, 88, 89] and Poincaré duality. The curvature of a vector bundle represents a characteristic cohomology class that can be integrated over homology cycles to produce topological invariants. By Poincaré duality this can be viewed as a homology class and the umbilics furnish a representative of this Poincaré dual. We shall develop this general topology of orientational order in terms of a natural connection on the vector bundle that the spin 2 transformation Δ takes values in.

As before, let n be a unit vector field in \mathbb{R}^3 ; then it defines a splitting of

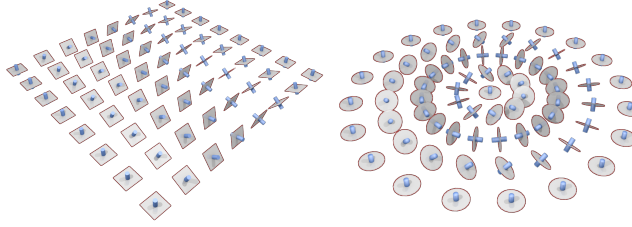


Figure 3.2: The splitting $T\mathbb{R}^3 \cong L_{\mathbf{n}} \oplus \xi$ induced by orientational order. *Left:* A simple helical director profile, corresponding to the ground state of a cholesteric liquid crystal or helimagnet. *Right:* An idealised, axisymmetric Skyrmiон profile, the central portion of which is a standard idealised model of double twist cylinders in blue phases.

the tangent bundle

$$T\mathbb{R}^3 \cong L_{\mathbf{n}} \oplus \xi, \quad (3.7)$$

into a real line bundle, $L_{\mathbf{n}}$, of vectors parallel to \mathbf{n} and a rank 2 real vector bundle, ξ , of vectors orthogonal to \mathbf{n} . Examples of this splitting are shown in Figure 3.2. The gradients of \mathbf{n} take values in $T\mathbb{R}^{3*} \otimes \xi \cong (L_{\mathbf{n}}^* \otimes \xi) \oplus (\xi^* \otimes \xi)$, with the first part containing the bend deformations and the second the perpendicular gradients given locally in (3.2). By complete analogy with the classical differential geometry of surfaces we call these perpendicular gradients the shape operator of the orientational order and think of it as a linear transformation on the orthogonal 2-planes.

The shape operator decomposes in the following way. Local rotations about the director field correspond to a local symmetry and endow the bundle ξ with a natural $SO(2)$ action, under which the tensor product $\xi^* \otimes \xi$ splits into a direct sum $\mathcal{I} \oplus \mathcal{J} \oplus E$, where \mathcal{I} and \mathcal{J} are trivial line bundles and E is a rank 2 vector bundle. Correspondingly, the shape operator has the decomposition

$$\nabla_{\perp} \mathbf{n} = \frac{\nabla \cdot \mathbf{n}}{2} \mathbb{I}_{\xi} + \frac{\mathbf{n} \cdot \nabla \times \mathbf{n}}{2} J + \Delta, \quad (3.8)$$

given previously in (3.2). Here, \mathbb{I}_{ξ} is the identity transformation and $J = \mathbf{n} \times$ is a complex structure on ξ , now defined globally, while Δ has the global

definition

$$\Delta(\mathbf{v}) = \frac{1}{2} \left[(\mathbf{v} \cdot \nabla) \mathbf{n} + \mathbf{n} \times (\mathbf{n} \times \mathbf{v} \cdot \nabla) \mathbf{n} \right], \quad (3.9)$$

for any \mathbf{v} that is a section of ξ . The umbilics are identified with the zeros of Δ ; they encode the topology of the orientational order.

Without repeating too much of the local description given previously, we note that composition with the complex structure again yields the chirality pseudotensor [78], $\chi = J \circ \nabla_{\perp} \mathbf{n}$, and that the spin 2 component of this, $\Pi = J \circ \Delta$, can be expressed globally as

$$\Pi(\mathbf{v}) = \frac{1}{2} \left[\mathbf{n} \times (\mathbf{v} \cdot \nabla) \mathbf{n} - (\mathbf{n} \times \mathbf{v}) \cdot \nabla \mathbf{n} \right], \quad (3.10)$$

for any \mathbf{v} that is a section of ξ , and is also a section of E . We reiterate that although Π and Δ may be obtained one from the other by composition with the complex structure, they are orthogonal with respect to the natural inner product $\langle \Pi, \Delta \rangle = \frac{1}{2} \text{Tr}(\Pi^T \Delta)$. At the same time, they share the same magnitude and the same zero set, the umbilics \mathcal{U} . Thus, away from umbilic lines, Π and Δ represent two non-zero orthogonal sections of E , and so they provide a basis for $E|_{\mathbb{R}^3 - \mathcal{U}}$ and also define a natural connection 1-form

$$A = \frac{\langle \Pi, \nabla \Delta \rangle}{\langle \Delta, \Delta \rangle}. \quad (3.11)$$

This 1-form conveys the fundamental topology of the orientational order.

We give in (3.11) a global definition of A that emphasises its naturality and makes clear how it arises. In a local chart it can be represented in terms of the eigenvectors, \mathbf{p}^+ and \mathbf{p}^- , of Δ and has components $A_i = 2p_a^- \partial_i p_a^+$, an expression perhaps closer in form to the usual way of writing Berry connections. However, one must keep in mind that this representation is only local in the present context; otherwise it only serves to obfuscate the natural structure. The exterior derivative of A , $\Omega_E = dA$, is the (Berry) curvature of the vector bundle E . It is equal to twice the curvature of ξ on account of

E being a spin 2 subbundle of $\xi^* \otimes \xi$. (This is also evident from the local expression in terms of the eigenvectors \mathbf{p}^\pm .)

A fundamental property of an umbilic is given by the integral of the connection 1-form (3.11) around any simple closed loop γ encircling the umbilic. This is the holonomy of the connection, or Berry phase. Let Σ be an oriented surface with boundary γ , as in Figure 3.3. If Σ is generic then the umbilics will intersect it transversally in some number of distinct points. Let $\{D_i\}$ be disjoint small discs in Σ about each of these intersection points and denote their boundaries by $\{C_i\}$. Then $|\Delta|$ is nowhere zero on $\Sigma - \{D_i\}$ and $\partial(\Sigma - \{D_i\}) = \gamma \sqcup \{\bar{C}_i\}$ so that by Stokes' theorem

$$\int_{\gamma} A - \sum_i \int_{C_i} A = \int_{\Sigma - \{D_i\}} dA = \int_{\Sigma - \{D_i\}} \Omega_E. \quad (3.12)$$

To extend the analysis over the umbilics, we can introduce a local trivialisation of $L_n \oplus \xi$ on each of the D_i , which we denote by the orthonormal basis $\{\mathbf{n}, \mathbf{d}_1, \mathbf{d}_2\}$. Then $\mathbf{e}_1 = \mathbf{d}_1 \otimes \mathbf{d}_1 - \mathbf{d}_2 \otimes \mathbf{d}_2$ and $\mathbf{e}_2 = \mathbf{d}_1 \otimes \mathbf{d}_2 + \mathbf{d}_2 \otimes \mathbf{d}_1$ form a local basis for E . In such a basis $\Delta = |\Delta| \cos \theta \mathbf{e}_1 + |\Delta| \sin \theta \mathbf{e}_2$ and $A = d\theta + 2\omega$ where $\omega_i = (\mathbf{d}_2)_a \partial_i (\mathbf{d}_1)_a$ is the connection 1-form on ξ for this basis (the factor of two accounts for E being a spin 2 bundle). With this, one finds at once the Gauss-Bonnet-Chern theorem [90] in the form

$$\begin{aligned} \frac{-1}{2\pi} \int_{\Sigma} \Omega_E + \frac{1}{2\pi} \int_{\gamma} A &= \sum_i \frac{1}{2\pi} \int_{C_i} d\theta, \\ &= \sum_i \text{index}_{\Sigma} U_i, \end{aligned} \quad (3.13)$$

which defines the index of an umbilic, an integer associated to its intersection with a surface. Note that, as alluded to earlier, the index of an umbilic is not simply the winding number of the angle θ that characterises the local profile as that is measured relative to a local basis for ξ , while the index uses the orientation on the surface Σ ; there is, therefore, an additional sign according to whether $d\theta$ is cooriented with C_i or not.

It is instructive to contrast this situation, where the type of profile does not carry topological information, with that of umbilical points of surfaces where it does. This occurs because in the case of surfaces \mathbf{n} is fixed to be the normal to Σ , and so $d\theta$ is always cooriented with C_i .

One can understand this relation between the profile and index in terms of oriented umbilics. The 1-form A circulates around umbilic lines, orienting them such that the circulation is right handed. If one orients umbilics in this way, the expression for the index in (3.13) is rewritten as

$$\text{index}_\Sigma U_i = s_i \text{Int}(U_i, \Sigma), \quad (3.14)$$

where $\text{Int}(U_i, \Sigma)$ is the signed number of intersections of U_i with Σ and $s_i \in \mathbb{N}$ is the absolute strength of the umbilic U_i . Examples illustrating this are shown in Figures 3.1 and 3.4; we describe only the latter (the former is essentially identical). Figure 3.4 shows a Skyrmion lattice, a well-known structure seen in a variety of systems [51, 52, 53, 54, 59, 91, 92, 93, 94]. The umbilics form a lattice, with $s = 2$ umbilics each surrounded by six $s = 1$ umbilics. The eigenvectors of Π show the central umbilic having a +1 profile, and the six outer umbilics a $-1/2$ profile. All the umbilics have the same orientation induced by A , and so their intersection numbers, and thus indices in (3.13), are all positive. For the +1 profile, $-1/2$ profile and the orientations to all be consistent, it is necessary that \mathbf{n} rotates by π when passing from the central umbilic to an outer one.

The curvature of the bundle ξ can be expressed in terms of the director field as

$$\Omega_\xi = -\frac{1}{2} \epsilon_{abc} n^a \partial_i n^b \partial_j n^c dx^i \wedge dx^j. \quad (3.15)$$

This is because each 2-plane of the bundle ξ is explicitly embedded in \mathbb{R}^3 (see Figure 3.2) and the expression is just the extrinsic definition of curvature in terms of the (generalised) Gauss map. Equally, it follows from an explicit calculation in local coordinates for any particular texture, say a radial

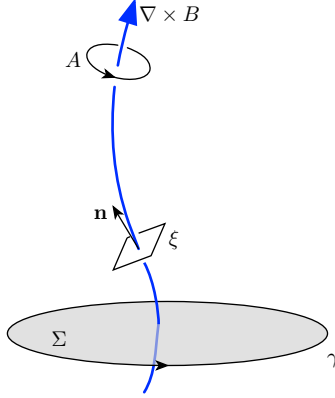


Figure 3.3: Anatomy of an umbilic line. *Top.* The vector $\nabla \times B$ is tangent to generic umbilic lines, giving them a natural orientation. This orientation is compatible with that induced by A . *Middle.* The vector field n and associated orthogonal plane ξ . Note that in general the tangent vector of the umbilic does not align with n . ξ is oriented by n and so gives a natural cycle along which to measure the winding. For a generic umbilic if $n \cdot \nabla \times B > 0$ then the eigenvectors of Δ have a $+1/2$ profile and if $n \cdot \nabla \times B < 0$ the eigenvectors have a $-1/2$ profile. *Bottom.* A measuring cycle γ bounding a surface Σ . Whether γ measures the winding of the umbilic as positive or negative depends on whether the umbilic – oriented by $\nabla \times B$ – intersects Σ positively or negatively.

hedgehog. A third way to establish it is through a calculation in the style of the Mermin-Ho relation [47], a good account of which has been given by Kamien [95]. The curvature of E is equal to twice this, $\Omega_E = 2\Omega_\xi$, since E is a spin 2 subbundle of $\xi^* \otimes \xi$. Therefore, when Σ is closed, or the boundary term vanishes, we have

$$\sum_i s_i \text{Int}(U_i, \Sigma) = \frac{1}{2\pi} \int_{\Sigma} \epsilon_{abc} n^a \partial_i n^b \partial_j n^c dx^i \wedge dx^j = 4q, \quad (3.16)$$

or the sum of the indices of the umbilics piercing Σ is equal to four times the Skyrmion number. This establishes a general relationship between Skyrmions and umbilics. This is illustrated in Figure 3.4 where each unit cell contains one $s = 2$ umbilic and six $s = 1$ umbilics, each of which are shared between three unit cells, giving a total count of $2 + 6 \times 1/3 = 4$, *i.e.* there is one Skyrmion in each unit cell.

This correspondence between Skyrmions and umbilics can be seen as a version of Poincaré duality, giving a natural way to localise Skyrmions to a

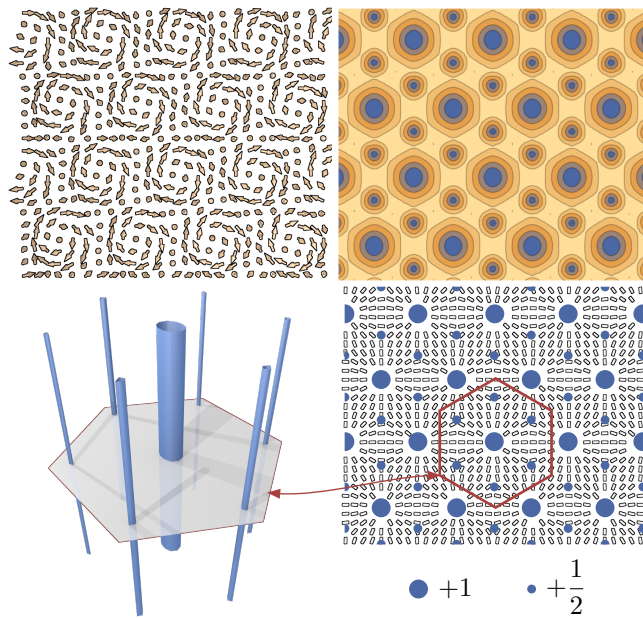


Figure 3.4: Skyrmion lattice. Each unit cell possesses a single central $s = 2$ umbilic, with the six outer $s = 1$ umbilics each shared between 3 unit cells giving a total count of $2 + 6 \times 1/3 = 4$ umbilics = 1 Skyrmion per unit cell. *Top Left:* Unit vector field n in a Skyrmion lattice. *Top Right:* Contour plot of $|\Delta|$ showing the umbilic lines forming a lattice of tubes. *Bottom Right:* Eigenvector field of Π , illustrating the $+1$ winding around the central umbilics and $-1/2$ winding around the outer umbilics. Note that both are counted with the same sign as the orientation of n changes from one to another. *Bottom Left:* Umbilics form lines in three dimensions.

set of points or lines. The set of umbilics \mathcal{U} in a three dimensional system M gives a representative of a cycle in $H_1(M)$. The Poincaré dual of this is the cocycle $e(E) \in H^2(M)$, the Euler class, which depends only on the topology of the bundle E and hence \mathbf{n} , and gives a global constraint on the total number of umbilic lines in the system in terms of the topology of \mathbf{n} . As a spin-2 vector bundle, $e(E) = 2e(\xi) = 4[\mathbf{n}]$, where $[\mathbf{n}] \in H^2(M)$ is the cocycle represented by \mathbf{n}^2 . In the absence of torsion in $H^2(M)$ ³, there is a canonical representative of the cocycle $4[\mathbf{n}]$ as a 2-form which is given through the Chern-Weil homomorphism by $\text{Pf}(-\Omega_E/2\pi)$, which leads to (3.13).

An example of the Euler class as a global constraint on umbilics is given by the case of monopoles, illustrated in Figure 3.5. These are point defects in the magnetisation that mediate changes in the number of Skyrmions [55]. In the local neighbourhood of a point defect the topology of \mathbf{n} is described by an integer $q \in \pi_2(S^2) \cong \mathbb{Z}$, the charge of the point defect. Through (3.16) one finds that a sphere surrounding this point defect must be pierced by umbilics of total index $4q$. In Figure 3.5 we show a simulation of two ± 1 point defects, or monopoles, in a chiral ferromagnet. There are four umbilics, each of generic type, ending on the point defects in a manner reminiscent of Dirac strings [86]. On a slice in the midplane of the cell \mathbf{n} contains a Skyrmion, illustrating the well-known creation and annihilation of Skyrmions in terms of point defects, observed experimentally [55].

3.3 LOCAL PROFILES OF UMBILIC LINES

Generic umbilic lines carry a canonical orientation through the vector B , defined as

$$B^i = \langle \Pi, \partial^i \Delta \rangle = \langle \Delta, \Delta \rangle \delta^{ij} A_j, \quad (3.17)$$

²If \mathbf{n} is considered as a map into S^2 , then homotopy classes are given by an element in H^2 with additional data associated to the Hopf invariant.

³Here, torsion is meant in the sense of group theory – *i.e.* $H^2(M)$ contains elements of finite order – and not in the geometric sense.

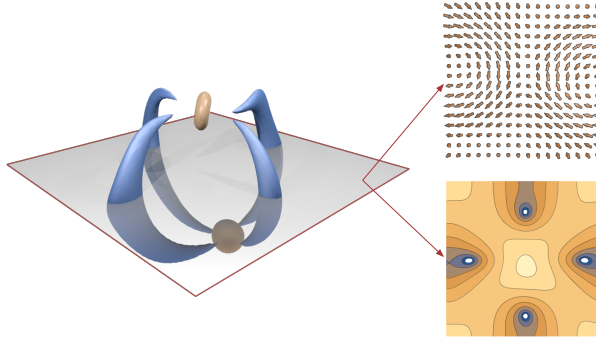


Figure 3.5: Transient monopoles and umbilic lines observed in a simulated quench of the free energy (3.1). *Left:* Contours of constant value of $|\Delta|$. The blue lines are umbilics, the beige spheres are monopoles (point defects). Each umbilic has winding $n = 1$. They are all oriented similarly, so that the sum of the umbilics entering/leaving the negative/positive point defect is 4, in accordance with (3.13) and corresponding to the Skyrmion created between the monopoles. *Top Right:* Cross-section showing \mathbf{n} on the shaded plane. As a map from the plane to S^2 , it has degree 1, indicating the presence of a Skyrmion. *Bottom Right:* Contour plot showing the magnitude of $\log(|\Delta|)$ on the shaded plane, the umbilics are clearly picked out.

which assigns a tangent vector to the umbilic, provided it is generic, as follows. If, in a local trivialisation, $\Delta = s_1 \mathbf{e}_1 + s_2 \mathbf{e}_2$ then an umbilic is defined as the intersection of the two surfaces $s_1 = 0$ and $s_2 = 0$ and so its tangent vector will be $\nabla s_1 \times \nabla s_2$. Note that while the values of s_1 and s_2 depend on the choice of basis, the tangent vector does not. In this local form we can write

$$B = s_1 \nabla s_2 - s_2 \nabla s_1 + 2(s_1^2 + s_2^2)\omega, \quad (3.18)$$

so that on an umbilic we have $\nabla \times B = 2\nabla s_1 \times \nabla s_2$ and hence the vector $\nabla \times B$ points along umbilic lines, canonically orienting them. As indicated in Figure 3.3 this orientation is compatible with that induced by the circulation in A previously discussed. As alluded to in Figures 3.1 and 3.4, the discrepancy between the type of profile and index of an umbilic depends on the relative orientation between \mathbf{n} and the umbilic line. To measure whether the eigenvectors of a generic umbilic have winding $\pm 1/2$ one should integrate A along a contour γ chosen such that its orientation matches the orientation imparted to ξ by \mathbf{n} . One can then show that the local profile is $\pm 1/2$ depend-

ing on

$$\text{Sgn}(\mathbf{n} \cdot \nabla \times B), \quad (3.19)$$

the analysis being identical to that given by Berry for C lines in electromagnetic fields [96].

This quantity $\mathbf{n} \cdot \nabla \times B$ can be used to further characterise the local structure of umbilic lines. Along an umbilic Δ vanishes and generically we can expect it to vanish linearly. Its local profile is then given by the form of the linear order terms in Δ in the immediate vicinity of the umbilic. Equivalently, generically we can expect the gradients of Δ to be non-zero on the umbilic and the local profile is then given by the structure of $\nabla\Delta$ evaluated on the umbilic. As usual, we split the gradients into the components parallel to \mathbf{n} and those perpendicular to it, and consider only the latter. The non-zero part of these transverse gradients, evaluated on the umbilics, takes values in $\xi^* \otimes E$, so it is this part that we need to focus on. A section of this bundle characterising the local profile of the umbilic can be constructed from $\nabla\Delta$ as follows. If \mathbb{I}_E is the projection onto E in $T\mathbb{R}^{3*} \otimes T\mathbb{R}^3$ then we define the differential operator ∇^ξ as $\nabla^\xi\Delta = \mathbb{I}_\xi\nabla\Delta\mathbb{I}_E$. By construction $\nabla^\xi\Delta$ is a section of the bundle $\xi^* \otimes E$. Under the action of $SO(2)$ the bundle $\xi^* \otimes E$ splits into two rank 2 subbundles, $F^+ \oplus F^-$, where F^+ is the spin 1 bundle corresponding to $+1/2$ profiles and F^- is the spin 3 bundle corresponding to $-1/2$ profiles, and we decompose $\nabla^\xi\Delta$ according to this splitting as

$$\nabla^\xi\Delta = \nabla^\xi\Delta^+ + \nabla^\xi\Delta^-. \quad (3.20)$$

A short calculation shows that $\mathbf{n} \cdot \nabla \times B = |\nabla^\xi\Delta^+|^2 - |\nabla^\xi\Delta^-|^2$ so that if $|\nabla^\xi\Delta^+| > |\nabla^\xi\Delta^-|$ the umbilic has a local $+1/2$ profile, while if the converse holds the profile is of type $-1/2$.

This analysis allows us to give a description of the space of local profiles for a generic umbilic. Since $\nabla^\xi\Delta|_{\mathcal{U}}$ is non-zero for a generic umbilic, but otherwise arbitrary, the space of local profiles has the homotopy type of the

three-sphere. However, there is more structure to it than that. The equality $|\nabla^\xi \Delta^+| = |\nabla^\xi \Delta^-|$ defines a Clifford torus separating the three-sphere into two solid tori corresponding to the different profiles. A natural constraint on an umbilic loop is for its profile to be of constant type, *i.e.* for $\mathbf{n} \cdot \nabla \times \mathbf{B}$ to be of constant sign or the profile to stay within a single solid torus. An umbilic loop which satisfies this constraint is called transverse, as its tangent vector is always transverse to the planes of ξ . This is not an unphysical constraint, transverse umbilic lines are commonly found in various chiral structures – typical λ lines in cholesterics have a local structure in which \mathbf{n} is either parallel or antiparallel with the tangent vector to an umbilic. Figure 3.6 shows the transverse umbilic loop found in toron excitations in frustrated cholesterics [7, 8].

The condition of an umbilic being transverse therefore translates as one of the two profiles having a higher ‘weight’ along the entire length of the umbilic. If this is the case then we have $|\nabla^\xi \Delta^\pm|^2 \neq 0$ with the sign depending on whether the umbilic is positively or negatively transverse. Suppose, for concreteness, that the umbilic is positively transverse. Then, in a local trivialisation, we will have $\nabla^\xi \Delta^+ = t_1 \mathbf{f}_1^+ + t_2 \mathbf{f}_2^+$, with $t_1^2 + t_2^2 \neq 0$, and the space of positively transverse umbilics has the homotopy type of a circle. The variation of the profile around a closed, transverse umbilic loop confers another integer winding number. This number depends on how the basis vectors of the trivialisation of F^+ wind around the umbilic. The ambiguity can be removed by demanding that each of the basis vectors in the trivialisation does not link with the umbilic. As we will show in §3.5, this winding number can be interpreted as twice a self-linking number for the umbilic loop, and is related to a relative Euler class of E .

3.4 THE LOCAL PROFILE OF TENSOR FIELD ZEROS IN 2D

An understanding of the profiles of higher order umbilics can be phrased in terms of the local structure of zeros of a spin-2 field in two dimensions.

This is a specific example of the more general case of zeros of an arbitrary spin field in two dimensions, which has an elegant structure when phrased in terms of vector bundles⁴ and forms an amusing digression.

We will begin with a trivial calculation. Suppose we have two rank 2 vector bundles E and F on a 2-manifold Σ . They have spin N and M meaning that under the action of $SO(2)$ corresponding to rotations a section s of E transforms as

$$s_1 \mathbf{e}_1 + s_2 \mathbf{e}_2 \mapsto s_1(\cos(N\theta)\mathbf{e}_1 + \sin(N\theta)\mathbf{e}_2) + s_2(\cos(N\theta)\mathbf{e}_2 - \sin(N\theta)\mathbf{e}_1), \quad (3.21)$$

or, writing as a vector

$$s \mapsto R_\theta^N s, \quad (3.22)$$

with a corresponding statement for F . Now consider the bundle $E \otimes F$. It has dimension four and under the rotation one finds that it splits into two irreducible two-dimensional subbundles as

$$E \otimes F \cong A \oplus B \quad (3.23)$$

where A consists of identity and antisymmetric tensors and has spin $N - M$ and basis $\mathbf{a}_1 = \mathbf{d}_1 \otimes \mathbf{e}_1 + \mathbf{d}_2 \otimes \mathbf{e}_2$ and $\mathbf{a}_2 = \mathbf{d}_2 \otimes \mathbf{e}_1 - \mathbf{d}_1 \otimes \mathbf{e}_2$; and B consists of traceless symmetric tensors, has spin $M + N$ and basis $\mathbf{b}_1 = \mathbf{d}_1 \otimes \mathbf{e}_1 - \mathbf{d}_2 \otimes \mathbf{e}_2$ and $\mathbf{b}_2 = \mathbf{d}_1 \otimes \mathbf{e}_2 + \mathbf{d}_2 \otimes \mathbf{e}_1$. Writing bundles with their spin as a subscript we have the equation

$$E_N \otimes F_M \cong A_{M-N} \oplus B_{M+N} \quad (3.24)$$

Now suppose we have a field $\sigma = s_1 \mathbf{e}_1 + s_2 \mathbf{e}_2$, a section of a rank-2 spin N vector bundle E . Now the first order derivative of σ will be a section of

⁴Of course, it can all be done in half the time by using complex numbers, but we would like to keep using vector bundles.

$T^*\Sigma \otimes E$, and by (3.24) this decomposes as

$$T^*\Sigma \otimes E_N \cong D^{(1)}E_{N-1} \oplus D^{(-1)}E_{N+1}, \quad (3.25)$$

since $T^*\Sigma$ has spin 1 and we have used the notation $D^{(a)}E_M$ to denote a subbundle corresponding to a spin M derivative of E , a is associated to the winding of a zero whose derivative only has values in the bundle, and will be explained below. To understand the full structure we will need to go one step further, and look at second derivatives. In this case we are looking at a section of the bundle

$$T^*\Sigma \otimes T^*\Sigma \otimes E_N \cong D^{(1,1)}E_{N-2} \oplus D^{(1,-1)}E_N \oplus D^{(-1,1)}E_N \oplus D^{(-1,-1)}E_{N+2}. \quad (3.26)$$

A short calculation in terms of basis vectors shows that the bundles $D^{(1,-1)}E_N$ and $D^{(-1,1)}E_N$ are the same. If we denote ∇^\pm to be the restriction of the derivative to the appropriate subbundle, then this structure can be summed up by the diagram.

$$\begin{array}{ccccc} & & E & & \\ & \swarrow \nabla^+ & & \searrow \nabla^- & \\ D^1E & & & & D^{-1}E \\ \swarrow \nabla^+ & & \searrow \nabla^- & \swarrow \nabla^+ & \searrow \nabla^- \\ D^{(1,1)}E & & D^{(1,-1)}E & & D^{(-1,-1)}E \end{array}$$

This diagram has a natural extension to arbitrary order, and it commutes up to the p^{th} row for a zero of order p . This is a consequence of the following. Suppose there is a point x such that $\sigma(x) = 0$. Then the order of the zero at x is the lowest p such that $\nabla^p\sigma \neq 0$. Now, if ω is a connection form for E then

$$\nabla\sigma = \partial\sigma + \omega_{ik}^j\sigma_j, \quad (3.27)$$

so that if we restrict the derivatives to be of order $\leq p$ we can consider the connection to be flat in the vicinity of the zero, since any terms coming from the connection will be multiplied by $\sigma(p) = 0$ or lower order gradients.

Now suppose there is a zero of order p , but that its p^{th} derivatives lie entirely in a single subbundle, as distinguished on symmetry grounds. Then, purely by symmetry, one can deduce the winding of the zero. To see this consider the field $\sigma(x)$ with $\sigma(0) = 0$. Then, if one considers a circuit around the zero, it is possible to deduce that the winding of a zero of a spin N field corresponding to a spin M subbundle is $N - M$. This is illustrated in Table 3.1. Finally, one can use this relationship to observe changes in the symmetry of a zero when one tries to change the symmetry of a field. The canonical example of this operation is decorating a line field with an orientation. Suppose one has a spin N field σ with a zero of spin M , then by trying to change the symmetry of the field, one creates a new field with spin N/p for an integer divisor p of N . One can see, then, that this will only be possible if the spin of the zero, M , is equal to pM' .

3.5 UMBILIC LOOPS

The umbilics of three-dimensional orientationally ordered materials are extended line-like objects, however most of the properties we have described so far can be associated to isolated points along these one-dimensional curves. For example the points of transverse intersection with an appropriate surface (or slice through the material) count numbers of Skyrmions, merons, or λ defects. It is clear, however, that these locally measurable objects do not represent all the information encoded by umbilic lines; if one has a closed umbilic loop then, as discussed above, the local properties at each point must stitch together consistently along the loop conveying both geometric and topological information about the orientational order.

Umbilic loops have been observed in experimental systems [9, 8, 72], and a motivating set of examples are the so-called torons [7], illustrated in Figure 3.6. These soliton structures can be generated in a frustrated cholesteric cell, with the director held vertical along the top and bottom. As shown in Figure 3.6(a), they display a characterisitc umbilic loop, in the form of a circle sitting

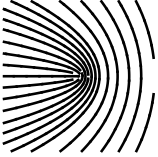
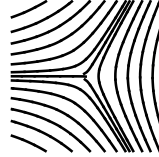
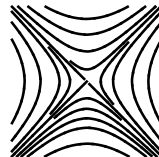
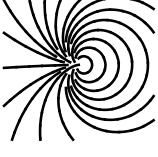
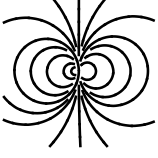
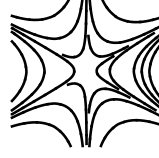
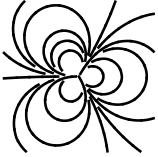
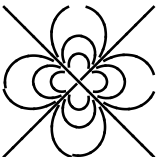
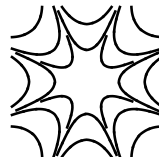
Order	Charge	Spin	Profile	Charge	Spin	Profile
1	$\frac{1}{2}$	1		$-\frac{1}{2}$	3	
2	1	0		-1	4	
3	$\frac{3}{2}$	-1		$-\frac{3}{2}$	5	
4	2	-2		-2	6	
5	$\frac{5}{2}$	-3		$-\frac{5}{2}$	7	
6	3	-4		-3	8	

Table 3.1: Local structure of zeros for a spin 2 field in two dimensions up to order 6. The spins of the profile correspond to the spins of the associated vector bundles. Note that the sum of the spins in a given order is equal to twice the spin of the original field, in this case 4. Also note that the charge 1 profile has spin zero, meaning one can distinguish a star and a centre on symmetry grounds.

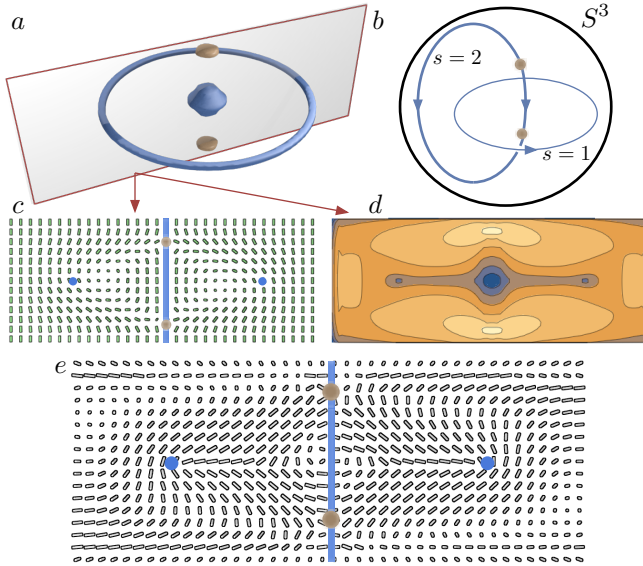


Figure 3.6: Umbilic lines in a toron. (a) Simulation results showing point defects and characteristic umbilic loop in a toron. The umbilic loop is transverse and has zero self-linking number. The point defects have opposite charge, due to lattice effects the simulation does not resolve the umbilic lines connecting them, though they are clear in the topology of the eigenvector field. (b) Diagram illustrating the umbilic structure of the toron in S^3 when the boundary of the cell is collapsed to a point, note that the umbilic loops connecting the point defects each have strength $s = 2$, for a total of 4, as required by (3.13). (c) Simulation results showing director field for the toron. (d) Contour plot showing the value of $|\Delta|$. (e) Eigenvector field of Π . Note that the umbilic loop is generic and has a monstar profile.

in the midplane of the cell. This loop is of generic type, with the eigenvectors of Π having a monstar profile.

As with local properties of umbilic lines, much of the structure of loops is encoded in the 1-form A . Previously we have obtained local information about umbilics by integrating A around a meridian. The first step to understanding their global structure is to integrate A along a longitude. Since A is singular on an umbilic, we must define this integral as a limit. If U_i is an umbilic, then let U'_i be a curve close to U_i that has zero linking number with it. The integral of A over U'_i is well defined and if all the umbilics in the system are closed loops we can take the limit $U'_i \rightarrow U_i$ to obtain

$$\int_{U_i} A = 2\pi \sum_j s_j \text{Lk}(U_i, U_j) + \int_{\Sigma} \Omega_E, \quad (3.28)$$

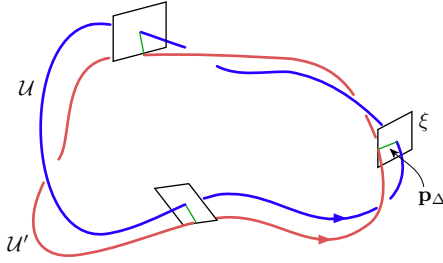


Figure 3.7: The self-linking number for transverse umbilic loops. The red curve U' is formed by pushing U along an eigenvector field p_Δ of Δ . The self-linking number is then computed as the linking number of U with U' . The umbilic must be transverse to ensure that U' does not cross U . Because the eigenvectors are degenerate on the umbilic, one evaluates p_Δ on a line close to U , \hat{U} , that has zero self-linking number with U . Such a line can be found by drawing an orientable surface whose boundary is U and pushing U into that surface. Note that because eigenvectors are line fields, the self-linking number can be a half-integer, corresponding to p being non-orientable along the longitude of U .

where Σ is an orientable surface bounded by U_i . The requirement that U'_i have zero linking with U_i ensures that the limit is well defined but in general the result depends upon this choice of framing. The quantity $\sum_j s_j \text{Lk}(U_i, U_j) = e(U_i)$ in (3.28) is an integer associated to the umbilic line, the relative Euler class, and counts the number of umbilics linking U_i . There are two natural questions to ask of this quantity. The first is whether it corresponds to any local geometric structure of the umbilic line; the second is whether it relates to a global property of n . On both counts the answer is yes. Geometrically (3.28) is related to both a self-linking number and the winding number defined in the previous section. Globally we will show that it is related to the Hopf invariant of n .

To see this suppose U is a transverse umbilic loop, then let \hat{U} be a loop close to U of zero linking number with U . Evaluate one of the eigenvectors of Δ , p_Δ^+ say, along \hat{U} and then push U along this eigenvector field to form a new loop, U' . The linking number $\text{Lk}(U, U')$ is then taken to define the self-linking number of the transverse umbilic, $\text{Sl}(U)$. This construction is shown in Figure 3.7. Note that since p_Δ^+ is a line field, $\text{Sl}(U)$ may be a half-integer corresponding to p being non-orientable along the longitude of U .

With this notion in hand the correspondence between the self-linking

number and the winding number coming from the variation of the local profile defined in the previous section can be established. Choose a trivialisation $\{d_1, d_2\}$ of ξ on a neighbourhood of U such that the linking number of U pushed off along d_1 (say) is zero, then the winding of $\nabla^\xi \Delta^+$ with respect to the chosen trivialisation will give twice the self-linking number. Note that the geometric definition of the self-linking number did not depend on the zero of Δ being of linear order. The relationship between the self-linking number and the relative Euler class of a transverse umbilic is then⁵

$$\text{Sl}(U) = \overline{\text{Sl}}(U) + \frac{1}{2}e(U). \quad (3.29)$$

There is a new term in this equation, $\overline{\text{Sl}}(U)$, the transverse self-linking number of U . $\overline{\text{Sl}}(U)$ is a geometric quantity, preserved under deformations that keep U transverse. A similar notion is studied in the context of contact topology [97] where it provides useful geometric information, but we do not know of a general discussion in the case of arbitrary n .

We now turn to the relationship between the linking of umbilics and global properties of n . Associated to the 1-form A is the Chern-Simons 3-form, $A \wedge dA$, and it is natural to ask whether the integral over the complement of U ,

$$\int A \wedge dA, \quad (3.30)$$

gives some information about umbilic lines and n . This integral can be compared to the similar helicity integral for a fluid flow and the Abelian Chern-Simons action. Both these quantities are related to linking numbers, of vortex lines in the case of helicity [98, 99, 100] and Wilson loops in Chern-Simons theory [101, 102] and, as we will show, it is no different for umbilics, (3.30) connects the linking numbers of the umbilic loops with the Hopf invariant of n . To proceed we will assume that the material domain is S^3 , with no defects and that the zero set of Δ is one-dimensional. By a compactification,

⁵To see that (3.29) is correct it is enough to show that increasing $e(U)$ by 1 increases $\text{Sl}(U)$ by $1/2$ coupled with standard arguments from contact topology [97].

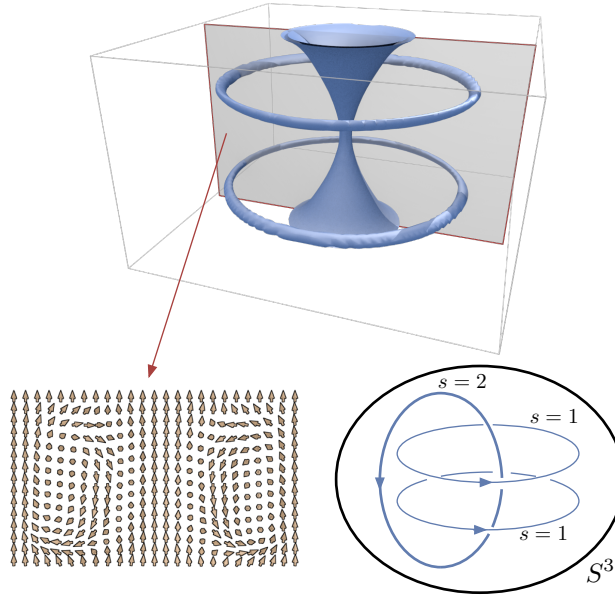


Figure 3.8: Umbilic lines in the Hopf fibration. *Top:* Umbilic lines given as isosurfaces of $|\Delta|$ for a simulated Hopf fibration. The two lines in the mid plane of the cell are both generic, with the same orientation. For symmetry reasons the central umbilic is not generic and has $s = 2$. On the boundary of the cell \mathbf{n} is uniform, which means that the Hopf invariant is well-defined. Note that the system is totally umbilic on the boundary. If you compactify the domain by collapsing the boundary to a point, then one can interpret the central vertical umbilic line as passing through this point. *Bottom Left:* director field for the Hopf texture. *Bottom Right:* Schematic of the relationship between umbilic lines in S^3 . Two generic $s = 1$ umbilic lines each link with one $s = 2$ umbilic line that passes through the point at infinity.

this assumption that the domain is S^3 is equivalent to examining a system in \mathbb{R}^3 for which $\lim_{x \rightarrow \infty} \mathbf{n}(x) = \mathbf{n}_0$, a constant. An example of such a system is illustrated by the Hopf fibration, which has been experimentally realised in frustrated cholesterics [8], illustrated in Figure 3.8, and the aforementioned toron. In both these systems \mathbf{n} is constant on the boundary of the cell. Because of this $\Delta = 0$ on the boundary and one should consider these systems as having an umbilic line passing through the point ‘at infinity’, which in Figures 3.6 and 3.8 is just the boundary of the system.

Topologically the configuration in Figure 3.8 is unusual, it is non-singular but not homotopically equivalent to a constant. The difference is that it has a non-zero Hopf invariant. This integer invariant distinguishes topologically distinct non-singular textures in \mathbb{R}^3 which are constrained to tend to a con-

stant at infinity and is typically visualised in terms of linking of pre-images of two orientations using the Pontryagin-Thom construction [8]. In our setting however one can give a slight re-interpretation of the famous Whitehead integral formula [103], similar to that given by Arnol'd [100], to show that the Hopf invariant is also the Chern-Simons invariant of the bundle ξ . In our interpretation, if one takes a ω to be a connection form for ξ , then $d\omega$ is the curvature of ξ and the Chern-Simons integral

$$\frac{1}{(4\pi)^2} \int_{S^3} \omega \wedge d\omega \quad (3.31)$$

computes the Hopf invariant of \mathbf{n} .

Now we turn back to our integral (3.30). As discussed, we assume the material domain is S^3 (or \mathbb{R}^3 with uniform boundary conditions). This means that we can give a global trivialisation of ξ with connection ω and our 1-form A can be written as $A = d\theta + 2\omega$. This allows us to write

$$\int_{S^3 - \mathcal{U}} A \wedge dA = 4 \int_{S^3 - \mathcal{U}} \omega \wedge d\omega + 2 \int_{S^3 - \mathcal{U}} d\theta \wedge d\omega \quad (3.32)$$

or, since \mathcal{U} has measure zero

$$\int_{S^3 - \mathcal{U}} A \wedge dA = 4(4\pi)^2 H + 2 \int_{S^3 - \mathcal{U}} d\theta \wedge d\omega \quad (3.33)$$

where H is the Hopf invariant of \mathbf{n} . Now we need to evaluate the integral of $d\theta \wedge d\omega$ over $S^3 - \mathcal{U}$. We will first do a simpler integral, over $S^3 - N(\mathcal{U})$, where $N(\mathcal{U})$ is a neighbourhood of the umbilic lines. By Stokes' theorem this can be reduced to an integral over the boundary of $N(\mathcal{U})$ as

$$\int_{S^3 - N(\mathcal{U})} d\theta \wedge d\omega = \sum_i \int_{\partial N(U_i)} \omega \wedge d\theta. \quad (3.34)$$

The boundary of the neighbourhood of each umbilic line is a torus and because our domain is S^3 we can choose a preferred longitude for each torus that has zero linking with the umbilic at its centre. This allows us to specify

a decomposition of each boundary component into $S_M^1 \times S_L^1$. If we choose $N(\mathcal{U})$ small enough, then along each meridian of the torus ω will be approximately constant and equal to its value on the umbilic line. The integral over each boundary component can then be written as:

$$\sum_i \int_{\partial N(U_i)} \omega \wedge d\theta = \sum_i \int_{S_L^1} \omega^* \left(\int_{S_M^1} d\theta^* \right) \quad (3.35)$$

where we have pulled the forms back to each S^1 .

The integral of $d\theta$ is trivial, it evaluates to $s_i 2\pi$, where s_i is the strength of the i^{th} umbilic. Finally, we take a limit as $N(\mathcal{U}) \rightarrow \mathcal{U}$ and obtain a sum of Wilson loop integrals

$$\lim_{N(\mathcal{U}) \rightarrow \mathcal{U}} \sum_i \int_{\partial N(U_i)} \omega \wedge d\theta = 2\pi \sum_i s_i \int_{U_i} \omega. \quad (3.36)$$

Now from the Gauss-Bonnet-Chern theorem (3.13) we can relate intergals of ω along umbilics to integrals of A . Putting this together with the above equations we obtain

$$\begin{aligned} & \frac{1}{(4\pi)^2} \int_{S^3 - \mathcal{U}} A \wedge dA - \frac{1}{8\pi} \sum_i s_i \int_{U_i} A \\ &= 4H - \frac{1}{4} \sum_{ij} s_i s_j \text{Lk}(U_i, U_j) \end{aligned} \quad (3.37)$$

This equation relates analytic data, the integral of $A \wedge dA$ and Wilson loop integrals, to topological data, namely the linking number of the umbilic lines and the Hopf invariant. We hope that this relationship will allow for an interpretation of the creation and destruction of Hopf solitons in terms of umbilic lines.

3.6 EXAMPLES OF LINE FIELDS: BLUE PHASES

So far in this chapter we have been concerned with the geometric properties of vector fields and our discussion of line fields has been confined to

the observation that a local orientating of a director is always possible and so a local definition⁶ of umbilics passes through to the non-orientable case, with the only effect of potential non-orientability relating to the global constraints on umbilic lines, which will be dealt with extensively in Chapter 4.

However, not all orientationally ordered systems are described by either a vector or a director field. In Chapter 1 we considered tensorial order parameters, in particular Q tensors, and it is natural to ask whether umbilic lines exist in these systems also. Much of this section is built around discussion of a beautiful set of examples, the cholesteric blue phases. These remarkable materials are characterised by periodic orientational order corresponding to crystalline space groups, while remaining three-dimensional fluids. Two distinct cubic structures, BPI with space group $O^{8-}(I4_132)$ and BPII with space group $O^2(P4_232)$, are observed on varying temperature or the amount of chiral dopant [104, 105, 106], while several other structures can be induced by applied electric field effects [107, 108, 109] or confinement [110], and there is also an amorphous phase, known as BPIII [111]. Their structure arises because the local optimal configuration for the chiral free energy is one of double twist (illustrated in Figures 3.1 and 3.2), but this is only locally favourable and the structure becomes energetically unstable if it extends too far. This leads to a frustrated arrangement where locally preferred regions of double twist form periodic arrays interwoven by a network of disclination lines [104, 106]. The blue phases have a long-standing association with Skyrmions in chiral magnets, with which they may be considered analogous, and this connection continues to stimulate considerable interchange of ideas between the two fields [112, 115, 113, 9, 114].

To begin our discussion of umbilic lines in Q tensors, we note that as $\xi^* \otimes \xi$ is a subbundle of $T\mathbb{R}^{3*} \otimes T\mathbb{R}^3$ the linear transformation Π , equation (3.10),

⁶Here local has the rather tautological definition of a region in which \mathbf{n} may be oriented, in liquid crystalline systems this will typically mean a region containing no disclination lines.

can be embedded in a 3×3 matrix and expressed, in a Cartesian basis, as

$$\begin{aligned}\Pi_{ij} = & \frac{1}{4}\epsilon_{ilk}\left[n_l\partial_k n_j + n_l\partial_j n_k - n_j n_l n_m \partial_m n_k\right] \\ & + \frac{1}{4}\epsilon_{jlk}\left[n_l\partial_k n_i + n_l\partial_i n_k - n_i n_l n_m \partial_m n_k\right].\end{aligned}\quad (3.38)$$

The issue at hand is what a suitable replacement should be if we express the orientational order using a Q-tensor rather than the director field. The usual approach to obtaining such a replacement is to adopt algebraic methods rather than geometric ones⁷; one constructs a list of potential expressions and selects on the basis of how they reduce when the Q-tensor is written in terms of the director field. Following this procedure, we find that the expression

$$\begin{aligned}\tilde{\Pi}_{ij} = & \frac{1}{4}\epsilon_{ilk}\left[2Q_{lm}\partial_k Q_{jm} + Q_{jm}\partial_k Q_{lm}\right. \\ & \left.+ Q_{lm}\partial_j Q_{km} - Q_{jl}\partial_m Q_{km}\right] \\ & + \frac{1}{4}\epsilon_{jlk}\left[2Q_{lm}\partial_k Q_{im} + Q_{im}\partial_k Q_{lm}\right. \\ & \left.+ Q_{lm}\partial_i Q_{km} - Q_{il}\partial_m Q_{km}\right],\end{aligned}\quad (3.39)$$

reduces to Π_{ij} when the Q-tensor is uniaxial, with constant magnitude, $Q_{ij} \propto n_i n_j - \frac{1}{3}\delta_{ij}$. We subtract its trace and adopt it as an appropriate Q-tensor analogue of Π . In simulations, the umbilic lines can then be identified using isosurfaces where the norm of $\tilde{\Pi}$ drops below a threshold value.

Illustrations are given in Figure 3.9 for some standard blue phase textures. The umbilics coincide with structural motifs that have been identified previously, either through symmetry considerations [116] or by taking a singular value decomposition of the Q-tensor [80]. These motifs are the axes of double twist cylinders [104, 106]. Two remarks are in order concerning this. First, the pattern of umbilic lines in BPII (see Figure 3.9) does not correspond

⁷We are reminded here of a sentiment put forth by Michael Atiyah: “*Algebra is the offer made by the devil to the mathematician. The devil says: ‘I will give you this powerful machine, it will answer any question you like. All you need to do is give me your soul: give up geometry and you will have this marvellous machine.’*”, from page 7 of M.F. Atiyah, *Mathematics in the 20th Century*, Bull. Lond. Math. Soc. **34**, 1-15 (2002).

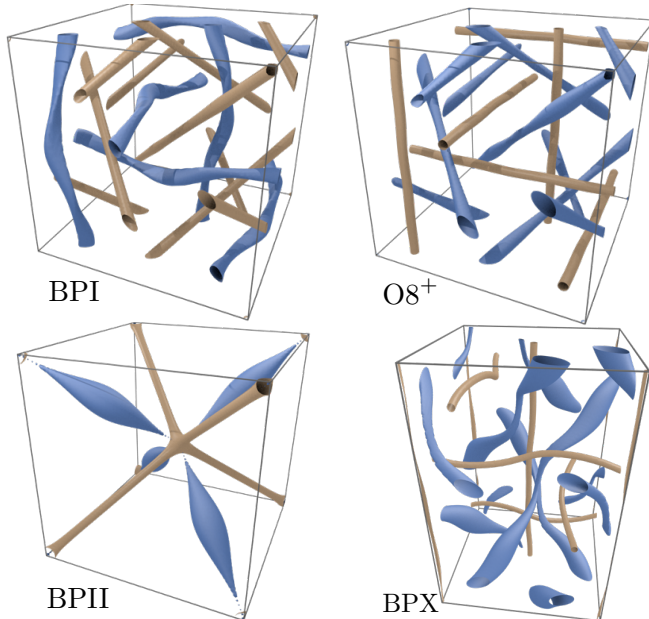


Figure 3.9: Umbilic lines in the blue phases. The umbilics are indicated by blue isosurfaces, while the network of disclination lines is shown by bronze isosurfaces. The textures BPI and BPII are the cubic structures observed experimentally. $O8^+$ is a cubic structure with the same space group as BPI but an interchange between disclination lines and umbilics. BPX is a tetragonal texture observed in an applied electric field. The arrangement of disclinations and umbilics is the same as in $O8^+$, although the symmetry is different.

to the array of double twist cylinders traditionally depicted in the literature. In the traditional depiction the double twist cylinders are taken along the 2-fold axes lying in the faces of the conventional unit cell and, indeed, inspection by eye reveals these lines to have the same general structure as model double twist cylinders [104] (see Figure 3.1). However, in a Q-tensor description of BPII these are not degeneracies where the local structure is axisymmetric, as in the standard idealised picture of a double twist cylinder; rather they are 2-fold lines where the Q-tensor is maximally biaxial [13, 117, 80]. Second, it is perhaps worth emphasising that the umbilics identified in all other blue phase textures also differ from the standard idealised picture of a double twist cylinder. This is because the idealised axisymmetry of the latter constrains it to be a degenerate winding +2 umbilic, whereas those that are found in periodic textures are generic umbilics, typically with a $-1/2$ profile for the eigenvectors of $\tilde{\Pi}$, *i.e.* a star umbilic.

We have given here only cursory illustrations for periodic blue phases with crystalline space groups. It would be of interest to also study the structure of the amorphous BPIII in terms of umbilics, as well as their behaviour in transitions and rheology. The Q-tensor version of the linear transformation Π that we introduced here was motivated on algebraic grounds rather than the geometrical considerations that the rest of our work is founded upon. It is clear that geometrical considerations can be developed for traceless symmetric tensors, parallel to our description of orientational order. It would be interesting to do so and compare the outcome with the algebraic construction we have given. We speculate that since the group of symmetries of the biaxial phase is discrete, the identification of an umbilic line in a Q tensor necessarily coincides with degeneracies in Q itself.

CHAPTER 4

SYNTHESIS: THE CASE OF THE CHOLESTERIC

In this chapter we will bring together ideas from the previous chapters, along with material from the field of contact topology and geometry to try to understand structures and defects in cholesteric liquid crystals.

Cholesterics are liquid crystals with chirality, typically though not always due to a chiral dopant. The result is a propensity for the cholesteric to twist, and the groundstate of such a system is given by

$$\mathbf{n} = \cos q_0 z \mathbf{e}_x + \sin q_0 z \mathbf{e}_y \quad (4.1)$$

which is periodic with period π/q_0 (\mathbf{n} is a director not a vector), a length-scale known as (half the) the pitch of the cholesteric [11]. The value of q_0 controls the rate of twisting, with the sign dictating whether the twisting is right or left handed. The value of q_0 is not only affected by chemical properties such as the amount of chiral dopant, but also physical variables such as temperature. Indeed it is possible to have helical sense inversion as a function of temperature, where the value of q_0 passes from being positive to negative. This process is continuous, and the system does not undergo any phase transition [1].

While this groundstate has a simple form, cholesterics themselves support a huge array of exotic twisted structures, particularly in confined environments, often accompanied by set of line-like features many of which

do not correspond to the singular disclination lines found in nematics, and are instead non-singular. These twisted structures include textures, soliton structures and other phenomena. Of interest to us include various solitons in frustrated cholesterics, including those related to topological objects such as baby Skyrmions [9, 7] and the Hopf fibration [8] and textures displayed by cholesterics such as oily streaks, which consist of various line defects against a helical background, and the related fingerprint and fan textures [118, 119].

Understanding these structures from the perspective of geometry and topology has long stood as a challenge, indeed in his 1979 review [25] Mermin described constructing a theory of defects in cholesterics as an “important challenge which the topological methods have yet to come to terms with” and while various descriptions have been given based on ideas such as the Volterra process [45] and applications of the homotopy theory [120, 44, 11], it is arguable that none of these truly capture the essence of the problem.

Our approach, which we do not claim offers a complete solution, is based on two central notions. The first is the identification of defect lines in cholesterics, which we will argue can be understood in terms of the spin-2 field Δ introduced in Chapter 3. These defect lines can then be related to the global properties of the director discussed in Chapter 2. The second is the idea of topological equivalence between two cholesteric textures, which we will relate to the mathematical idea of contact structures. Attempting to combine these two facets of our description leads one towards areas of Floer theory and contact homologies. Indeed, it seems that ultimately the natural theory of the topology and geometry of cholesterics will be an as-yet undefined form of contact homology.

4.1 OBSERVED DEFECTS IN CHOLESTERICS

Defects in cholesterics have traditionally been studied in model settings such as Grandjean-Cano wedges [121, 122, 123, 46, 43]. In these systems a cholesteric is placed between two plates with strong planar surface anchoring. If the

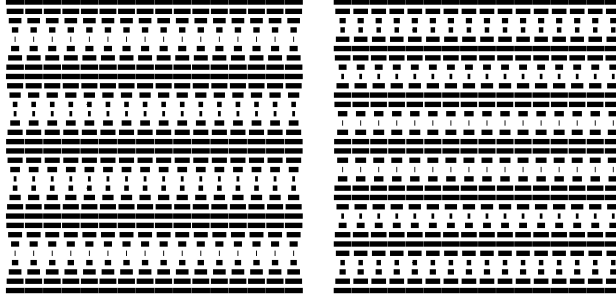


Figure 4.1: Two helical cholesterics in a slab of height L . The left has four twists and the right six.

plates are parallel then the cholesteric will form its helical phase, illustrated in Figure 4.1, with \mathbf{n} undergoing an integer, p , number of twists from one plate to another. Note that if the separation of the plates L is not equal to an integer multiplied by π/q_0 , then the cholesteric will not be at a minimum of the free energy and will be frustrated. The wedge is formed by arranging the plates such that they are at a small angle with respect to each other. At this point one observes a change from p twists to $p + 1$ or $p + 2$ twists as the separation increases. This change in the number of twists is typically mediated by a line defect, pointing in the direction orthogonal to that of increasing cell width. These defects may take several forms, and were first understood using the Volterra process by Kléman and Friedel [45] and were grouped into three categories, λ , τ and χ defect lines, some of which are shown in Figure 4.2.

While wedge and slab geometries provide a controlled setting for the study of defect lines in cholesterics, the same set of lines has, of course, been observed in many other contexts, for example, in simulations of cholesteric droplets [124], frustrated cholesteric cells [125] and in the work of Bouligand [118, 119].

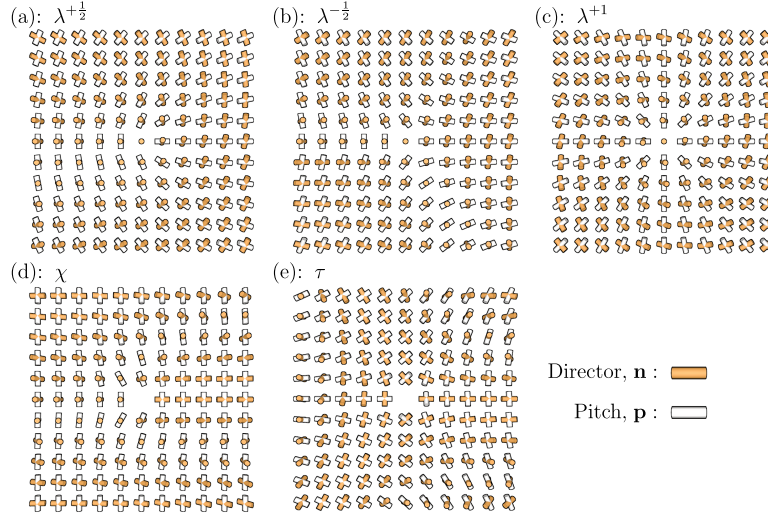


Figure 4.2: Defects in cholesterics and an associated pitch axis, constructed as an eigenvector of Δ . λ defects are defects in the pitch axis, or umbilic lines. χ defects are defects in n . τ lines are defects in n around which the pitch axis is non-orientable.

4.2 THE THEORY OF THE PITCH AXIS

Historically these line defects have been organised through a homotopy theoretic approach involving the introduction of an auxiliary direction in space known as the pitch axis[120, 44, 11]. The theory is centred around the observation that the helical groundstate of the cholesteric, for example

$$\mathbf{n} = \cos q_0 z \mathbf{e}_x + \sin q_0 z \mathbf{e}_y \quad (4.2)$$

consists of n rotating about an axis, in (4.2) this is the z -axis, though in general it is an arbitrary direction p , with $p \cdot n = 0$ and of course one can form a third direction as $n \times p$ ¹. As such, one obtains a triad of directors T . The direction p is also a director, rather than a vector, since directions of twisting are apolar² – think of a helix or corkscrew – and do not distinguish a direction but only an axis. Though, of course, it is apolar for a different reason

¹Some feel that this direction should be called $\not n$ for ‘not n ’.

²In fact a helix, which has a handedness and an apolar direction, is a nice example of an elementary object whose moduli space is a tensor, specifically a rank (in the sense of a matrix) 1 symmetric section of $T\mathbb{R}^{3 \otimes 2}$.

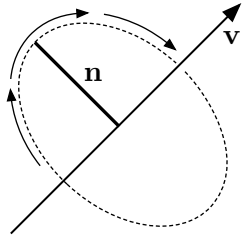


Figure 4.3: The twist of \mathbf{n} along \mathbf{v} can be thought of as the rate of change of \mathbf{n} about \mathbf{v} in the direction along \mathbf{v} .

than \mathbf{n} is apolar, and so one should also allow for a theory of the pitch axis in polar materials as well as liquid crystals.

With the direction \mathbf{p} given, the theory of the pitch axis states that the triad \mathbf{T} is an element in a regular order parameter space which, as a triad of directors, is the biaxial nematic order parameter space. This predicts then, that cholesterics contain no point defects, only line defects. This theory fits remarkably well with the structures found in oily streak cholesterics, as shown in Figure 1.7, where we see that λ lines, which are non-singular in \mathbf{n} , are associated with defects in the pitch axis, χ lines which are simply standard disclinations and τ lines which are singularities in both the pitch axis and the director.

Despite the observational successes of this theory – which indicate that it should be along the right lines – it has a conceptual difficulty. The difficulty is precisely the one raised implicitly by Mermin[25] and Chen[19], in that the direction \mathbf{p} cannot be incorporated into a regular order parameter as it is a quantity derived from \mathbf{n} and as such cannot be varied independently from \mathbf{n} . One can only vary the director and examine the consequences on the pitch axis. Indeed, all one needs to define a cholesteric is a director field, which contains all the information about the phase. One should, therefore, be able to construct a coherent theory of these structures entirely in terms of singularities in the director.

4.2.1 REMEDIES FOR THE PITCH AXIS

To fix the difficulty with this theory, one should try to define the pitch axis as a properly derived quantity in terms of \mathbf{n} . The first point to note is that it is apolar, and as such should be an eigenvector of a particular tensor. Our heuristic notion was that the pitch axis should be ‘the axis along which the cholesteric is twisting’. Following this intuition, one can define the twisting of \mathbf{n} in a direction \mathbf{v} to be the rate of change of \mathbf{n} about \mathbf{v} , shown in Figure 4.3. In a similar vein to Efrati and Irvine’s [78] work in chirality in materials, one can consider the twisting $T(\mathbf{v})$ as

$$T(\mathbf{v}) = \mathbf{v} \cdot (\nabla \mathbf{n}) \cdot (\mathbf{n} \times \mathbf{v}) \quad (4.3)$$

the pitch axis should then be considered as the unit vector \mathbf{p} which maximises $T(\mathbf{p})$. This problem has a simple solution, in index notation one should maximise

$$T(\mathbf{p}) = p_i \partial_i n_j \epsilon_{jkl} n_k p_l - \lambda p_i p_i. \quad (4.4)$$

or

$$T(\mathbf{p}) = p_i M_{il} p_l - \lambda p_i p_i. \quad (4.5)$$

which has the solution

$$\frac{1}{2}(M + M^T) \cdot \mathbf{p} = \lambda \mathbf{p} \quad (4.6)$$

There is one additional assumption to make, that is that $\mathbf{p} \cdot \mathbf{n} = 0$. If one does not account for this then $T(\mathbf{p})$ is affected by the value of $(\mathbf{n} \cdot \nabla) \mathbf{n}$ which is a bend deformation (in particular one can show that (4.6) implies that $\mathbf{p} \cdot \mathbf{n} \propto (\mathbf{n} \cdot \nabla) \mathbf{n}$). Demanding this orthogonality condition one finds that \mathbf{p} should be an eigenvector of the tensor

$$-\frac{1}{2}(\mathbf{n} \cdot \nabla \times \mathbf{n}) I_\xi + \Pi \quad (4.7)$$

where the tensors I_ξ and Π are defined in Chapter 3, and the tensor acts on ξ , the orthogonal 2-plane bundle. The pitch axis \mathbf{p} should then be the eigenvector with largest (in magnitude) eigenvalue.

4.3 UMBILIC LINES AND CHOLESTERIC DEFECTS

With our definition of the pitch axis, we are in a position to describe the types of lines seen in cholesterics. The first, χ lines, are regular disclinations and discontinuities in \mathbf{n} . λ lines then become singularities in the pitch. These are degeneracies in the tensor $-(\mathbf{n} \cdot \nabla \times \mathbf{n}/2)I_\xi + \Pi$, and so are simply generic umbilics, and we can import our entire theory from the previous chapter. The last class of lines, τ lines, correspond to disclination lines around which \mathbf{p} is non-orientable. Note the slightly different definition in comparison with the τ lines found in the biaxial theory. Since the pitch axis is defined in terms of \mathbf{n} , one cannot evaluate the pitch axis along a disclination.

In terms of Π (or indeed Δ) we therefore obtain a consistent theory of defects in cholesterics, in which the various types of defects can all be explicitly derived from the gradients of the director \mathbf{n} ³. As we will show, an advantage of this description is that we immediately obtain a global constraint of the λ and τ defects in the system from the Euler class of the orthogonal 2-plane bundle. Moreover, because we defined the defects in terms of the gradients in \mathbf{n} we can always forget about this additional structure and examine the topology as a nematic.

The relationship between the Euler class and umbilics in simple cases such as in connection to point defects and baby Skyrmions has already been discussed in Chapter 3. Of more interest is the case where one has knotted and linked defect lines. Recalling Chapter 2, if one has a set of disclination lines L in \mathbb{R}^3 with \mathbf{n} null-homotopic at infinity, then, ignoring the equivalence relation, the topological class of \mathbf{n} is given by an element of $H^2(\Sigma(L))$,

³Note that this also allows for ‘orientable cholesterics’ where \mathbf{n} is a vector rather than a director, such as chiral ferromagnets.

where $\Sigma(L)$ is the branched double cover of S^3 over L . We then suppose that the cholesteric defects in the system are described by the tensor Π , which is a section of the vector bundle E . The global constraint on the zeros of Π is then the Poincaré dual of the Euler class of E , which is $e(E) = 4[\mathbf{n}] \in H^2(\Sigma(L))$. If $H^2(\Sigma(L))$ consists wholly of integer summands then the situation is more or less as illustrated in Chapter 3. Of interest are the cases where $H^2(\Sigma(L))$ contains elements of order 2 and 4, since these correspond to no required zeros in Π (or a trivial Euler class).

Suppose one had a director field \mathbf{n} containing a linked disclination set L such that $e(E) = 0$, *i.e.* the element in $H^2(\Sigma(L))$ describing \mathbf{n} is of order 2 or 4. Furthermore, suppose that Π contains no zeros, that is there are no umbilic lines in the system. Our task is to analyse the cholesteric defects in this situation.

Now the vector bundle E is a subbundle of $\xi^* \otimes \xi$ consisting of symmetric tensors and therefore non-zero sections of E have corresponding eigenvectors, \mathbf{p}_1 and \mathbf{p}_2 , previously identified as potential pitch axes. Since, by assumption, \mathbf{n} does not contain any umbilic lines, these eigenvectors are globally defined and are sections of the projectivisation of ξ , $P(\xi)$. There are two possibilities: either the eigenvector fields are orientable, or they are not. If the eigenvector fields are orientable then one can find a non-zero vector field \mathbf{v} parallel to \mathbf{p}_1 . Since $\mathbf{v} \cdot \mathbf{n} = 0$, \mathbf{v} is a section of ξ . Since \mathbf{v} is non-zero, ξ must have vanishing Euler class. The Euler class of ξ is $2[\mathbf{n}]$, and so this corresponds to an element of order 2. Physically, this situation corresponds to no cholesteric defects – since Π is non-zero there are no λ lines and since its eigenvectors are orientable there are no τ lines. As an example take the Hopf link, for which $H^2(\Sigma(L)) \cong \mathbb{Z}_2$. Both these elements are of order two, so there is no obstruction to either of these textures being realised in a cholesteric without either τ or λ lines. Of course, in an actual realisation these may exist for energetic, kinetic or more subtle topological reasons which will be discussed below.

Now we consider the case where the eigenvectors are not orientable. By similar reasoning to that given above, we therefore conclude that $[n]$ is an element of order 4. What of the cholesteric defects in this case? By assumption there are no umbilic lines in the system, and yet the eigenvectors of Π must be non-orientable. This implies that there are closed loops in $\mathbb{R}^3 - L$ around which these eigenvectors are non-orientable. The only closed loops in $\mathbb{R}^3 - L$ are those that encircle defect lines, hence there must be disclination lines around which Π is non-orientable – these are τ lines.

The natural question to ask at this point is: given a defect set L with an associated homotopy class which is an element of order 4, can one determine where the τ defect lines can be? If one has a system containing only disclination lines, some of which are τ lines, then the τ lines can be represented by a set of longitudes. The homotopy class of n can then be determined by deducing which element in $H_1(\Sigma(L))$ gives, up to cobordism, a longitude when multiplied by 4.

An example is shown in Figure 4.4. The link known as Solomon's Seal has an associated group \mathbb{Z}_4 , which contains two elements of order 4 and one element of order 2, therefore there is no obstruction to every possible homotopy class of texture in its complement having no umbilic or λ lines. Textures corresponding to the two elements of order 4, however, must contain τ lines. To understand this, note that a generator of this group can be represented as a tether connecting the link components. Denote this tether by t , then $4t$ is equivalent to either of the longitudes. Hence, the elements of order 4 can be realised as one χ line (disclination) and one τ line. Note that if one would bring together the two defect lines, the result would be a λ line.

An amusing counterexample to this case is the Hopf link. One can ask whether it is possible to have a τ line linking with a regular disclination. This would imply that there was an element of order 4 in the group $H_1(\Sigma(L))$ for the Hopf link. But we know that in this case the group is \mathbb{Z}_2 , which has maximum order 2, and so one cannot find a τ line linking a regular disclination.

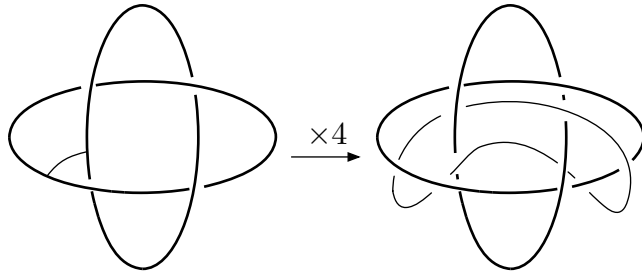


Figure 4.4: Solomon's Seal and τ lines in a cholesteric. For Solomon's Seal $H_1(\Sigma(L)) = \mathbb{Z}_4$, this implies that for textures corresponding to elements 1 and 3, there is no topological obstruction to the removal of umbilic lines, but that such a removal would result in the pitch axis being non-orientable, indicating the existence of τ lines. A generator of $H_1(\Sigma(L))$ is indicated on the left, as a tether connecting the two components. Multiplying this by 4, one finds a cycle that is cobordant to a longitude of either of the link components. Either of these, therefore can be realised as τ lines. Finally, note that if one would bring together the two defect lines, the result would be a λ line.

This statement has its analogue in the theory of biaxial nematics (and thus the theory illustrated in §4.2), defects of type i and j may not link without a tether. The technical statement of this constraint is that there must exist a homomorphism from the fundamental group of the link complement onto the group Q [29]. Given this, it is natural to ask if other phenomena in the biaxial theory have their analogues in our construction. One natural question to ask is if a λ line may cross a disclination. In the biaxial case we know the following: recalling the definitions in Chapter 1, the fundamental group of the biaxial order parameter space is the set of quaternions generated by $\{i, j\}$ and has four classes of defects given by $-1, \pm i, \pm j$ and $\pm k$. The crossing of two defect lines of type x and y leaves a tether of type given by the commutator $xyx^{-1}y^{-1}$ (if the group is abelian then crossing of defect lines is possible). If one uses the theory of biaxials as a model for cholesterics, then it predicts that the crossing of λ defects and disclinations will lead to a tether. If one identifies a disclination (χ defect) as i and a λ line as j , then the tether created by their crossing is of type $i \cdot j \cdot -i \cdot -j = -1$.

Let us consider the corresponding situation where now the λ line is a generic umbilic. As discussed, the Euler class supplies a global constraint for

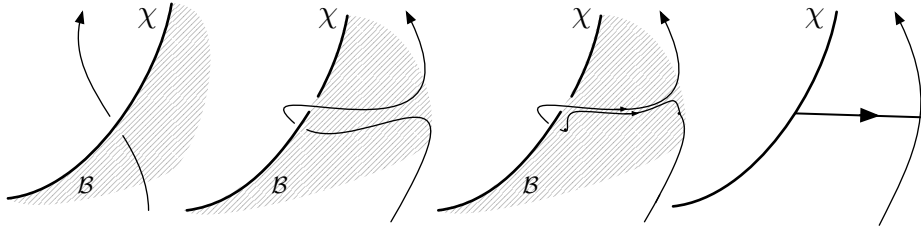


Figure 4.5: Umbilic Crossing a Disclination. From left to right. A disclination χ and an umbilic, B is a branch set for the disclination lines in the system. The umbilic line is moved in such a way as to preempt crossing the disclination line, because it does not cross B it can be given a consistent orientation. The umbilic line is homotoped so that it crosses B , its orientation must be reversed at these crossing points. A further homotopy is performed, creating a $s = 2$ strength umbilic as a ‘tether’ connecting the two defect lines.

the umbilics, and hence λ lines, in the system. The constraint is in the form of an element of the first homology of the double cover of the complement of the defect set. As such, one expects that λ lines should not be able to simply cross disclination lines in nematics, since this would change their homology class. In fact, considering λ lines as umbilic lines leads to precisely the same conclusion as the biaxial based theory. This is illustrated in Figure 4.5, which shows that an attempt to make a generic umbilic line cross a disclination creates a ‘tether’ comprising a non-generic umbilic. The standard non-generic umbilic corresponds exactly to the standard -1 disclination.

4.4 TWO-DIMENSIONAL SMECTICS

At this point, it is instructive to consider the topology of two-dimensional smectic liquid crystals[126, 19], with which our work shares many similarities. Smectics are liquid crystals with an additional layered structure, typically forming at lower temperatures than nematics, that is the system has 1 dimensional positional order, where d is the dimension of the space. This layered structure is such that the director in a smectic (type A) points in a normal direction to the layers. A naive approach to understanding this system is then to have two objects describing the order, a phase ϕ describing the layer structure, along with the regular director \mathbf{n} , and then studying the

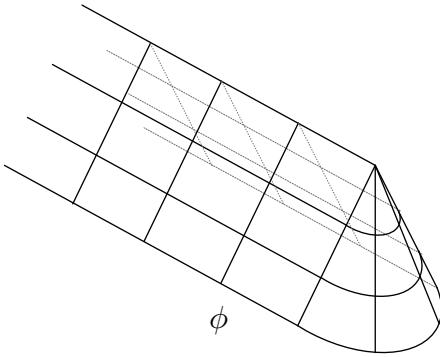


Figure 4.6: A surface corresponding to a phase field ϕ in 2d smectic, the associated director $\mathbf{n} = \nabla\phi/|\nabla\phi|$ contains a $+1/2$ defect at the end of the ridge.

topology of each separately. As observed by Mermin[25], this fails because the director and the phase are related, $\mathbf{n} = \nabla\phi/|\nabla\phi|$, a condition that must be satisfied at all times. Indeed, as shown by Poénaru [127], this implies that a two dimensional smectic can have no defects of winding higher than $+1$.

The resolution of this problem can be phrased in many equivalent ways. \mathbf{n} is completely determined by ϕ , which can be visualised as a surface [126], shown in Figure 4.6, and as such serves as the description of the order. Singularities in \mathbf{n} , or disclinations in the smectic, are then entirely determined by this surface, and can be thought of as an additional structure sitting on top of the basic description, which is simply the phase field ϕ . As discussed above we find an analogous situation in cholesterics, where the observed λ lines are described as umbilics. In the same way that disclinations in the 2d smectic are derived from ϕ , λ lines are derived from \mathbf{n} , which serves as the basic description of the order.

4.5 THE WEAKLY TWISTED CASE

This perspective, in which the additional cholesteric defects sit on top of the basic nematic description, has an advantage when considering systems such as weakly twisted cholesterics. The identification of and emphasis on λ , τ and χ lines in experimental cholesteric systems comes from their easy

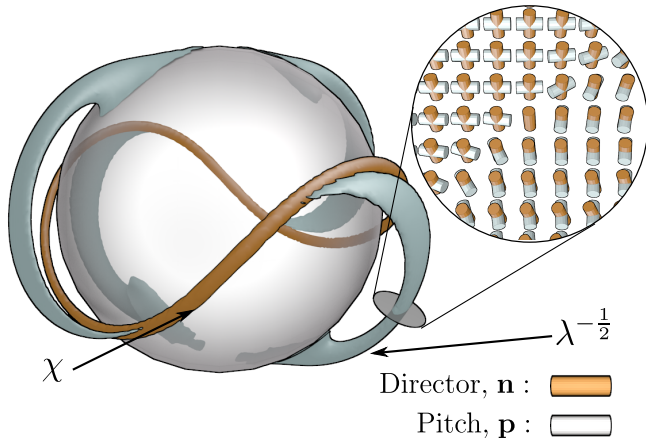


Figure 4.7: Simulation of umbilic lines in a Saturn's ring configuration. Placing a colloid with homeotropic anchoring conditions into a cholesteric liquid crystal can induce the type of twisted disclination line seen here. From topological considerations, one expects (and observes) the existence of four generic umbilic lines, given in blue, connecting the disclination line to the colloid. These lines do not have a strong optical signature experimentally, as opposed to those that correspond to λ lines.

optical identification in strongly twisted cells. Focussing on λ lines, which we have identified as umbilics, one might wonder whether all umbilic lines in a cholesteric always correspond to λ lines as they are identified experimentally. The answer to this question is no. Essentially this is because umbilics are perfectly well defined in nematics, and one can continuously transform a nematic into a cholesteric. Indeed, in weakly twisted systems ($Lq_0 \ll 1$, where L is the system size) one can observe bare charge 1 point defects in $n[11]$. While such a point defect necessarily has umbilic lines of total strength 4 emerging from it, they are not experimentally visible. A similar situation occurs for Saturn's ring structures. In cholesterics, with $Lq_0 \sim 1$ the familiar defect loop twists up around the colloid [128, 129, 130]. Optical images do not reveal any noticeable umbilic lines, though simulations, shown in Figure 4.7 show that they exist.

4.6 THE FREE ENERGY AND GEOMETRY OF A CHOLESTERIC

So far we have only discussed the identification of defects in the cholesteric. A more subtle question is that of topological equivalence of different configurations. Again making the analogy to the case of two dimensional smectics, we know that deformations of a texture can be visualised by deformations of the surface corresponding to ϕ . Our task is finding the equivalent structure in the case of cholesterics.

To do this, we must first examine the elastic energy of the cholesteric. One of the essential characteristics of the cholesteric is that in its ground-state the director field has non-zero gradients. A short inspection of possible elastic free energies reveals that, not only is the cholesteric the lowest order extension of the nematic having a groundstate with non-zero gradients, but that the geometric characterisation of the cholesteric is $\mathbf{n} \cdot \nabla \times \mathbf{n} = -q_0$.

Since a cholesteric can be obtained from a nematic by varying temperature without a phase transition, the description of a cholesteric must reduce to that of nematic, and its description must be given completely in terms of a director field. Recalling our discussion in Chapter 1, we know that the free energy for a unit vector field, including only first order derivatives, can be written (excluding saddle-splay) as

$$F = \int \frac{K_1}{2} (\nabla \cdot \mathbf{n} + s_0)^2 + \frac{K_2}{2} (\mathbf{n} \cdot \nabla \times \mathbf{n} + q_0)^2 + \frac{K_3}{2} ((\mathbf{n} \cdot \nabla) \mathbf{n})^2 dV. \quad (4.8)$$

From this we can clearly see that the only two linear terms allowed correspond to s_0 and q_0 being non-zero, since these are identified with sections of line bundles. However, for a director field, we cannot have $s_0 \neq 0$, since we cannot distinguish \mathbf{n} from $-\mathbf{n}$. Hence we find that for a director field, the lowest order adjustment to the gradients to ensure the groundstate is non-zero is to make $q_0 \neq 0$, at which point we find that $\mathbf{n} \cdot \nabla \times \mathbf{n} = -q_0$ characterises the propensity of the cholesteric to twist. This requirement has a

natural geometric meaning, \mathbf{n} is never the normal to a system of layers. To see this note the following. Suppose \mathbf{n} is the normal to a system of layers. If Σ is an arbitrary patch of one of the layers, with boundary $\partial\Sigma$, then we know that

$$\int_{\partial\Sigma} \mathbf{n} \cdot d\mathbf{l} = 0, \quad (4.9)$$

but by Stokes' theorem we have

$$\int_{\partial\Sigma} \mathbf{n} \cdot d\mathbf{l} = \int_{\Sigma} (\mathbf{n} \cdot \nabla \times \mathbf{n}) dA. \quad (4.10)$$

Since Σ was arbitrary this gives $\mathbf{n} \cdot \nabla \times \mathbf{n} = 0$ as the requirement for \mathbf{n} to be the normal to a foliation.

4.7 CHOLESTERICS AND CONTACT STRUCTURES

With the energetic and geometrical condition of $\mathbf{n} \cdot \nabla \times \mathbf{n} = -q_0 \neq 0$ of the cholesteric we can begin to understand the topology of deformations. Suppose that a cholesteric undergoes a deformation induced by, say, a change of boundary conditions, or an external field. Then, given the form of the static elastic energy, there is a strong energetic preference for $\mathbf{n} \cdot \nabla \times \mathbf{n} \approx -q_0$ throughout the material during this process. A simple scale-free constraint on the system is therefore to demand that $\mathbf{n} \cdot \nabla \times \mathbf{n} \neq 0$. Note that this constraint is natural both geometrically and energetically. In mathematics there is a similar class of objects known as contact structures [97], and we will consider the consequences of making this analogy. Contact structures are non-integrable rank 2 subbundles of the tangent bundles of a given manifold, note that if one has a metric there is a simple equivalence between rank-2 subbundles and director fields. Contact structures are defined locally as (the kernel of) a one-form α such that $\alpha \wedge d\alpha > 0$. The local restriction here is the same as the fact that a director field can locally be thought of as a unit vector field.

Making the connection explicit, we will think of cholesterics as a unit

vector field \mathbf{n} such that the orthogonal 2-plane bundle ξ is non-integrable. The notion of equivalence between two cholesteric field configurations is then an isotopy, that is \mathbf{n} and \mathbf{n}' are isotopic if there is a one parameter family of director fields \mathbf{n}_t , $t \in [0, 1]$, with $\mathbf{n}_0 = \mathbf{n}$ and $\mathbf{n}_1 = \mathbf{n}'$, such that for each t , the corresponding 2-plane bundle, ξ_t , is non-integrable⁴, or that $\mathbf{n}_t \cdot \nabla \times \mathbf{n}_t \neq 0$.

This formulation has immediate consequences for the topological classification of cholesterics. Two director fields that are topologically equivalent as nematic textures can fail to be equivalent as cholesterics, that is to pass from one texture to another requires going through a state where at some point in the material $\mathbf{n} \cdot \nabla \times \mathbf{n} = 0$, which is energetically costly. The most elementary of these properties is that a helical state with $\mathbf{n} \cdot \nabla \times \mathbf{n} > 0$ is not equivalent to its mirror image with $\mathbf{n} \cdot \nabla \times \mathbf{n} < 0$ (though they are equivalent as nematics). Therefore, as one might hope, the handedness of the system is preserved in this theory and cholesterics of opposite chirality are considered distinct. This trivial distinction is always present, and for every isotopy class of contact structure we consider with $\mathbf{n} \cdot \nabla \times \mathbf{n} > 0$, there is a corresponding one with $\mathbf{n} \cdot \nabla \times \mathbf{n} < 0$. Henceforth we will consider only so-called ‘positive’ contact structures with $\mathbf{n} \cdot \nabla \times \mathbf{n} > 0$, but all our statements have their equivalents regarding negative contact structures.

While the distinction of handedness is trivial, what is surprising is that the theory of contact structures allows more subtle distinctions between cholesteric configurations. To understand this one needs to know the classification of isotopy classes of contact structures for a given manifold. This problem is in general unsolved though in many cases much is known. The principal distinction in this direction is the tight/overtwisted dichotomy. A contact structure is called overtwisted if one can find an embedded disk Σ such that the tangent vectors on each point of $\partial\Sigma$ are orthogonal to \mathbf{n} and the normal

⁴As a note we should mention that for contact structures on open manifolds, such as \mathbb{R}^3 , it is common in the mathematical literature to consider proper isotopies, those that are induced by diffeomorphisms of the underlying manifold.

to Σ coincides with \mathbf{n} on $\partial\Sigma$. The condition of tight or overtwisted is preserved by isotopy and so can distinguish contact structures.

Mathematically this notion induces distinctions that are strictly finer than the homotopy classification of director field. One can convert any tight contact structure into an overtwisted one without changing its homotopy class as a 2-plane field [131, 97], through a process known as a Lutz twist. In fact, overtwisted contact structures have considerable topological freedom and in a seminal paper Eliashberg showed that the isotopy classes of overtwisted contact structures coincide with the homotopy classes of 2-plane fields [132]. In the language of liquid crystalline order this implies that the topological classification of overtwisted cholesterics is the same as nematics. Tight contact structures are more elusive, and their classification is not yet fully understood mathematically, though many known results correspond to experimentally relevant situations.

This perspective suggests an explanation for why chiral systems exhibit many soliton structures that are not found in regular nematics. If one has an overtwisted cholesteric, then it cannot relax to a helical state – which is shown below to be tight – without either passing through a region where it is not twisted or creating defects. Such an operation will be energetically costly, indeed a region of zero twist has a local free energy density cost bounded below by $K_2 q_0^2/2$. As such, solitons in cholesterics that correspond to overtwisted contact structures may well enjoy increased stability.

Amusingly, the standard examples of tight and overtwisted contact structures are very familiar to those who study cholesteric liquid crystals. The first is the standard helical cholesteric phase, given by

$$\mathbf{n} = \cos q_0 z \mathbf{e}_x + \sin q_0 z \mathbf{e}_y \quad (4.11)$$

where $\{x, y, z\}$ are standard cartesian coordinates in \mathbb{R}^3 , and $\{\mathbf{e}_x, \mathbf{e}_y, \mathbf{e}_z\}$ the corresponding basis for $T\mathbb{R}^3$. The second is the ‘double twist cylinder’ tex-

ture, given by

$$\mathbf{n}_{ot} = \cos q_0 \rho \mathbf{e}_z - \sin q_0 \rho \mathbf{e}_\phi \quad (4.12)$$

where $\{\rho, \phi, z\}$ are cylindrical coordinates. Both (4.11) and (4.12) define contact structures, with $\mathbf{n} \cdot \nabla \times \mathbf{n} < 0$ (if $q_0 > 0$). The double twist cylinder is overtwisted, the disk defined by $z = 0$ and $\rho \leq \pi/q_0$ has a boundary curve whose tangent vector is orthogonal to \mathbf{n} . The standard helical cholesteric is tight, since there is an isotopy of contact structures given by

$$\mathbf{n}_t = \cos \phi_t \mathbf{e}_x + \sin \phi_t \mathbf{e}_y \quad (4.13)$$

with

$$\phi_t = tq_0 z - (1-t)\arctan z, \quad (4.14)$$

from the standard tight contact structure on \mathbb{R}^3 to the helical cholesteric. As such, the standard cholesteric helical phase and the double twist cylinder are not isotopic as cholesterics, though they are as director fields.

While this example is a nice illustration of the distinctions induced by these considerations, it is only a toy set-up, the double twist cylinder is typically only used as a local model in the vicinity of the axis. Nevertheless it indicates that one might try to associate double twist cylinders, and hence umbilic lines, to measures of overtwistedness. This will be done in §4.8, where we will show that self-linking of umbilic lines in a cholesteric can relate to overtwistedness. Before this, however, we will go through an example of a physical situation where the notion of contact structures can help us understand chiral systems.

4.7.1 SOLITONS IN A CHOLESTERIC BACKGROUND

As mentioned in the introduction, cholesteric liquid crystals support a large number of metastable soliton structures. A beautiful series of examples are given by Bouligand, who shows a large number of soliton structures in cholesterics against a helical background [43]. To construct a model for this situation

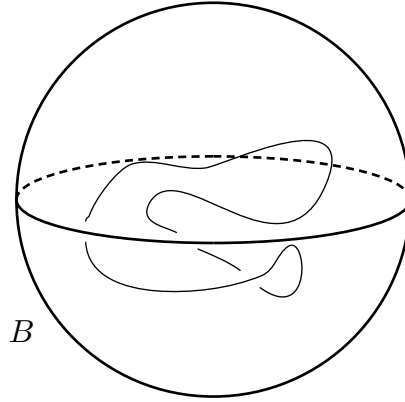


Figure 4.8: The setup for §4.7.1, outside of a ball B , the texture is the standard helical texture. Inside B is a non-singular soliton structure, S . The isotopy class of S relative to the boundary of B is given by the following information. If it is tight, then it is unique. If it is overtwisted then it is given by an integer, corresponding to the Hopf invariant.

we proceed as follows. We will assume that our soliton contains no disclinations lines, in fact we assume that \mathbf{n} has no singularities, and that it is contained in a ball B such that \mathbf{n} coincides with a standard helical phase on the complement of the interior of B .

We will first analyse this situation as a nematic. In this case we have to consider homotopy classes of maps $B \rightarrow \mathbb{RP}^2$ relative to the boundary. Restricted to ∂B we have a map $S^2 \rightarrow \mathbb{RP}^2$. This map must be null homotopic, since it extends to a non-singular map in the interior. The homotopy classes are therefore equivalent to maps $S^3 \rightarrow \mathbb{RP}^2$, which are classified by an integer, $h \in \mathbb{Z}$, the Hopf invariant.

Now we consider the case of contact structures. Our problem is isotopy classes of contact structures in a ball, relative to the boundary, where the contact structure on the boundary comes from the tight helical contact structure. This problem has been solved, see [133], for example. The solution states that up to isotopy there is a unique tight positive contact structure which has $h = 0$, and a single overtwisted positive contact structure in every homotopy class of \mathbf{n} as a director field. As such, we gain an extra topological distinction between configurations, the tight and overtwisted contact struc-

tures with $h = 0$, that does not exist in the nematic case. It is also interesting to note that all Hopf solitons are overtwisted.

The overtwisted $h = 0$ soliton would, therefore, be a cholesteric that was homotopic to the helical phase, but not isotopic as a contact structure. A transition to the helical phase would necessarily require passing through an energetically costly state where, in some portion of the material, $\mathbf{n} \cdot \nabla \times \mathbf{n} = 0$, and so may be suppressed.

4.8 OVERTWISTEDNESS AND UMBILIC LINES

So far, our discussion of cholesterics has been split into two halves, the half concerned with contact topology and the half concerned with umbilic lines. The discussion of overtwisted contact structures suggests that one might find a connection between umbilics and overtwisted contact structures. Such a connection does indeed exist, though we feel that what we present here represents only elementary aspects of a deeper theory.

Suppose one has a cholesteric with a transverse umbilic line. Recalling the definition in Chapter 3, these are umbilic lines whose tangent vector is always transverse to the 2-planes defined by \mathbf{n} . Amusingly such lines are intimately connected with the non-integrability of \mathbf{n} . More formally, in a simply connected domain transverse umbilics can only exist if $\mathbf{n} \cdot \nabla \times \mathbf{n} \neq 0$. If we are in such a domain and \mathbf{n} defines a non-singular foliation then there is a function ϕ such that $\nabla \phi$ is parallel to \mathbf{n} . Then integrating along an umbilic loop we have

$$\int_U d\phi = 0 \quad (4.15)$$

and so $\nabla \phi$ must be orthogonal to the tangent vector at at least two points and the umbilic is not transverse. Hence transverse umbilics can only exist if $\mathbf{n} \cdot \nabla \times \mathbf{n} \neq 0$ somewhere in the material. Given such a transverse umbilic

U , we defined a self-linking number which decomposes as

$$\text{Sl}(U) = \overline{\text{Sl}}(U) + \frac{1}{2}e(U). \quad (4.16)$$

In terms of the pitch axis, this can be thought of as the twisting of the pitch axis along a λ line. For us, the important component is $\overline{\text{Sl}}(U)$. If n defines a (positive) contact structure, then a transverse U is a transverse knot in this structure. The definition of such a knot is simply a curve whose tangent vector is transverse to the contact structure. A theorem of Etnyre's states that, for such a knot U with Seifert surface Σ , if

$$\overline{\text{Sl}}(U) > -\chi(\Sigma), \quad (4.17)$$

where $\chi(\Sigma)$ is the Euler characteristic, then the contact structure is overtwisted [134]. In particular, if U is an unknot, then its Seifert surface is a disk, which has $\chi = 1$ and so the existence of a transverse unknotted umbilic (λ line), such as those observed in both torons and Hopf solitons discussed in Chapter 3, in a cholesteric implies that the cholesteric is overtwisted and as such cannot relax to a helical configuration without untwisting.

4.9 FLOER THEORIES AND BEYOND

So far, throughout this entire thesis we have been primarily concerned with static configurations and have given only a cursory amount of attention towards dynamic configurations. Doing so reveals that the structure we have given so far is incomplete. Suppose one has a director field n_1 in \mathbb{R}^3 with an initial set of defects \mathcal{D}_1 and then, after some time, the configuration changes to n_2 with a new set of defects \mathcal{D}_2 . To model this situation one can introduce a cobordism with the 4-manifold $M = \mathbb{R}^3 \times [0, 1] - \mathcal{E}$, where one considers the fourth dimension as time and the set \mathcal{E} is such that $\mathcal{E} \cap \mathbb{R}^3 \times \{0\} = \mathcal{D}_1$ and $\mathcal{E} \cap \mathbb{R}^3 \times \{1\} = \mathcal{D}_2$. M therefore represents the changing domain. Finally, one

equips M with a director field \mathbf{n} , considered as a map $\mathbf{n} : M \rightarrow \mathbb{RP}^2$. Now, let $G(\mathcal{D}_1)$ denote the space of homotopy classes of textures with a given defect set. From Chapter 2 we know that this is equal to an abelian group $V(\mathcal{D}_1)$ modulo the equivalence relation $x \sim -x$. If we fix a lift to S^2 then we can, without ambiguity, consider both the beginning and final configurations as corresponding to elements in the groups $V(\mathcal{D}_1)$ and $V(\mathcal{D}_2)$. We would like to understand how one can go from an initial state to a final state. Ideally, there would be a map induced by the cobordism, that is $h_M : V(\mathcal{D}_1) \rightarrow V(\mathcal{D}_2)$. It is clear, through inspecting several examples, however, that in terms of the structures we have been considering, such a map cannot exist. However, there is a large class of theories associated to 3 manifolds, known under the umbrella term of Floer homology theories, which have precisely this property, they are functorial with respect to cobordisms [135]. Of particular interest are the class of such theories known as contact homology theories, such as embedded contact homology [136, 137] and symplectic field theory [138]. These theories are typically generated by closed orbits of the Reeb vector field. In physical terms these are vortex lines, closed orbits of $\nabla \times \mathbf{n}$. It seems that a natural extension, therefore, of the perspective that we have developed is to construct a Floer theory of cholesterics, which is generated by either umbilic lines or vortex lines, and which is consequently functorial with respect to cobordisms, and thus changes in the defect topology. A further potential advantage of such a theory would be specific to cholesterics. Theories of contact homology are often sensitive to properties involving the tight/overtwisted dichotomy and, as such, one may be able to understand distinct tight cholesteric structures associated to defect lines and as a consequence the topology of various cholesteric solitons associated to knotted defects, such as those shown in Figure 4.9.

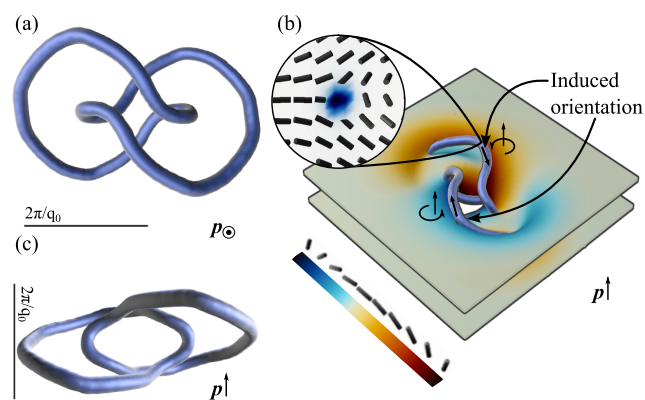


Figure 4.9: Stable Hopf link disclination embedded into a helical background. Note that the shape of the defect line is similar to that of a transverse knot in a contact structure [97]. It is hoped that such structures may be understood with a Floer theory.

CHAPTER 5

DEFECTS INDUCED BY NON-ORIENTABLE COLLOIDS

In modern experiments the most common way to manipulate and create defect-laden structures of liquid crystals on a fine scale is the use of colloidal particles. These micro- or nano-metre particles are dispersed into a liquid crystalline system with a particular material or coating inducing a particular alignment of the liquid crystal on the surface. These boundary conditions and the far field boundary conditions that are also controlled are often topologically incompatible leading to the creation of defects. A thorough review of these systems is available in [139].

Perhaps the most famous example of this is the saturn's ring defect produced around a spherical colloid with homeotropic (normal) anchoring, illustrated in Figure 5.1. As we will discuss, in a system with a uniform far-field, the topology of a spherical colloid with homeotropic anchoring demands the creation of a defect. While this defect can be realised as a point defect in a dipolar configuration with the colloid [140], it may also be elongated to form a loop encircling the colloid [141]. This system and its extensions has produced many beautiful results, many of which inspired much of the work presented in this thesis.

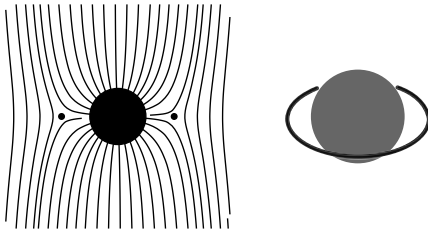


Figure 5.1: Saturn's ring defect line around a spherical colloid with homeotropic anchoring. The defect line has a $-1/2$ profile.

5.1 COLLOIDS AND THE TOPOLOGY OF SURFACES

As mentioned, for a spherical colloid, the defect created can be either a point defect or a line defect. This suggests that the distinction between the line and the point defect is not a topological one but rather energetic¹ and so a discussion of the topological aspects of colloids is useful. From the point of view of the liquid crystal, colloids are determined entirely by their surface, as it is only the surface that comes into contact with the liquid crystal. As such, the topology of the defects created should be a direct consequence of the topology – as a surface – of the colloidal particle. Fortunately for us the topology of surfaces is a classical subject and so the analysis can be done with a minimum of effort.

A colloidal particle is always contained within a small region of space and we all assume that it is not particularly pathological, for example it has no fractal structure. Mathematically we will say that it is a compact surface. The classification theorem of surfaces [142] states that any compact surface can be classified up to homeomorphism by its genus, orientability and number of boundary components. The genus is equal to the number of holes or handlebodies possessed by a surface; for example, a torus has genus one and a sphere genus zero. Orientability implies a consistent choice of normal vector can be made on a surface. The one-sided Möbius strip is the classic non-orientable surface; any normal vector on the strip will be flipped by going

¹We are not suggesting that a loop and a point are topologically equivalent!

around the strip once, forbidding a consistent choice of surface normal. Finally, the number of boundary components is simply the number of distinct connected components in the surface boundary, *e.g.* a disk has one boundary component and a torus has none.

While this is a complete topological classification of surfaces in an abstract setting, for applications they must also be embedded (no self-intersections) into ordinary three-dimensional space, \mathbb{R}^3 . Different embeddings are interesting in their own right – the whole of knot theory concerns embeddings of a circle into \mathbb{R}^3 – but they do not affect the local class of the defect necessitated in the bulk, which we focus on first. Thus, with the classification of surfaces in mind it is natural to ask what topological implications each type of surface has for accompanying defects in the surrounding liquid crystal. The complete classification, summarised in Fig. 5.2, naturally separates into four classes of surfaces; orientable or non-orientable and closed or with boundary.

Closed, orientable surfaces are known to induce defects corresponding to the element $1 - g = \chi/2$ of $\pi_2(\mathbb{RP}^2)$, where g is the genus of the surface and χ is the Euler characteristic [35, 143]. Briefly, this relation comes through computing the degree of the Gauss map of the surface. The Gauss map, \mathcal{G} , of a surface, X , is a map $\mathcal{G} : X \rightarrow S^2$ that sends every point of the surface to the direction of the surface normal at that point. For orientable surfaces with normal anchoring, the director can be given the orientation of the Gauss map, so that \mathcal{G} describes precisely the molecular orientation at the surface. The degree of this map – the number of times every point on S^2 is visited, counted with sign – is a homotopy invariant [35] characterising the type of defect that the surface generates [143]. Although experimentally the same surface can produce seemingly different defects, they are always characterised by this same element of $\pi_2(\mathbb{RP}^2)$. As in our example, where spherical colloids can nucleate either a point defect [140] or disclination loop [141] but the loop can always be shrunk continuously into a point [144], so that it

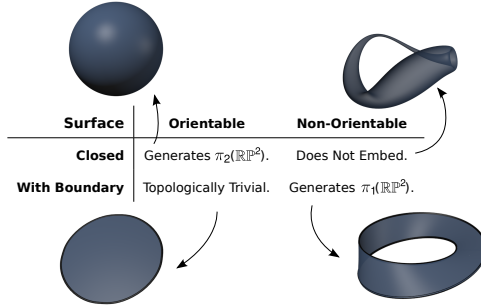


Figure 5.2: Topological characterisation of compact surfaces with homeotropic boundary conditions, embedded in a three-dimensional, nematic liquid crystal. Closed orientable surfaces generate elements of $\pi_2(\mathbb{RP}^2)$, equal to one minus the genus of the surface. Non-orientable surfaces with boundary generate the non-trivial element of $\pi_1(\mathbb{RP}^2)$, which forces the nucleation of disclination lines in the bulk.

is more properly classified by $\pi_2(\mathbb{RP}^2)$. More generally, orientable surfaces can never generate elements of $\pi_1(\mathbb{RP}^2)$, *i.e.* disclinations, as a topological requirement. Their orientability ensures that any disclination loops formed can always be removed in pairs or shrunk into points.

Closed, non-orientable surfaces cannot be embedded in \mathbb{R}^3 without self-intersection, meaning that a true representation of any of these (*e.g.* the real projective plane or the Klein bottle) in a liquid crystal is not possible. For this reason, we do not consider closed, non-orientable surfaces any further.

Orientable surfaces with boundaries have trivial topological implications for the surrounding liquid crystal. Their orientability, as in the closed case, forbids them from generating elements of $\pi_1(\mathbb{RP}^2)$ as a topological necessity. In addition, since they have a boundary, they cannot generate any elements of $\pi_2(\mathbb{RP}^2)$. We argue as follows. Closed, orientable surfaces separate space into an inside and an outside and they generate point defects in *both* regions. If one cuts a hole in the surface, creating a boundary component, then these defects can be combined to leave a defect-free texture. Cutting more holes in the surface will not change things as one could always make the texture on the new hole identical to the surface normal that was removed.

Non-orientable surfaces with boundary necessarily generate a non-trivial element of $\pi_1(\mathbb{RP}^2)$. A generalisation of the Gauss map to non-orientable

surfaces $\bar{\mathcal{G}} : X \rightarrow \mathbb{RP}^2$ assigns to every point of the surface the line element (point in \mathbb{RP}^2) corresponding to the direction of the (unoriented) surface normal². Now consider the loop space of our surface, ΩX . Composition with the non-orientable Gauss map $\bar{\mathcal{G}}$ creates a set of representatives of $\pi_1(\mathbb{RP}^2)$. If X is non-orientable then there must be at least one map in this set which represents the non-trivial element (and generates a disclination). Suppose there was no such map, then every map in $\bar{\mathcal{G}}[\Omega X]$ could be lifted from \mathbb{RP}^2 to S^2 and we would have created an orientable Gauss map, \mathcal{G} , implying the surface is orientable, a contradiction. The disclinations created in this way *must* entangle the surface, since any disk spanning a non-orientable loop on the surface must be pierced by the defect.

5.2 SIMULATIONS OF NON-ORIENTABLE COLLOIDS

Non-orientability of the surface enforces the existence of a disclination loop but it leaves open the precise form of the defects and their equilibrium configuration. These are determined by energetics and by the nature of the embedding of the surface. While surfaces with boundary are unavoidably two-dimensional, experimentally realisable, but topologically equivalent, surfaces may be constructed by using thin material with homeotropic boundary conditions on the faces and planar anchoring on the thin edges, as shown schematically in Fig. 5.3. In this way a colloid with varying surface anchoring conditions can be made to faithfully represent a two-dimensional surface. Such boundary conditions are essential to mimic non-orientable surfaces and ensure the topological properties we describe – fully homeotropic boundary conditions simply replicate an orientable torus. Modern fabrication techniques allow for the manufacture of such exotic surfaces [145].

As the Möbius strip is the prototypical non-orientable surface – *all* non-

²It is more common, and more useful in general, to think of the non-orientable version of the Gauss map as a map to the Grassmannian $\text{Gr}_2(\mathbb{R}^3)$ – see, e.g. J.W. Milnor, J.D. Stasheff *Characteristic Classes* (Princeton University Press, Princeton, 1974) – but since $\text{Gr}_2(\mathbb{R}^3)$ is canonically homeomorphic to \mathbb{RP}^2 there is no loss in our discussion.

orientable surfaces contain the Möbius strip as a subset – it serves as an elementary guide to the behaviour of non-orientable surfaces in liquid crystals. A Möbius strip with homeotropic boundary conditions will generate a non-trivial element of $\pi_1(\mathbb{RP}^2)$ as one passes around the strip and hence must be threaded by a disclination loop of zero hedgehog charge, entangling the surface. The shape of disclination loops around colloidal particles is governed largely by the requirement to minimise the distortion energy of the surrounding director field. A simple heuristic for this can be constructed as follows. As one passes through a disclination line a rotation of approximately $\pi/2$ is induced in the director. This rotation mediates the transition from the surface normal orientation to that of the far-field and will best minimise the distortion in the director field when it is concentrated along those parts of the surface where the local anchoring and far-field directions are perpendicular. Since we consider colloids with homeotropic anchoring this simply gives the requirement that

$$\mathbf{S}_n \cdot \mathbf{n}_0 = 0, \quad (5.1)$$

along the disclination, where \mathbf{S}_n is the surface normal and \mathbf{n}_0 is the far-field director. For a spherical particle in a uniform far-field, this predicts that the disclination will lie on a great circle in a plane perpendicular to this far-field direction, which is the observed position of Saturn ring defects [141]. Likewise the twisted shape of disclinations around spherical colloids in a cholesteric [128, 130] is correctly predicted by the same heuristic.

The preferred defect configuration for a Möbius strip can be found by numerical simulation using continuum Landau-de Gennes modelling (see Chapter 1). As shown in Fig. 5.3, the minimum energy configuration is a single disclination loop entangling the strip, in the location predicted by (5.1). Of course, the precise configuration depends on the strip's orientation relative to the far-field, but we have found that the orientation shown, with the strip's centreline in a plane perpendicular to the far-field orientation, has the lowest observed energy. The cross-section of the disclination loop shows a

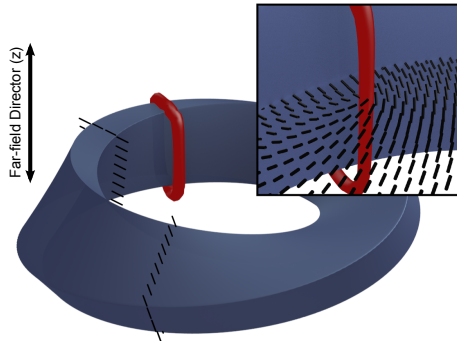


Figure 5.3: Simulation results of a Möbius strip with homeotropic boundary conditions on the flat faces, shown schematically in black along the strip. Note the planar anchoring on the short edge required to correctly represent a two-dimensional surface. The two-dimensional surface can then be thought of as living in the centre of the strip. The defect line (red) is clearly visible entangling the strip, as predicted by (5.1). The inset shows the local director profile near the defect, showing the $+1/2$ twist disclination on the inside of the strip; there is a corresponding $-1/2$ twist profile on the outside.

twisted $-1/2$ profile on the outside of the strip and a $+1/2$ twisted profile on the inside, as it has to in order to carry no hedgehog charge [146]. This hedgehog charge may be computed by several methods. The recently developed Pontryagin-Thom construction [8] and methods related to disclination profile switching [146] both assert that the charge of the disclination is zero, as required on topological grounds.

Perhaps the simplest generalisation of the Möbius strip topology is to vary its embedding in \mathbb{R}^3 . Different embeddings can be obtained by changing the number, p , of half-twists that the strip contains. The ‘canonical’ Möbius strip has one half-twist ($p = 1$), but more generally if p is odd then the surface is still non-orientable and has the same topology as the Möbius strip. When p is even the surface is orientable and has the topology of an annulus. Nonetheless, the embeddings are distinct and carry their own topological embellishments. The boundary of a Möbius strip is a circle. For a single half-twist this is a simple unknot, but for p half-twists it is a $(p, 2)$ torus knot (p odd) or link (p even). To see this, note that the boundary of a p -twisted strip (p odd) lives on a torus whose major radius is that of the strip and whose minor radius is half the strip width. The curve the boundary draws on this torus goes round the meridional cycle p times – once for each half-twist – while

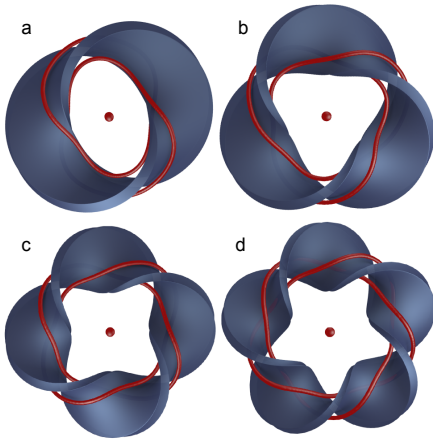


Figure 5.4: Knotted and linked disclinations in chiral nematics stabilised by the presence of twisted surfaces with homeotropic boundary conditions on the flat faces, and planar on the thin edges. They are torus knots and links of the form $(p, 2)$. Shown are: (a) $p = 2$ Hopf link, (b) $p = 3$ trefoil knot, (c) $p = 4$ Solomon's Seal and (d) $p = 5$ cinquefoil knot. The defects in the centre are hedgehogs, existing in pairs above and below the strip.

traversing the longitudinal cycle twice, which is the definition of a $(p, 2)$ torus knot. The story is the same for orientable strips with p even, except that there are two components to the boundary and they form a link.

Can this structure, coming from the nature of the embedding, be exploited to controllably produce knotted and linked disclination loops in liquid crystals? Disclination lines that follow the surface of such a multiply-twisted Möbius strip will have the same shape and properties as the colloid boundary, yielding precisely constructed knots and links. Here we show that such configurations can be stabilised in chiral nematics; examples for doubly, triply, quadruply and quintuply twisted strips are shown in Fig. 5.4. They produce the $p = 2$ Hopf link, the $p = 3$ trefoil knot, the $p = 4$ Solomon's Seal and the $p = 5$ cinquefoil knot, respectively. All these knots and links obey the topological requirements set out in the first section; the strips with an even number of twists are topologically trivial and the strip is entangled by an *even* number of disclinations, those with an odd number of twists are non-orientable and so enclose an *odd* number of disclinations.

The stabilisation of these knotted structures is not just a question of topology, energetics also come into play. In this regard, the chirality (inverse pitch)

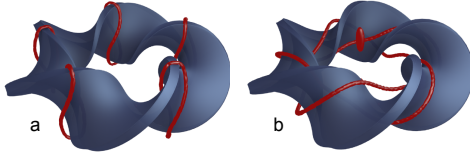


Figure 5.5: Comparison of configurations for a quintuply twisted strip. (a) Ground-state configuration consisting of 5 small disclination loops at the locations predicted by (5.1). They have a slightly twisted profile, caused by both the twisting of the strip and the chiral nature of the system. (b) (5, 2) torus knot entangling the strip, with two hyperbolic hedgehogs nucleated above and below. The energy difference between these configurations is approximately 1.2%.

of the system has an important role in the stability of these configurations. Indeed it is generally true that chiral systems allow for more exotic structures [130, 7]. In the achiral nematic system, the knotted defects are unstable and the liquid crystal assumes a ground state configuration consisting of p small disclination loops entangling the strip along the contours where $\mathbf{S}_n \cdot \mathbf{n}_0 = 0$, as predicted by (5.1). A similar configuration, with slightly twisted loops (Fig. 5.5), is also the ground state in cholesterics – the knots are metastable – although the difference in energies is small (of order 1-2%) and decreases both with increasing chirality and knot complexity p . The behaviour with increasing p can be understood in terms of the total length of disclination line, which scales as p for the isolated loops and as $\sqrt{4 + p^2}$ for the knots. If the chirality is increased such that the pitch becomes smaller than the width of the colloid then the disclinations develop twists analogous to those around spherical colloids [128, 130].

Like cholesterics, torus knots have a handedness – the $(p, 2)$ and $(p, -2)$ knots are mirror pairs – and it is not surprising to find that the relative handedness influences the stability of the textures. The handedness of the knot is set by the shape of the colloid, and if this matches that of the cholesteric then knotted textures are stable, otherwise the system tries to expel the reverse twist in the configuration, resulting in an unstable knot.

The disclination lines themselves represent just a small portion of the entire system. Their knottedness imprints a complex orientational order on everything that is *not* the knot. Fig. 5.6a shows a slice through the director

field of a quintuply twisted Möbius strip in a cell with fixed normal boundary conditions. To match the boundary conditions of the cell, the knotted disclination is accompanied by two hyperbolic hedgehogs, expanded into small loops, above and below the strip. The disclination-colloid pair has a constant profile that simply rotates uniformly as one moves around the strip; qualitatively, this structure does not depend on p , the number of half-twists. The cross-section through the colloid has a profile reminiscent of a double twist cylinder [106], split apart by the colloid into two separate $+1/2$ twist disclinations.

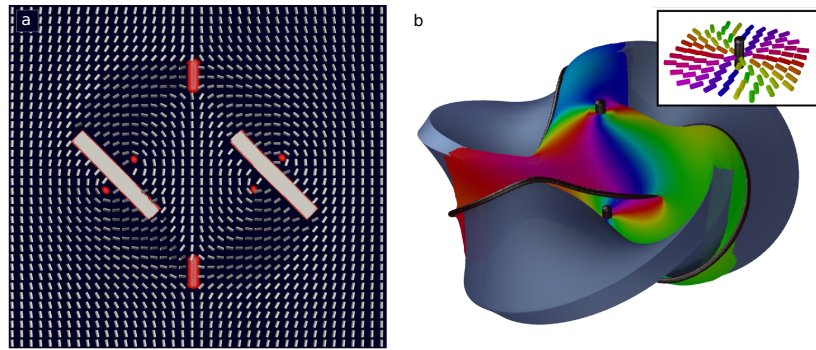


Figure 5.6: Field Structure. (a): Director field profile of a $(5, 2)$ torus knot and the two accompanying hyperbolic hedgehogs, opened up into small rings, above and below the strip, with disclinations bound to the colloid's surface. The local disclination-colloid profile is largely constant up to a rotation as one moves around the strip. Though this profile is for a $p = 5$ configuration, qualitatively the director field does not change as one varies p . The far-field director is fixed to be vertical on the boundary of the cell. (b): Pontryagin-Thom surface [8] for the trefoil knot-colloid pair. The surface is constructed by considering all points where the director field is perpendicular to the far-field. The surface is then coloured with the remaining \mathbb{RP}^1 degree of freedom (as illustrated in the inset). The defects, disclination line and two accompanying hedgehogs, are shown in black. The colour winding around the hedgehogs establishes them as unit charge defects. The surface can be patched by removing the hedgehogs, and allowing the surface to pass through the colloid. One then obtains a Seifert surface for the knot, composed of two disks (top and bottom) connected by 3 (generally p) twisted bands. It is readily verified that this surface has genus 1 (generally $(p - 1)/2$, for p odd), the genus of the trefoil knot. While there is also a colour winding around the disclination, this is a four-fold winding, giving the disclination even (equivalent to zero) hedgehog charge, as required.

CHAPTER 6

CONSTRUCTING KNOTTED TEXTURES WITH MILNOR FIBRATIONS

This chapter is concerned with giving explicit expressions for director fields containing knotted defect lines and their associated nematic textures, which have been the focus of much of this thesis. These expressions can be particularly useful in computational studies where they serve as interesting examples of initial conditions, and indeed were used in the previous chapter. The primary structure we exploit is that of Milnor fibrations [147]. These beautiful objects, at least the ones we're concerned with, are fibrations of S^3 associated to critical points of functions $\mathbb{C}^2 \rightarrow \mathbb{C}$ or $\mathbb{R}^4 \rightarrow \mathbb{C}$, though there is a far richer theory, the details of which can be found in the excellent books by Milnor [147] and Seade [148]. These structures have been used, in a very similar manner, by Mark Dennis [149] for the purpose of writing down knotted phase fields. Our use is similar, but the additional richness of nematic order as opposed to a section of a trivial $U(1)$ bundle (a phase field) allows us more freedom. A brief summary of the structure is as follows, one takes a polynomial $f : \mathbb{C}^2 \rightarrow \mathbb{C}$ with an isolated critical point at the origin. Restrict this polynomial to a 3-sphere surrounding the critical point. Let $L = f^{-1}(0) \cap S^3$ be the (dimension one) intersection of the zero set of f with S^3 , then the

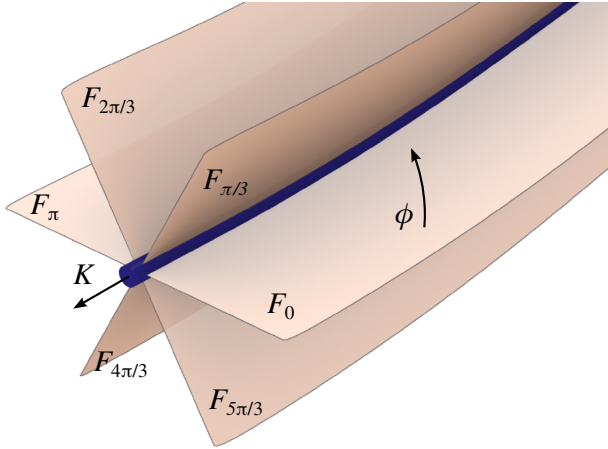


Figure 6.1: Milnor fibration of $S^3 - L$. The fibres, indexed by the phase ϕ , all join along the link L , which forms the binding of an open book decomposition of S^3 .

map

$$\phi : S^3 - L \rightarrow S^1 \quad (6.1)$$

$$x \mapsto \text{Arg}(f(x)). \quad (6.2)$$

defines a fibration of $S^3 - L$ over S^1 with fibre an orientable surface spanning L , as shown in Figure 6.1. The classic examples are given by the Brieskorn polynomials[150, 151]

$$f(z, w) = z^p + w^q, \quad (6.3)$$

with the neighbourhood S^3 chosen as the set $|z|^2 + |w|^2 = 1$. The zero set of f on S^3 is a (p, q) torus knot, has $d = \gcd(p, q)$ components and is given by the formula

$$L_j(t) = (r_1 e^{iqt}, r_2 e^{i(pt+2\pi j/d)}), \quad (6.4)$$

where $j \in \mathbb{Z}_d$ denotes the component of L and $r_1^{2p} + r_2^{2q} = 1$. The function $\phi = \text{Arg}(f)$ then gives a fibration of the complement of the (p, q) torus knot. Note that if L has d components then one can write

$$f = \prod_{i \in \mathbb{Z}_d} f_i^{n_i}, \quad (6.5)$$

where each f_i is a polynomial whose zero set restricted to S^3 is L_i and n_i is an integer. For example, the $p = 2, q = 2$ Brieskorn polynomial for the Hopf link can be written

$$f_{2,2} = (z + iw)(z - iw). \quad (6.6)$$

To apply this to the construction of textures we use stereographic projection to turn ϕ into a function $\bar{\phi} : \mathbb{R}^3 - L \rightarrow S^1 = \phi \circ \pi^{-1}$ where $\pi^{-1} : \mathbb{R}^3 \rightarrow S^3$ is an inverse three-dimensional stereographic projection. At this point it is useful to make some choices. We will choose the point $(0, i) \in \mathbb{C}^2$ as the projection point for π and demand that $f = 1$ at $(0, i)$. With these choices we can write the Brieskorn polynomials as

$$f(z, w) = z^p + (-iw)^q. \quad (6.7)$$

With these conventions we are now studying the map $\bar{\phi} : \mathbb{R}^3 - L \rightarrow S^1$. Consider a loop γ_i going around the i^{th} component of L , then the degree of $\bar{\phi}$ restricted to γ_i is

$$\deg(\bar{\phi}|_{\gamma_i}) = n_i. \quad (6.8)$$

Assume that $|n_i| = 1$ for each component. We can guarantee this by ensuring that the multiplicity of each factor in (6.5) is 1, and in general the magnitude of n_i is equal to the multiplicity of the corresponding factor [148].

6.1 CONSTRUCTING KNOTTED TEXTURES

We can use these polynomials to construct knotted textures. Essentially the observation is that if $\text{Arg}(f)$ winds by 2π around L then $\text{Arg}(\sqrt{f})$ will wind by π , and thus make L a nematic disclination. Formally we take a director field, considered as a map $\mathbf{n} : \mathbb{R}^3 - L \rightarrow \mathbb{RP}^2$, where L is a set of line defects. We assume that the director field is always orthogonal to some fixed direction \mathbf{v}_0 , for examples we will choose $\mathbf{v}_0 = \mathbf{e}_y$ in the standard Cartesian basis. Then we can regard \mathbf{n} as a map $\mathbf{n} : \mathbb{R}^3 - L \rightarrow \mathbb{RP}^1$. Passing to the double cover

of the complement of L , $\widehat{\Sigma(L)}$ we can write \mathbf{n} as an oriented map $\tilde{\mathbf{n}} : \widehat{\Sigma(L)} \rightarrow S^1$, equivariant with respect to the deck transformation that exchanges the two sheets of the cover (as discussed extensively earlier). Now if we take a new path γ_i going around L_i in the double cover (which can be thought of as going around L_i in \mathbb{R}^3 twice) then the fact that the lines L_i are line defects is given by the requirement that

$$\deg(\tilde{\mathbf{n}}|_{\gamma_i}) = 1. \quad (6.9)$$

So if we can find an equivariant map $\widehat{\Sigma}(L) \rightarrow S^1$ such that (6.9) is satisfied then we have constructed a texture with L as a defect set and with \mathbf{n} always pointing orthogonal to \mathbf{e}_y . Such a function is supplied by $\text{Arg}(f^{\frac{1}{2}})$.

So to summarise, let $\varphi = \text{Arg}(f^{\frac{1}{2}})$. Then the director field

$$\mathbf{n} = (\cos(\varphi), 0, \sin(\varphi)) \quad (6.10)$$

contains a defect line L , defined by f . Of course \mathbf{n} has discontinuities (with a branching given by an appropriate branching set as constructed in Chapter 2), but the associated Q tensor:

$$Q = \frac{s}{2} \left(\mathbf{n} \otimes \mathbf{n} - \frac{1}{3} \mathbb{I} \right), \quad (6.11)$$

is continuous and defines the appropriate uniaxial nematic texture.

6.1.1 THE TOPOLOGY OF THE TEXTURE

Constructing nematic textures in this way strongly constrains their topology. Because \mathbf{n} is always pointing orthogonal to a particular direction, its topological class $[\mathbf{n}]$ in the group $H_1(\Sigma(L))$ must be of order two, that is $2[\mathbf{n}] \in H_1(\Sigma(L)) = 0$.

To show this, let ξ be the vector bundle of vectors orthogonal to $\tilde{\mathbf{n}}$ on the double cover of the link complement defined by the splitting, $T\widehat{\Sigma(L)} =$

$L_{\tilde{\mathbf{n}}} \oplus \xi$. By construction our texture is locally of the form $\tilde{\mathbf{n}}(x) = (a(x), 0, b(x))$, and hence sections of ξ consist of vector fields that are locally of the form $\alpha(0, 1, 0) + \beta(-b(x), 0, a(x))$. The vector field $(0, 1, 0)$ is therefore a non-zero section of ξ (*i.e.* a non-zero vector field that is everywhere orthogonal to $\tilde{\mathbf{n}}$). As ξ admits two non-zero linearly independent sections it must be a trivial bundle, and hence have vanishing Euler class. As we know, the topological type of \mathbf{n} , up to sign ambiguity, is an element of the group $H_1(\Sigma(L))$. Then the Euler class of ξ is twice $[\tilde{\mathbf{n}}]$, but this must be zero, as we constructed a non-zero section. Hence

$$2[\mathbf{n}] \in H_1(\Sigma(L)) = 0. \quad (6.12)$$

which does not depend on the choice of orientation in the lift of \mathbf{n} to the double cover.

One can also obtain insight using the Pontryagin-Thom construction. Take $\lim_{x \rightarrow \infty} \mathbf{n} = (0, 0, 1)$ as the chosen direction, then the PT surface will be regions where $\mathbf{n} = (1, 0, 0)$ and will be of one colour, and of course this is just a fibre of f .

6.2 THE HOPF LINK AND CONJUGATE POLYNOMIALS

We will illustrate these ideas with our favourite example – the Hopf link. The Brieskorn polynomial is

$$f(z, w) = z^2 - w^2. \quad (6.13)$$

We use the stereographic projection

$$\pi^{-1}(x, y, z) = \frac{(2x + i2y, 2z + i(x^2 + y^2 + z^2 - 1))}{1 + x^2 + y^2 + z^2}. \quad (6.14)$$

The polynomial f , as a function of Cartesian coordinates (x, y, z) , is then given as

$$f(x, y, z) = \left(1 + \frac{8(1+x^2) - 8(1+x^2+y^2+z^2)}{(1+x^2+y^2+z^2)^2}\right) + i4 \left(\frac{2xy - z(x^2+y^2+z^2-1)}{(1+x^2+y^2+z^2)^2}\right). \quad (6.15)$$

Then the phase field $\varphi = \text{Arg}(f^{\frac{1}{2}})$ takes the form

$$\varphi = \frac{1}{2} \arctan \left(\frac{\text{Im}(f)}{\text{Re}(f)} \right) \quad (6.16)$$

and one constructs the texture \mathbf{n} as

$$\mathbf{n} = (\sin \varphi, 0, \cos \varphi). \quad (6.17)$$

The PT surface can be plotted as the intersection of the sets $\text{Im}(f) = 0$ and $\text{Re}(f) > 0$ and is shown in Figure 6.2.

In §6.1.1 we showed that textures generated in this manner are given by order two elements of $H_1(\Sigma(L))$. In the case of the Hopf link we know that $H_1(\Sigma(L)) = \mathbb{Z}_2$, both elements of which are of order two. Hence one might ask if we can create representatives of both textures with this method. The example illustrated above can be assigned a linking number invariant of +1 by considering the orientation on the boundary defined by the PT surface. The corresponding -1 texture can be constructed by conjugating one of the component polynomials:

$$f_{-1} = (z+w)\overline{(z-w)} \quad (6.18)$$

which can be thought of as reversing the orientation of one of the link components. This procedure can be made more general, indeed each factor in the expression (6.5) may be conjugated to form a new fibration. Plots of the Milnor surfaces are shown in Figure 6.2. There is a slight subtlety, in particular one might like to ask which of the textures is $0 \in \mathbb{Z}_2$ and which of the textures is 1 . The two textures can be related by a reflection, and so the

choice of which texture corresponds to which element of \mathbb{Z}_2 is arbitrary. In fact, considerations of this type leads one to conjecture that for a given link, the order of the first homology of the branched double cover is bounded from below by $2^{|L|-1}$. We do not know the status of this conjecture in the mathematics literature.

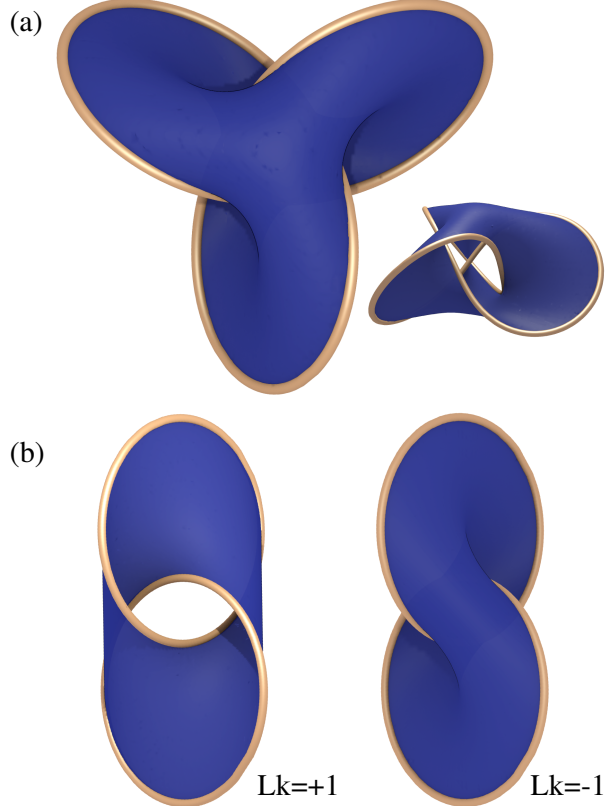


Figure 6.2: Pontryagin-Thom surfaces for a texture containing a knotted nematic defect line. (a) PT surface for a nematic containing a trefoil knot. (b) & (c) PT surfaces for nematic textures containing linked defects with linking numbers ± 1 respectively. These are generated using the equations (6.13) and (6.18). The linking number of ± 1 can be found by assigning orientations to the boundary that are induced by choosing an orientation of the surface. Note that choice of surface orientation changes the induced boundary orientations by a global sign, so that the overall linking number is the same.

6.3 ADDING SKYRMIONS AND HEDGEHOGS

By construction, the technique we have used so far gives textures which permit an everywhere orthogonal direction, the Euler class of the orthogonal

2-plane bundle must be of order 2. An alternative way of saying this is that one can construct a PT surface for these textures which can be of a single, solid colour, as shown in Figure 6.2. The next step is, of course, to construct textures for which the associated Euler class is not of order 2. To do this is simple, and requires but a small extension of our previous work.

The first step is to extend our formula (6.10) for \mathbf{n} as follows

$$\mathbf{n} = (\sin \varphi \cos \chi, \sin \varphi \sin \chi, \cos \varphi) \quad (6.19)$$

for arbitrary maps $\varphi, \chi : \mathbb{R}^3 - L \rightarrow S^1$ this formula can give any texture. We have specified φ using the Milnor polynomials, so it remains to specify χ . A natural choice is to make $\chi = \text{Arg}(h(x + iy, z))$, where $h(x + iy, z)$ is a smooth one-parameter family of meromorphic functions indexed by z (the Cartesian coordinate). While (6.19) contains singularities along the lines in \mathbb{R}^3 corresponding to the poles and zeros of h , they can be made removable by ensuring that the lines do not intersect the surface where $\varphi = \pi/2$. In fact, in this way, one can choose the surface $\varphi = \pi/2$ as a ‘canonical’ PT surface, $\Sigma_{\pi/2}$, and consider the poles and zeros of h as entangling it. A schematic of this situation is shown in Figure 6.3.

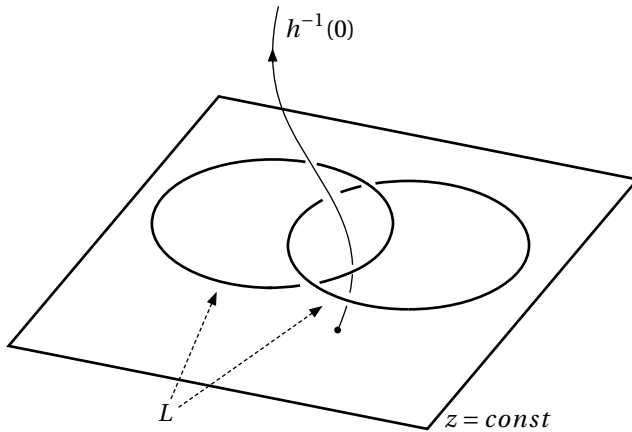


Figure 6.3: Extending the construction. The data from the Milnor polynomial is supplemented with a family of meromorphic functions h , which are indexed by z , the zeros of which entangle the link L . The homology class of the zeros and poles of h determine the topological class of the texture generated in this way.

Once one makes this choice, it remains to identify the topological class to which it belongs. We need to do two things to achieve this, we first need to remove the removable singularities from (6.19) and then identify the topology of the texture. As before we have the director \mathbf{n} given by

$$\mathbf{n} = (\cos \varphi \cos \chi, \cos \varphi \sin \chi, \sin \varphi) \quad (6.20)$$

along with this there is the natural orthogonal direction given by

$$\mathbf{b} = (-\sin \chi, \cos \chi, 0). \quad (6.21)$$

Now \mathbf{n} has singularities along the zeros and poles of h . We have promised they are removable, so we will remove them. Since h is a smooth 1-parameter family of meromorphic functions, its zeros and poles must intersect the $x-y$ planes transversely, except at a set of isolated points, where zeros and poles merge. If one assigns a line corresponding to a zero of h to be pointing along the positive z -axis direction, and poles to be pointing along the negative z -axis direction, then one obtains a set of cycles \mathcal{C} in $S^3 - \Sigma_{\pi/2}$ ¹; note that this is only possible because of the transverse intersection guaranteed by h . These cycles are precisely the locations of the singularities in \mathbf{n} .

By construction, \mathcal{C} does not intersect the surface $\Sigma_{\pi/2}$. Now consider a particular component $C_i \in \mathcal{C}$, φ restricted to C_i is a map² $S^1 \rightarrow \mathbb{RP}^1$. Because \mathcal{C} does not intersect the surface $\Sigma_{\pi/2}$ the degree of the map $S^1 \rightarrow \mathbb{RP}^1$ must be zero, since it is not surjective. Take a neighbourhood $N(C_i)$, fix φ on $\partial N(C_i)$. Since φ is null-homotopic on $\partial N(C_i)$, one can perform a homotopy of φ in $N(C_i)$, such that $\varphi|_{C_i} = \pi/2$ (*i.e.* \mathbf{n} is vertical). In doing so one has removed the singularities in \mathbf{n} , but \mathbf{b} remains orthogonal.

The singularities in \mathbf{b} are precisely the same as the original singularities in \mathbf{n} . Hence they are also the set of cycles \mathcal{C} . Passing to the cyclic double

¹In principle, one obtains a singular set; arcs joined at nodes, but a perturbation of h removes these.

²The target space is \mathbb{RP}^1 because we took the square root of ϕ .

cover, this set \mathcal{C} becomes an element (up to sign) $[\mathcal{C}] \in H_1(\Sigma(L))$, defined by the oriented cycles corresponding to the poles and zeros of h . The sign depends on the choice that zeros are oriented ‘upwards’ and poles oriented ‘downwards’, but there is a global sign ambiguity in the classification of nematic textures anyway, so it all comes out in the wash. Hence we have constructed a direction orthogonal to $\tilde{\mathbf{n}}$ whose singularities lie on \mathcal{C} . Since the Euler class is given by the Poincaré dual to zeros of a generic section, the Euler class of $\tilde{\mathbf{n}}$ is given by $PD([\mathcal{C}])$, which determines the topology of \mathbf{n} up to elements of order 2 in $H_1(\Sigma(L))$. Aspects of order two textures can, as we have illustrated with the Hopf link, be explored by changing the orientations of the link components through partial conjugation of the appropriate Milnor polynomial, though we do not currently have a full theory for this.

Finally, we will briefly mention how one may add point defects to this system. The answer is predictably simple, one simply allows the zeros or poles of h to intersect the surface $\Sigma_{\pi/2}$.

6.3.1 EXAMPLES AND PRACTICALITIES

While conceptually the process outlined above is clear, actually choosing a family of meromorphic functions h can be difficult. The simplest choice is to set $h(x + iy, z) = h(x + iy)$, *i.e.* have no dependence on the z -direction. In this case the lines corresponding to the poles and zeros of h will be vertical, and will meet ‘at infinity’ in \mathbb{R}^3 . As such, this violates the assumption that $\lim_{|x| \rightarrow \infty} \mathbf{n} = \mathbf{n}_0$, and the knotted defect line will have an overall charge corresponding to the sum of the poles and zeros of h . Nevertheless, doing things in this way is by far the easiest, and a large gallery of examples are shown in Figure 6.4.

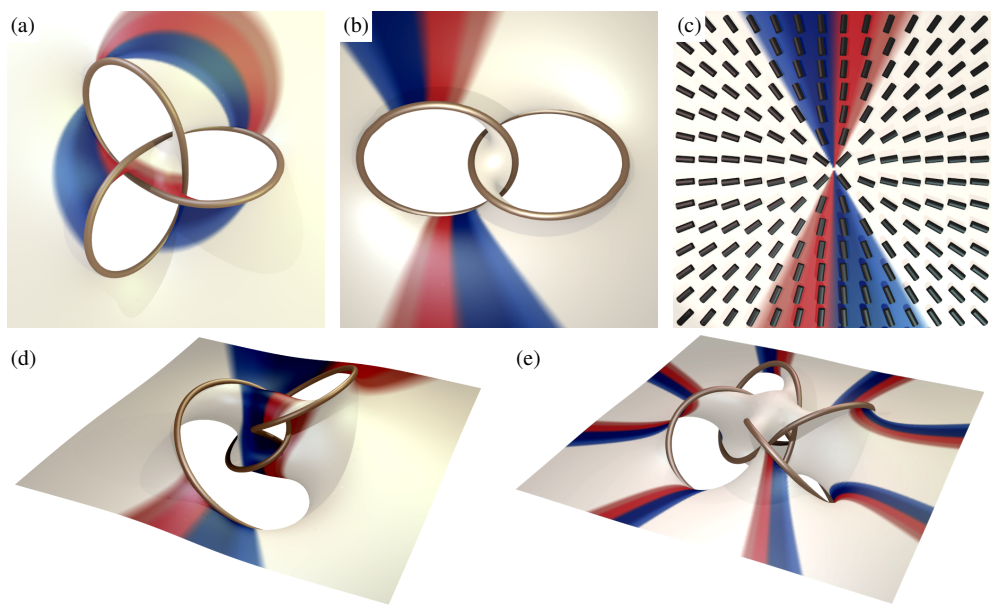


Figure 6.4: Gallery of knotted defect textures. The surfaces are where the director is horizontal, the colour is given by the horizontal orientation, and is indicated in (c). Note of particular interest the texture in (a), which has zero total hedgehog charge.

BIBLIOGRAPHY

- [1] P.G. de Gennes and J. Prost, *The Physics of Liquid Crystals*, 2nd Edition, (Oxford University Press, Oxford, 1993).
- [2] P.M. Chaikin and T.C. Lubensky, *Principles of condensed matter physics* (Cambridge University Press, Cambridge, 1995).
- [3] I.W. Stewart, *The Static and Dynamic Continuum Theory of Liquid Crystals: A Mathematical Introduction* (Taylor & Francis, London, 2004).
- [4] U. Tkalec, M. Ravnik, S. Čopar, S. Žumer, and I. Muševič, *Reconfigurable Knots and Links in Chiral Nematic Colloids*, Science **333**, 62 (2011).
- [5] A. Martinez, M. Ravnik, B. Lucero, R. Visvanathan, S. Žumer, and I.I. Smalyukh, *Mutually tangled colloidal knots and induced defect loops in nematic fields*, Nat. Mater. **13**, 258 (2014).
- [6] Tasinkevych, M.G. Campbell and I.I. Smalyukh, *Splitting, linking, knotting, and solitonic escape of topological defects in nematic drops with handles*, Proc. Natl. Acad. Sci. USA **111**, 16268 (2014).
- [7] I.I. Smalyukh, Y. Lansac, N.A. Clark, and R.P. Trivedi, *Three-dimensional structure and multistable optical switching of triple-twisted particle-like excitations in anisotropic fluids*, Nat. Mater. **9**, 139 (2010).
- [8] B.G. Chen, P.J. Ackerman, G.P. Alexander, R.D. Kamien, and I.I. Smalyukh, *Generating the Hopf Fibration Experimentally in Nematic Liquid Crystals*, Phys. Rev. Lett. **110**, 237801 (2013).

- [9] P.J. Ackerman, R.P. Trivedi, B. Senyuk, J. van de Lagemaat, and I.I. Smalyukh, *Two-dimensional skyrmions and other solitonic structures in confinement-frustrated chiral nematics*, Phys. Rev. E **90**, 012505 (2014).
- [10] R.D. Kamien and J.V. Selinger. *Order and frustration in chiral liquid crystals*. J. Phys. Condens. Matter **13**, R1 (2001).
- [11] O. Lavrentovich and M. Kleman, *Cholesteric liquid crystals: defects and topology* in *Chirality in Liquid Crystals*, ed: H.S. Kitzerow and C. Bahr (Springer-Verlag, Berlin, 2001), 115.
- [12] S. Chandrasekhar, *Liquid Crystals* (2nd ed.). (Cambridge University Press, Cambridge, 1992).
- [13] G.P. Alexander, *Liquid Crystalline Blue Phases and Swimmer Hydrodynamics* (DPhil thesis, University of Oxford, 2008).
- [14] M. Ravnik and S. Žumer, *Nematic colloids entangled by topological defects*, Soft Matter **5**, 269 (2009).
- [15] M. Ravnik and S. Žumer, *Landau-de Gennes modelling of nematic liquid crystal colloid*, Liq. Cryst. **36**, 1201 (2009).
- [16] M. Ravnik and S. Žumer, *Nematic braids: 2D entangled nematic liquid crystal colloids*, Soft Matter **5**, 4520 (2009).
- [17] I. Dierking, *Textures of Liquid Crystals* (Wiley-VCH, Weinheim, 2003).
- [18] https://commons.wikimedia.org/wiki/File:Nematische_Phase_Schlierentextur.jpg
- [19] B.G. Chen, Ph.D. thesis, University of Pennsylvania, 2012.
- [20] G.P. Alexander, B.G. Chen, E.A. Matsumoto, and R.D. Kamien, *Colloquium: Disclination loops, point defects, and all that in nematic liquid crystals*, Rev. Mod. Phys. **84**, 497 (2012).
- [21] P.E. Cladis and M. Kléman, *Non-singular disclinations of strength $s = +1$ in nematics*, J. Phys. (France) **33**, 591 (1972).

- [22] R.B. Meyer, *On the existence of even indexed disclinations in nematic liquid crystals*, Philos. Mag. **27**, 405 (1973).
- [23] C. Williams and Y. Bouligand, *Fils et disinclinaisons dans un nématique en tube capillaire*, J. Phys. (France) **35**, 589 (1974).
- [24] P.S. Drzaic, *Liquid Crystal Dispersions* (World Scientific, Singapore, 1995).
- [25] N.D. Mermin, *The topological theory of defects in ordered media*, Rev. Mod. Phys. **51**, 591 (1979).
- [26] A. Hatcher, *Algebraic Topology* (Cambridge University Press, Cambridge, 2001).
- [27] N.S. Manton and P.M. Sutcliffe, *Topological Solitons*, (Cambridge University Press, Cambridge, 2004).
- [28] V. Poénaru and G. Toulouse, *The crossing of defects in ordered media and the topology of three-manifolds*, J. Physique **38**, 887 (1977).
- [29] M.I. Monastyrsky and V.S. Retakh, *Topology of linked defects in condensed matter*, Comm. Math. Phys. **103**, 445 (1986).
- [30] K Jänich, *Topological properties of ordinary nematics in 3-space*, Acta. Appl. Math. **8**, 65 (1987).
- [31] S. Čopar and S. Žumer, *Nematic braids: topological invariants and rewiring of disclinations*, Phys. Rev. Lett. **106**, 117801 (2011).
- [32] L. Pontryagin, *A classification of continuous transformations of a complex into a sphere*, Dokl. Akad. Nauk SSSR **19**, 361 (1938).
- [33] L. Pontryagin, *A classification of mappings of the three-dimensional complex into the two dimensional sphere*, Rec. Math. [Mat. Sbornik] N.S. **9**, 5, 331 (1941).

- [34] R. Thom, *Quelques propriétés globales des variétés différentiables*, Comm. Math. Helv. **28**, 17 (1954).
- [35] J.W. Milnor, *Topology from the Differential Viewpoint*, (Princeton University Press, Princeton, 1965).
- [36] T. tom Dieck. *Algebraic Topology*, (European Mathematical Society, 2008).
- [37] S. Bechluft-Sachs and M. Hien, *The Global Defect Index*, Commun. Math. Phys. **202**, 403 (1998).
- [38] D. DeTurck, H. Gluck, R. Komendarczyk, P. Melvin, C. Shonkwiler and D.S. Vela-Vick, *Triple linking numbers, ambiguous Hopf invariants and integral formulas for three-component links*, Mat. Contemp. **34**, 251 (2008).
- [39] D. DeTurck, H. Gluck, R. Komendarczyk, P. Melvin, C. Shonkwiler and D.S. Vela-Vick, *Generalized Gauss maps and integrals for three-components links: Toward higher helicities for magnetic field and fluid flows*, J. Math. Phys. **54**, 013515 (2013). arXiv:1207.1793.
- [40] W.B.R. Lickorish, *An Introduction to Knot Theory*, (Springer-Verlag, New York, 1997).
- [41] D. Rolfsen, *Knots and Links*, (AMS Chelsea Publishing, Providence, 2003).
- [42] J.W. Milnor and J.D. Stasheff, *Characteristic Classes*, (Princeton University Press, Princeton, 1974).
- [43] Y. Bouligand, *Recherches sur les textures des états mésomorphes. 6 Dislocations coins et signification des cloisons de Grandjean-Cano dans les cholestériques*, J. Phys. (France) **35**, 959-981 (1974).

- [44] Y. Bouligand, B. Derrida, V. Poénaru, Y. Pomeau, and G. Toulouse, *Distortions with double topological character: the case of cholesterics*, J. Phys. (France) **39**, 863 (1978).
- [45] M. Kléman and J. Friedel, *Lignes de dislocation dans les cholestériques*, J. Phys. France Colloq. **30**, 43 (1969).
- [46] I.I. Smalyukh and O.D. Lavrentovich, *Three-dimensional director structures of defects in Grandjean-Cano wedges of cholesteric liquid crystals studied by fluorescence confocal polarizing microscopy*, Phys. Rev. E **66**, 051703 (2002).
- [47] N.D. Mermin and T.L. Ho, *Circulation and Angular Momentum in the A Phase of Superfluid Helium-3*, Phys. Rev. Lett. **36**, 594 (1976).
- [48] G.E. Volovik and V.P. Mineev, *Vortices with free ends in superfluid He^3 -A*, JETP Lett. **23**, 593-595 (1976). [Pis'ma Zh. Eksp. Teor. Fiz. **23**, 647 (1976).]
- [49] P.W. Anderson and G. Toulouse, *Phase Slippage without Vortex Cores: Vortex Textures in Superfluid ${}^3\text{He}$* , Phys. Rev. Lett. **38**, 508 (1977).
- [50] P.M. Walmsley and A.I. Golov, *Chirality of Superfluid ${}^3\text{He}$ -A*, Phys. Rev. Lett. **109**, 215301 (2012).
- [51] U.K. Rößler, A.N. Bogdanov, and C. Pfleiderer, *Spontaneous skyrmion ground states in magnetic metals*, Nature **442**, 797 (2006).
- [52] S. Mühlbauer, B. Binz, F. Jonietz, C. Pfleiderer, A. Rosch, A. Neubauer, R. Georgii, and P. Böni, *Skyrmion Lattice in a Chiral Magnet*, Science **323**, 915 (2009).
- [53] X.Z. Yu, Y. Onose, N. Kanazawa, J.H. Park, J.H. Han, Y. Matsui, N. Nagaosa, and Y. Tokura, *Real-space observation of a two-dimensional skyrmion crystal*, Nature **465**, 901 (2010).

- [54] X. Yu, M. Mostovoy, Y. Tokunaga, W. Zhang, K. Kimoto, Y. Matsui, Y. Kaneko, N. Nagaosa, and Y. Tokura, *Magnetic stripes and skyrmions with helicity reversals*, Proc. Natl. Acad. Sci. USA **109**, 8856 (2012).
- [55] P. Milde, D. Köhler, J. Seidel, L.M. Eng, A. Bauer, A. Chacon, J. Kinder-vater, S. Mühlbauer, C. Pfleiderer, S. Buhrandt, C. Schütte, and A. Rosch, *Unwinding of a Skyrmion Lattice by Magnetic Monopoles*, Science **340**, 1076 (2013).
- [56] U. Al Khawaja and H. Stoof, *Skyrmions in a ferromagnetic Bose-Einstein condensate*, Nature **411**, 918 (2001).
- [57] L.S. Leslie, A. Hansen, K.C. Wright, B.M. Deutsch, and N.P. Bigelow, *Creation and Detection of Skyrmions in a Bose-Einstein Condensate*, Phys. Rev. Lett. **103**, 250401 (2009).
- [58] J.Y. Choi, W.J. Kwon, and Y.I. Shin, *Observation of topologically stable 2d Skyrmions in an antiferromagnetic spinor Bose-Einstein condensate*, Phys. Rev. Lett. **108**, 035301 (2012).
- [59] J.Y. Choi, S. Kang, S.W. Seo, W.J. Kwon, and Y.I. Shin, *Observation of a Geometric Hall Effect in a Spinor Bose-Einstein Condensate with a Skyrmion Spin Texture*, Phys. Rev. Lett. **111**, 245301 (2013).
- [60] M.J.H. Ku, W. Ji, B. Mukherjee, E. Guardado-Sánchez, L.W. Cheuk, T. Yefsah, and M. Zwierlein, *Motion of a Solitonic Vortex in the BEC-BCS Crossover*, Phys. Rev. Lett. **113**, 065301 (2014).
- [61] S. Donadello, S. Serafini, M. Tylutki, L.P. Pitaevskii, F. Dalfovo, G. Lam-poresi, and G. Ferrari, *Observation of Solitonic Vortices in Bose-Einstein Condensates*, Phys. Rev. Lett. **113**, 065302 (2014).
- [62] J.F. Nye, *Lines of circular polarization in electromagnetic wave fields*, Proc. R. Soc. A **389**, 279 (1983).

- [63] J.F. Nye and J.V. Hajnal, *The wave structure of monochromatic electromagnetic radiation*, Proc. R. Soc. A **409**, 21 (1987).
- [64] J.V. Hajnal, *Singularities in the transverse fields of electromagnetic waves. I. Theory*, Proc. R. Soc. A **414**, 433 (1987).
- [65] J.V. Hajnal, *Singularities in the transverse fields of electromagnetic waves. II. Observations on the electric field*, Proc. R. Soc. A **414**, 447 (1987).
- [66] D. Hilbert and S. Cohn-Vossen, *Geometry and the Imagination*, (AMS Chelsea Publishing, New York, 1999).
- [67] M.V. Berry and J.H. Hannay, *Umbilic points on Gaussian random surfaces*, J. Phys. A: Math. Gen. **10**, 1809 (1977).
- [68] M.V. Berry and M.R. Dennis, *Polarization singularities in isotropic random waves*, Proc. R. Soc. A **456**, 2059 (2000).
- [69] M.V. Berry and M.R. Dennis, *Polarization singularities in isotropic random vector waves*, Proc. R. Soc. A **457**, 141 (2001).
- [70] M.R. Dennis, *Polarization singularities in paraxial vector fields: morphology and statistics*, Opt. Commun. **213**, 201 (2002).
- [71] F. Flossmann, U.T. Schwarz, M. Maier, and M.R. Dennis, *Polarization singularities from unfolding an optical vortex through a birefringent crystal*, Phys. Rev. Lett. **95**, 253901 (2005).
- [72] F. Flossmann, K. O'Holleran, M.R. Dennis, and M.J. Padgett, *Polarization singularities in 2D and 3D speckle fields*, Phys. Rev. Lett. **100**, 203902 (2008).
- [73] V. Vitelli, B. Jain, and R.D. Kamien, *Topological defects in gravitational lensing shear fields*, J. Cosmol. Astropart. Phys. **09**, 034 (2009).

- [74] T.H. Beuman, A.M. Turner, and V. Vitelli, *Stochastic geometry and topology of non-Gaussian fields*, Proc. Natl. Acad. Sci. USA **109**, 19943 (2012).
- [75] T.H. Beuman, A.M. Turner, and V. Vitelli, *Critical and umbilical points of a non-Gaussian random field*, Phys. Rev. E **88**, 012115 (2013).
- [76] I. Dzyaloshinsky, *A thermodynamic theory of “weak” ferromagnetism of antiferromagnetics*, J. Phys. Chem. Solids **4**, 241 (1958).
- [77] T. Moriya, *Anisotropic superexchange interaction and weak ferromagnetism*, Phys. Rev. **120**, 91 (1960).
- [78] E. Efrati and W.T.M. Irvine, *Orientation-Dependent Handedness and Chiral Design*, Phys. Rev. X **4**, 011003 (2014).
- [79] A.S. Thorndike, C.R. Cooley, and J.F. Nye, *The structure and evolution of flow fields and other vector fields*, J. Phys. A: Math. Gen. **11**, 1455 (1978).
- [80] S. Čopar, M.R. Dennis, R.D. Kamien, and S. Žumer, *Singular values, nematic disclinations, and emergent biaxiality*, Phys. Rev. E **87**, 050504(R) (2013).
- [81] D.A. Beller, T. Machon, S. Čopar, D.M. Sussman, G.P. Alexander, R.D. Kamien, and R.A. Mosna, *Geometry of the Cholesteric Phase*, Phys. Rev. X **4**, 031050 (2014).
- [82] R.A.P. Rogers, *Some Differential Properties of the Orthogonal Trajectories of a Congruence of Curves, with an Application to Curl and Divergence of Vectors*, Proc. R. Irish Soc. A **29**, 92 (1912).
- [83] Yu. Aminov, *The Geometry of Vector Fields*, (Gordon and Breach Science Publishers, Amsterdam, 2000).
- [84] A.A. Belavin and A.M. Polyakov, *Metastable states of two-dimensional isotropic ferromagnets*, JETP Lett. **22**, 245-247 (1975). [Pis'ma v. Zh. Eksp. Teor. Fiz. **22**, 503 (1975).]

- [85] S. Armon, E. Efrati, R. Kupferman, and E. Sharon, *Geometry and Mechanics in the Opening of Chiral Seed Pods*, Science **333**, 1726 (2011).
- [86] P.A.M. Dirac, *Quantised singularities in the electromagnetic field*, Proc. R. Soc. Lond. A **133**, 60 (1931).
- [87] S.S. Chern, *A Simple Intrinsic Proof of the Gauss-Bonnet Formula for Closed Riemannian Manifolds*, Ann. Math. **45**, 747 (1944).
- [88] S.S. Chern, *On the curvatura integra in a Riemannian manifold*, Ann. Math. **46**, 674 (1945).
- [89] S.S. Chern, *Characteristic classes of Hermitian manifolds*, Ann. Math. **47**, 85 (1946).
- [90] R. Bott and L.W. Tu, *Differential Forms in Algebraic Topology*, (Springer-Verlag, New York, 1982).
- [91] S. Seki, X.Z. Yu, S. Ishiwata, and Y. Tokura, *Observation of skyrmions in a multiferroic material*, Science **336**, 198 (2012).
- [92] X.Z. Yu, N. Kanazawa, Y. Onose, K. Kimoto, W.Z. Zhang, S. Ishiwata, Y. Matsui, and Y. Tokura, *Near room-temperature formation of a skyrmion crystal in thin-films of helimagnet FeGe*, Nat. Mater. **10**, 106 (2011).
- [93] A. Tonomura, X. Yu, K. Yanagisawa, T. Matsuda, Y. Onose, N. Kanazawa, H.S. Park, and Y. Tokura, *Real-Space Observation of Skyrmion Lattice in Helimagnet MnSi Thin Samples*, Nano Lett. **12**, 1673 (2012).
- [94] N.S. Kiselev, A.N. Bogdanov, R. Schäfer, and U.K. Rößler, *Chiral skyrmions in thin magnetic films: new objects for magnetic storage technologies?*, J. Phys. D: Appl. Phys. **44**, 392001 (2011).
- [95] R.D. Kamien, *Geometry of soft materials: a primer*, Rev. Mod. Phys. **74**, 953 (2002).

- [96] M.V. Berry, *Index formulae for singular lines of polarization*, J. Opt. A **6**, 675 (2004).
- [97] H. Geiges, *An Introduction to Contact Topology*, (Cambridge University Press, Cambridge, 2008).
- [98] H.K. Moffatt, *The degree of knottedness of tangled vortex lines*, J. Fluid Mech. **35**, 117 (1969).
- [99] H.K. Moffatt and R.L. Ricca, *Helicity and the Călugăreanu Invariant*, Proc. R. Soc. A **439**, 411 (1992).
- [100] V.I. Arnold, *The Asymptotic Hopf Invariant and Its Applications*, Sel. Math. Sov. **5**, 327 (1986).
- [101] E. Witten, *Quantum field theory and the Jones polynomial*, Commun. Math. Phys. **121**, 351 (1989).
- [102] A.M. Polyakov, *One physical problem with possible mathematical significance*, J. Geom. Phys. **5**, 595 (1988).
- [103] J. H. C. Whitehead, *An expression of Hopf's invariant as an integral*, Proc. Nat. Acad. Sci. USA **33**, 117 (1947).
- [104] S. Meiboom, J.P. Sethna, P.W. Anderson, and W.F. Brinkman, *Theory of the blue phase of cholesteric liquid crystals*, Phys. Rev. Lett. **46**, 1216 (1981).
- [105] H. Grebel, R.M. Hornreich, and S. Shtrikman, *Landau theory of cholesteric blue phases*, Phys. Rev. A **28**, 1114-1138 (1983).
- [106] D.C. Wright and N.D. Mermin, *Crystalline liquids: the blue phases*, Rev. Mod. Phys. **61**, 385 (1989).
- [107] P. Pieranski, P.E. Cladis, and R. Barbet-Massin, *Experimental evidence for a hexagonal Blue Phase*, J. Phys. France Lett. **46**, 973 (1985).

- [108] P. Pieranski and P.E. Cladis, *Field-induced tetragonal blue phase (BP X)*, Phys. Rev. A **35**, 355 (1987).
- [109] R.M. Hornreich and S. Shtrikman, *Field-induced hexagonal blue phases in positive and negative dielectric anisotropy systems: Phase diagrams and topological properties*, Phys. Rev. A **41**, 1978 (1990).
- [110] J. Fukuda and S. Žumer, *Cholesteric blue phases: effect of strong confinement*, Liq. Cryst. **37**, 875 (2010).
- [111] O. Henrich, K. Stratford, M.E. Cates, and D. Marenduzzo, *Structure of Blue Phase III of Cholesteric Liquid Crystals*, Phys. Rev. Lett. **106**, 107801 (2011).
- [112] B Binz, A. Vishwanath, and V. Aji, *Theory of the Helical Spin Crystal: A Candidate for the Partially Ordered State of MnSi*, Phys. Rev. Lett. **96**, 207202 (2006).
- [113] A. Hamann, D. Lamago, Th. Wolf, H. v Löhneysen, and D. Reznik, *Magnetic Blue Phase in the Chiral Itinerant Magnet MnSi*, Phys. Rev. Lett. **107**, 037207 (2011).
- [114] A.O. Leonov, I.E. Dragunov, U.K. Rößler, and A.N. Bogdanov, *Theory of skyrmion states in liquid crystals*, Phys. Rev. E **90**, 042502 (2014).
- [115] J.I. Fukuda and S. Žumer, *Quasi-two-dimensional Skyrmion lattices in a chiral nematic liquid crystal*, Nat. Commun. **2**, 246 (2010).
- [116] R.M. Hornreich and S. Shtrikman, *Topological properties of cholesteric blue phases*, Phys. Rev. A **38**, 4843 (1988).
- [117] M. Ravnik, G.P. Alexander, J.M. Yeomans, and S. Žumer, *Three-dimensional colloidal crystals in liquid crystalline blue phases*, Proc. Natl. Acad. Sci. USA **108**, 5188 (2011).

- [118] Y. Bouligand. *Recherches sur les textures des états mésomorphes-2. – Les champs polygonaux dans les cholestériques.* Journal de Physique **33**, 715 (1972).
- [119] Y. Bouligand. *Recherches sur les textures des états mésomorphes. 3. Les plages à éventails dans les cholestériques.* Journal de Physique **34**, 603 (1973).
- [120] G.E. Volovik and V.P. Mineev, *Investigations of singularities in superluid He^3 in liquid crystals by the homotopic topology methods.* Zh. Eksp. Teor. Fiz. **72**, 2256 (1977).
- [121] F. Grandjean, C.R. Hebd. Seances Acad. Sci. **172**, 71 (1921).
- [122] R. Cano, Bull. Soc. Fr. Mineral. Cristallogr. **90**, 333 (1967).
- [123] R. Cano, Bull. Soc. Fr. Mineral. Cristallogr. **91**. 20 (1968).
- [124] D. Seč, T. Porenta, M. Ravnik and S. Žumer, *Geometrical frustration of chiral ordering in cholesteric droplets,* Soft Matter **8**, 11982 (2012).
- [125] P. J. Ackerman, R. P. Trivedi, B. Senyuk, J. van de Lagemaat, and I. I. Smalyukh *Two-dimensional skyrmions and other solitonic structures in confinement-frustrated chiral nematics,* Phys. Rev. E **90**, 012505 (2014).
- [126] B.G. Chen, G.P. Alexander and R.D. Kamien, *Symmetry breaking in smectics and surface models of their singularities,* Proc. Natl. Acad. Sci. USA **106**, 15577 (2009).
- [127] V. Poénaru, *Some aspects of the theory of defects of ordered media and gauge fields related to foliations,* Commun. Math. Phys. **80**, 127 (1981).
- [128] J.S. Lintuvuori, D. Marenduzzo, K. Stratford and M.E. Cates, *Colloids in liquid crystals: a lattice Boltzmann study.* J. Mater. Chem. **20**, 10547 (2010).

- [129] J.S. Lintuvuori, K. Stratford, M.E. Cates, D. Marenduzzo, *Colloids in cholesterics: size-dependent defects and non-Stokesian microrheology*, Phys. Rev. Lett. **105**, 178302 (2010).
- [130] V.S.R. Jampani, M. Škarabot, M. Ravnik, S. Čopar, S. Žumer, and I. Muševič *Colloidal entanglement in highly twisted chiral nematic colloids: twisted loops, Hopflinks, and trefoil knots*, Phys. Rev. E **84**, 031703 (2011).
- [131] J. Martinet, *Formes de contact sur les variétés de dimension 3*, in Proceedings of the Liverpool Singularities Symposium II, Lecture Notes in Math. 209, (Springer-Verlag, Berlin, 1971).
- [132] Y. Eliashberg, *Classification of overtwisted contact structures on 3-manifolds*, Invent. Math. **98**, 623 (1989).
- [133] Y. Eliashberg, *Contact Manifolds Twenty Years Since J. Martinet's Work*, Ann. Inst. Fourier (Grenoble) **42**, 165 (1992).
- [134] J.B. Etnyre, *On knots in overtwisted contact structures*, ArXiv:1012.3745 (2012).
- [135] P. Kronheimer and T. Mrowka, *Monopoles and Three-Manifolds*, (Cambridge University Press, Cambridge, 2007).
- [136] M. Hutchings and M. Sullivan, *Rounding corners of polygons and embedded contact homology*, Geometry and Topology **10**, 169 (2006).
- [137] M. Hutchings and C.H. Taubes, *Gluing pseudoholomorphic curves along branched covered cylinders I*, J. Symplect. Geom. **5**, 43 (2007).
- [138] Y. Eliashberg, A. Givental and H. Hofer, *Introduction to Symplectic Field Theory*, ArXiv:math/0010059 (2000).
- [139] R.D. Kamien, *Colloidal Inclusions in Liquid Crystals*, Lecture Notes, ArXiv:1506.06815 (2015).

- [140] P. Poulin, H. Stark, T.C. Lubensky, D.A. Weitz, *Novel colloidal interactions in anisotropic fluids*, Science **275**, 1770 (1997).
- [141] E.M.Terentjev, *Disclination loops, standing alone and around solid particles, in nematic liquid crystals*, Phys. Rev. E **51**, 1330 (1995).
- [142] S.K. Donaldson, *Riemann Surfaces*, (Oxford University Press, Oxford, 2011).
- [143] B. Senyuk, Q. Liu, S. He, R.D. Kamien, R.B. Kusner, T.C. Lubenskuy and I.I. Smalyukh, *Topological colloids*, Nature **493**, 200 (2013).
- [144] H. Stark, *Physics of colloidal dispersions in nematic liquid crystals*, Phys. Rep. **351**, 387 (2001).
- [145] I. Muševič, private communication.
- [146] S. Čopar, PhD Thesis, University of Ljubljana (2012).
- [147] J. Milnor, *Singular Points of Complex Hypersurfaces*, (Princeton University Press, Princeton NJ, 1968).
- [148] J. Seade, *On the Topology of Isolated Singularities in Analytic Spaces*, (Birkhäuser Verlag, Basel, 2006).
- [149] M.R. Dennis, R.P. King, B. Jack, K. O'Holleran, and M.J. Padgett, *Isolated optical vortex knots*, Nat. Phys. **6**, 118-121 (2010).
- [150] F. Pham, *Formules de Picard-Lefschetz généralisées et ramification des intégrales*, Bull. Soc. Math. France **93**, 333 (1965).
- [151] E. Brieskorn, *Beispiele zur Differentialtopologie von Singularitäten*, Invent. Math. **2**, 1 (1966).